

POLITECNICO DI TORINO
CORSO DI LAUREA MAGISTRALE
IN INGEGNERIA CIVILE

**Effects of nano-sized additives on
bituminous binders: rheological and
morphological characterization**

Tesi di Laurea Magistrale



Relatori:

Prof. Orazio Baglieri

Prof. Ezio Santagata

Ing. Lucia Tsantilis

Candidata:

Lidia Santoro

7 Dicembre 2018

Contents

List of figures	5
List of tables	7

INTRODUCTION

Research Methodology	8
----------------------------	---

CHAPTER 1 NANO-REINFORCED BITUMINOUS BLENDS

1. Materials.....	10
1.1 Bitumen	10
1.2 Nanoclays	11
1.3 Carbon Nanotubes	12
2. Nano-reinforced blends	13
2.1 Dosages Selection.....	13
2.2 Mixing Protocols	14
2.3 First Phase: Shear mixing.....	15
2.4 Low-Shear Mixing	15
2.4.1 Protocol	16
2.5 High-Shear Mixing (Silverson)	17
.....	18
2.5.1 Silverson work head functioning	18
2.5.2 Protocol	19
2.6 Sonication	23
2.6.1 Protocol	25
.....	25
2.7 The four protocols (A/B/C/D)	26
3. Acronyms	27

CHAPTER 2 RHEOLOGICAL ANALYSIS AND RESULTS

1. Experimental tests	29
2. Literature review	29
3. Performed tests	31
3.1 Frequency Sweep Test.....	33
3.2 Sample preparation.....	33
3.3 RTFOT	34
3.3.1 RTFO Test - Protocol.....	36
3.4 Linear Amplitude Sweep (LAS) Test.....	37
4. Black diagrams.....	38
3.1 Result's discussion: protocols comparison	39
3.2 Result's discussion: materials comparison.....	42
5. Master Curves	45
5.1 Literature review	45
5.2 Results discussion: protocols comparison	48
5.3 Results discussion: materials comparison	52
5.4 Comparison of variables from CA model	54
6. Damage curves from LAS Test.....	57
6.1 TP 101-14 standard	57
6.2 TP 101-16 standard	59
6.3 TP 101-14 Results discussion and analysis	60
6.3.1 Protocol comparison.....	60
6.3.2 Fatigue parameters normalization	62
6.4 TP 101-16 Results discussion and analysis	64
7. Apparent Molecular Weight Distribution (AMWD).....	66
7.1 MWDs from the linear viscoelastic behaviour	67
7.2 Results discussion.....	69

CHAPTER 3 ESEM OBSERVATION

1. Introduction	74
2. SEM drawbacks	76
3. ESEM technique.....	77
4. ESEM procedure	79

4.1 Protocol and mould description.....	81
4.2 ESEM observation.....	82
4.3 Results discussion.....	83
4.3.1 NB and NC results	84
4.3.2 CNT results	89
4.3.3 Aged samples: NB and NC results.....	93
4.3.4 Aged samples: CNT results.....	96
CONCLUSIONS AND PERSPECTIVES	
Bibliography and sitography	102

List of figures

Figure 1 AZALT 70/100 technical specifications provided by the refinery	11
Figure 2 Molecular structure 1	12
Figure 3 NC7000 micrograph scale: 100 nm - TEM	13
Figure 4 Heidolph RZR-2041	15
Figure 5 Silverson-type head	16
Figure 6 Low-Shear Mixing	17
Figure 7 Silverson L5M-A	18
Figure 8 Standard Mixing Assembly	20
Figure 9 Standard Mixing Assembly - 2	20
Figure 10 Vertical Slotted Disintegrating Head	21
Figure 11 Square Hole High Shear Screen	21
Figure 12 Base assembly	22
Figure 13 Correct rotor position	22
Figure 14 High-Shear Mixing procedure	23
Figure 15 ultrasonic device UP200S	24
Figure 16 Sonication procedure	25
Figure 17 Protocol A	26
Figure 18 Protocol B	26
Figure 19 Protocol C	27
Figure 20 Protocol D	27
Figure 21 Complex shear modulus and phase angle - Vector representation	31
Figure 22 DSR plate system	31
Figure 23 DSR 8-mm and 25-mm plates	32
Figure 24 Plate dimensions	32
Figure 25 DSR MCR 302 from Anton Paar	32
Figure 26 8-mm plate sample preparation phases (a-d)	33
Figure 27 RTFOT device	34
Figure 28 Air flow front view	35
Figure 29 RTFO glass bottles	35
Figure 30 RTFO equipment	36
Figure 31 Pouring phase	36
Figure 32 LAS - Loading scheme	38
Figure 33 Black diagrams - All blends	39
Figure 34 Black diagrams - Neat bitumen, Protocol comparison	40
Figure 35 Black diagrams - Nanoclay 3% by weight , Protocol comparison	40
Figure 36 Black diagrams - Nanoclay 6% by weight , Protocol comparison	41
Figure 37 Black diagrams - Carbon nanotubes 0.5% by weight, Protocol comparison	41

Figure 38 Black diagrams - Carbon nanotubes 1% by weight, Protocol comparison	42
Figure 39 Black diagrams - Protocol A, material comparison	43
Figure 40 Black diagrams - Protocol B, material comparison	43
Figure 41 Black diagrams - Protocol C, material comparison	44
Figure 42 Black diagrams - Protocol D, material comparison	44
Figure 43 A typical mastercurve and physical properties	47
Figure 44 Master Curves- All Blends	48
Figure 45 Master curve neat bitumen - Protocol comparison	49
Figure 46 Master curve 3% nanoclay blends - Protocol comparison	50
Figure 47 Master curve 6% nanoclay blends - Protocol comparison	50
Figure 48 Master curve 0.5% carbon nanotube blends - Protocol comparison	51
Figure 49 Master curve 1% carbon nanotube blends - Protocol comparison	51
Figure 50 Master curve Protocol A, materials comparison	52
Figure 51 Master curve Protocol B, materials comparison	53
Figure 52 Master curve Protocol C, materials comparison	53
Figure 53 Master curve Protocol D, materials comparison	54
Figure 54 Shift factors plot in time	56
Figure 55 Plot of Fatigue Parameter Nf versus applied shear strain	59
Figure 56 Fatigue parameter Nf - Neat bitumen, protocol comparison	60
Figure 57 Fatigue parameter Nf - 3% nanoclay blends, protocol comparison	61
Figure 58 Fatigue parameter Nf - 6% nanoclay blends, protocol comparison	61
Figure 59 Fatigue parameter Nf - 0.5% carbon nanotube blends, protocol comparison	62
Figure 60 Fatigue parameter Nf - 1% carbon nanotube blends, protocol comparison	62
Figure 61 A parameter comparison - NC blends	63
Figure 62 A parameter comparison - CNT blends	63
Figure 63 Fatigue parameter Nf - Neat bitumen, protocol comparison	64
Figure 64 Fatigue parameter Nf - 3% nanoclay blends, protocol comparison	64
Figure 65 Fatigue parameter Nf - 6% nanoclay blends, protocol comparison	65
Figure 66 Fatigue parameter Nf - 0.5% carbon nanotube blends, protocol comparison	65
Figure 67 Fatigue parameter Nf - 1% carbon nanotube blends, protocol comparison	66
Figure 68 Modulus and phase-angle master curves	68
Figure 69 AMWD Material comparison - Protocol A	69
Figure 70 AMWD Material comparison - Protocol B	70
Figure 71 AMWD Material comparison - Protocol C	70
Figure 72 AMWD Material comparison - Protocol D	71
Figure 73 f(MW) average values, Materials comparison - Protocol A	71
Figure 74 f(MW) average values, Materials comparison - Protocol B	72
Figure 75 f(MW) average values, Materials comparison - Protocol C	72

Figure 76 f(MW) average values, Materials comparison - Protocol D.....	73
Figure 77 SEM interaction model.....	75
Figure 78 SEM System representation.....	75
Figure 79 Respectively, SE and BSE image	76
Figure 80 ESEM System representation	78
Figure 81 Example of SE images derived from ESEM observation.....	79
Figure 82 Sample stage	80
Figure 83 Stainless steel mould	81
Figure 84 Mould pouring phase	82
Figure 85 Sample flattened on a heater.....	82
Figure 86 ESEM observation.....	83

List of tables

Table 1 Cloisite 15A technical specifications.....	12
Table 2 NC7000 technical specifications.....	13
Table 3 Summary of the names.....	28
Table 4 Plate dimensions	32
Table 5 Master curve rheological modelled variables	55
Table 6 Error Sum of Squares - Complex shear modulus and phase angle	55
Table 7 shift factors - variables.....	57
Table 8 ESEM evaluation – NB, NC samples	88
Table 9 ESEM observation CNTs 1000 x magnification.....	89
Table 10 ESEM evaluation: CNT samples	92
Table 11 ESEM evaluation – NB, NC aged samples.....	96
Table 12 ESEM evaluation – CNT aged samples.....	99

Introduction

The use of nano-sized particles as reinforcing additives for bituminous binders has become, in recent times, increasingly popular, due to the positive effects that nanoparticles induce on a wide range of materials.

A considerable literature has grown up around the theme, and the experimental work presented here will contribute to a deeper understanding of nano-additives effects on rheological and morphological properties, with the main purpose to improve the performance of bituminous materials.

Much less is known about the connection between rheological parameters and microstructure morphology, thus our dissertation has thrown up many questions in need of further investigation.

Research Methodology

In our specific case-study, one type of nanoclays (NC) and one type of carbon nanotubes (CNT) were added into a single base bitumen at several dosages, assessed in compliance with experimental researches led in the past.

Four different operating protocols were adopted for the mixing phase. Each protocol was characterized by a specific multi-stage process, differentiated on the base of:

- shear mixing equipment (low or high mixing speed);
- wave amplitude during sonication phase;
- disintegrating head type, just in case of high speed.

A two-phase blends preparation was adopted: the shear-mixing procedure leads to a more homogeneous dispersion of the nanoparticles into the bituminous matrix; on the other hand, the sonication-mixing procedure allows the reduction of particles agglomeration, in order to reach a dispersion as much uniform as possible.

Rheological tests were performed in both the linear and non-linear domain, performing respectively frequency sweeps on unaged samples and linear amplitude sweeps, after the simulation of short-term aging of asphalt binders with the Rolling Thin-Film Over Test (RTFOT).

From measurements carried out in the linear domain, black diagrams and master curves were constructed, as well as damage curves in the non-linear range.

Black diagrams are useful tools to identify inconsistencies in rheological data and to highlight and compare the revealing differences between the mixtures: they allowed to identify anomalies in rheological data, due to mistakes occurred using inappropriately DSR plates and device. Moreover, Master curves are effective to provide a relationship between stiffness and reduced frequency, over a wide range of temperatures and frequencies. Prediction of viscoelastic properties was allowed at any temperature.

Furthermore, developing the δ -method provided in literature, the bitumen's apparent molecular weight distribution (AMWD) was determined, by means of the phase angle and the complex modulus measured in the linear viscoelastic domain. All the information about AMWD can be found in the rubbery zone of the linear viscoelastic behaviour and a plot of MW and phase angle was pictured.

Recent developments in microscope technology broaden research horizons to morphological investigation of both uncoated, non-conductive and "wet" specimens, as bitumen and polymers, with a non-destructive procedure.

In order to investigate bituminous blends morphology, ESEM technology was used, with the main intention to estimate the mixing procedure influence on nanoparticles dispersion degree and to examine the relationship between the microstructure and the rheological properties.

The ESEM study gave us pictures and videos as output, for that reason we were not able to easily jump to quantitative conclusions, since previous researches have not treated the topic in much details.

However, the final conclusions showed findings that, doubtlessly, are as stimulating as innovative.

Chapter 1

Nano-reinforced bituminous blends

1.Materials

In the area of engineering, noteworthy advantages have been attained in terms of mechanical properties and long-lasting service life by using nano-sized particles in polymeric matrices (1) (2).

Approaching to our peculiar case-study, first of all, the dissertation presents a description of the materials involved in the experimental analysis.

The choice of the single base bitumen utilized has consequences on the outcomes, in terms of effects of nano-sized additives on the bituminous matrix.

1.1 Bitumen

According to its scientific definition, bitumen is a complex mixture of high molecular weight hydrocarbons insoluble in water, mostly obtained as a residue of crude oil distillation (3). The components percentage is strictly connected to the crude's origin and the distillation process. Bitumen may also be available in natural deposits, where it's directly extracted, but nowadays is preferably produced along petroleum refining process.

Bitumen material can be described as a thermoplastic and viscoelastic liquid, whose behaviour seems close to an elastic solid at low temperatures or under fast loading, and to a viscous fluid at high temperatures or under slow loading phases. As a consequence of its viscoelastic properties, bitumen exhibits both elastic and viscous responses, and shows temperature-time dependent relationship between applied stresses and outcome strains.

The single base bitumen used is an AZALT70/100, characterized by the following technical specifications:

CARATTERISTICHE		METODO	SPECIFICHE
Penetrazione a 25 °C	1/10 mm	EN 1426	70 - 100
Punto di Rammollimento (Palla & Anello)	°C	EN 1427	43 - 51
Infiammabilità Cleveland	°C	EN ISO 2592	≥ 230
Temperatura di rottura Fraass	°C	EN 12593	≤ -10
Solubilità	% massa	EN 12592	≥ 99,0
Resistenza all'indurimento a 163°C (RTFOT)		EN 12607-1	
Variazione di massa	%		≤ 0,8
Penetrazione residua	%	EN 1426	≥ 46
Aumento del punto di Rammollimento	°C	EN 1427	≤ 11

Figure 1 AZALT 70/100 technical specifications provided by the refinery

The origin refinery was sited in Volpiano (TO) establishment, and bitumen was provided by Total Erg.

1.2 Nanoclays

A commercial organophilic montmorillonite was used as a second component to reinforce our reference neat bitumen (1).

Nanoclays can be described as layered mineral particles able of yielding an exceptionally high interfacial surface as a consequence of clay sheet slight separation (4).

Specifically, the Cloisite 15A nanoclay is a montmorillonite, organically modified with different quaternary ammonium salts, characterized by the following chemical structure:

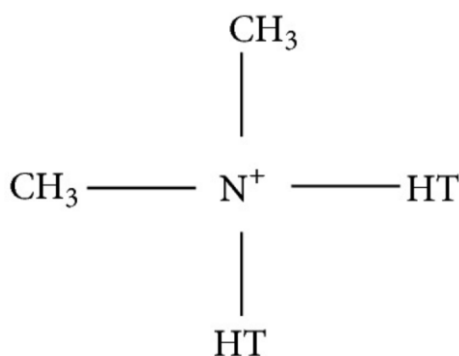


Figure 2 Molecular structure 1

T is the abbreviation form of “Tallow”, a lipid compound, which is responsible for the organic characters of the sodium montmorillonite.

The Cloisite 15A was provided by the Southern Clay Company, having the following technical characteristics:

Montmorillonite	Basal spacing d_{001} [nm]	Cation Exchange Capacity (CEC)	Organic modifier
Cloisite 15A	3.15	125 meq/100g	Dimethyl- dihydrogenated tallow quaternary ammonium salt

Table 1 Cloisite 15A technical specifications

1.3 Carbon Nanotubes

The carbon nanotubes involved in our research project came from the Nanocyl company, a worldwide industry leader in manufacturing of multiwall carbon nanotubes (MWCNT). They are classified with the acronym of NC7000™, and produced via the Catalytic Chemical Vapor Deposition (CCVD) process (5).

A Carbon nanotube is a one-atom thick sheet of graphite rolled up into a seamless hollow cylinder with a nano-scale diameter. CNTs are characterized, with some evidence, by superior mechanical properties compared to other construction materials (6).

Regarding the morphological composition, NC7000™ carbon nanotubes are tube-shaped materials, exclusively composed of carbon atoms and having a nanometric diameter .

Thanks to van der Waals forces, NC7000™ carbon nanotubes tends to cluster into agglomerates. Consequently, they look like a black powder. At nanoscale, they have a spaghetti-like structure.

Their micrograph, provided by the company, is shown in Figure 2.

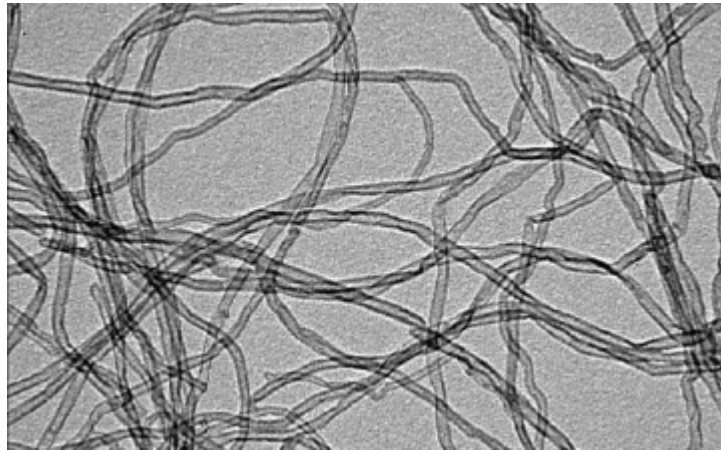


Figure 3 NC7000 micrograph scale: 100 nm - TEM

Focusing on the technical specifications, they're provided by the company and described in the following table (7):

Properties		Unit	Value	Method of measurement	
Average Diameter		10^{-9} m	9.5	Transmission Microscopy (TEM)	Electron
Average length		μm	1.5	Transmission Microscopy (TEM)	Electron
Carbon purity		%	90	Thermogravimetric (TGA)	analysis
Transition Metal oxide	%		<1%	Inductively Coupled Plasma Mass Spectrometry (ICP-MS)	
Amorphous carbon		-	*	High resolution Transmission Electron Microscopy (HRTEM)	
Surface Area		m^2/g	250-300	BET surface area analysis	
Volume resistivity		ωcm	10^{-4}	Internal test method (resistivity on powder)	

*Pyrolytically deposited carbon on the surface of the NC7000

Table 2 NC7000 technical specifications

Carbon nanotubes presents several benefits: high recyclability in thermoplastics, high electrical conductivity and UV resistance are just an example of the surprising properties they own.

2.Nano-reinforced blends

2.1 Dosages Selection

[San_Bag_Tsa_Chi_Aim_CONDBUILDMAT] [12,13,22]

Several nano-reinforced blends were prepared in the laboratory by combining the previously described base bitumen with the nano-sized materials at various dosages (8).

In order to establish such dosages, the blends preparation phase required a preliminary study concerning nanoparticles quantity estimation in terms of percentage by weight of the base bitumen (9).

Previous experimental researches have explored and deeply investigated the adequate amount to be added in order to achieve the satisfactory and expected improvements (10). In other words, it's decisive to select the right dosage that can sufficiently affect the rheological response of neat bitumen. The hard role played by that choice deals with the purpose to bridge the gap between restricting base materials' costs and limiting excessive viscosity of blends at mixing temperatures, since mixing operations have influence on the rheological behaviour.

Thus, the main experimental factor kept variable in our case-study was the mixing process.

Twofold percentage was finally chosen for each nano-additive material, to perform a further investigation of the dosage influence on the rheological properties. Percentages by weight of the base bitumen were fixed at 0.5% and 1%, respectively, for carbon nanotubes and at 3% and 6% for nanoclays (8).

It was found that higher *CNTs* content has consequences on nanoparticles agglomeration level and produces troubles in mixing phase, due to the very high viscosity.

2.2 Mixing Protocols

In order to produce reinforced bituminous binders, four different mixing protocols were adopted. The twenty blends were prepared within the department laboratory, sited on the ground floor of the Politecnico main building, by means of a technique consisting in two separate steps: a simple shear mixing phase followed by sonication.

The selected procedures were chosen according to a previously developed protocol, matured after many trials and accurate studies, according to the main aim to achieve uniformity in dispersion and fine separation of nanomaterials (5), (4).

The mixing phase plays a role of maximum importance, as the reader can easily understand, since the nano-additive dispersion degree has a direct influence on the expected results, in terms of rheological and mechanical properties.

The number of twenty blends comes out from the combination of the single base bitumen and the two nano-additive types, added in a twofold percentage and prepared following four mixing protocols.

2.3 First Phase: Shear mixing

To accomplish the first blends preparation phase, two shear mixing equipment was used, whose main differential parameter is given by the maximum speed the device can bear.

2.4 Low-Shear Mixing

The low-shear mixing device employed for Protocols A and B is an Heidolph product, model RZR-2041[®], and shows the following technical specifications (11): it has two gear speeds, whose ranges are 40 to 400 rpm for the first gear and 200 to 2000 rpm for the second one.



Technical Specifications

- Motor power: 37 W
- Speed range: 40-2000 rpm range 1: 40 – 400 rpm
range 2: 200 – 2000 rpm
- Maximum torque: 520 N·cm
- Maximum viscosity: 100000 mPa·s
- Dimensions: 82 *211*176 mm

Figure 4 Heidolph RZR-2041

To perform the first step of the mixing protocol, the spindle in the picture was employed, realized according to Silverson-head model.

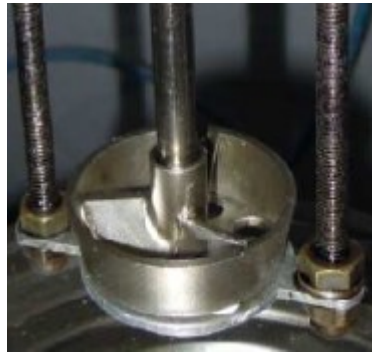


Figure 5 Silverson-type head

2.4.1 Protocol

Once the base bitumen was melted inside the oven, approximately 450 g of binder was poured in twenty metal cans, labelled with the appropriate acronym, in order to unequivocally recognize each blend.

By means of the protection measure provided by the laboratory fume hood, which is a ventilation device designed to limit exposure to hazardous or toxic fumes and dusts, we manually mixed the single base bitumen and the nano-additive, performing a first basic incorporation. Both nanoclays and carbon nanotubes are a powder, so they're high volatile.

Hence, the can was placed on a heater at 150°C to keep the viscosity within acceptable yielding ranges.

Once we've fulfilled that preliminary steps, low-shear mixing procedure took place following a thorough procedure. The tin cans were singularly soaked into a steaming silicon oil, heated at about 150°C, with a tolerance in temperature floating of $\pm 5^\circ\text{C}$, in order to keep blend's temperature as constant as possible, since a rapid changing would burn the can, weakening its functionality. There are a number of large cross-sectional studies which suggest such temperature's choice as valid, nevertheless slight variations wouldn't modify materials properties.

Then, the mixing head was immersed until the distance with the can's bottom was about 20 mm, letting a complete and effortless rotation, and the speed set at 1500 rpm. According to previous experimental researches, that speed has successfully utilised in several cases; the mixing procedure lasted 90 minutes.

The adopted protocol consists of the following steps, described in details (5):

- Place the tin can, filled with about 400-450 g of neat bitumen, into the oven at 150°C, until the bitumen will become quite fluid. It could take a

variable time from 60 to 120 minutes, depending on many environmental factors, like the base bitumen or the oven warmup;

- Assemble the Silverson-type head to the low-shear mixing;
- Turn on the heater placed under the silicon oil container, increasing the temperature until 160°C. We reserved a 10 degree tolerance, taking into account every possible heat loss. We recommend to let the temperature increase gradually to prevent oil from burning;
- Arrange the can on a heater at 160°C inside the fume hood;
- Manually incorporate and mix the nano-additive, previously weighted on the high precision scale, into the base bitumen by means of a paddle. This operation must take place in the fume hood, to prevent dust inhalation;
- Soak the can in the silicon oil and lower the shaft until around 20-30 mm to the bottom;
- Gradually increase rotation speed to 1550 rpm;
- Keep the speed constant for 90 minutes;
- Once the time has arrested, turn off the mixing device and the silicon oil;
- Lift carefully the shaft, to avoid squirts;
- Remove the can and dry off oil's drops along the metal's surface.



Figure 6 Low-Shear Mixing

2.5 High-Shear Mixing (Silverson)

The high-shear mixing equipment was adopted in protocols C and D. Specifically, we used a Silverson L5M-A model, realized by the homonym company.

The advantages of Silverson's high shear rotor laboratory mixer over simple conventional stirrers or agitators stem take the first step from the multistage shear

mixing action, since materials have been drawn through the specially designed Silverson working-head (12).



Technical Specifications

- Motor power: 750 W
- Nominal maximum speed: 8000 rpm (6000 rpm under full load)
- Capacity: up to 12 liters.
- Dimensions: length 290mm, width 57mm

Figure 7 Silverson L5M-A

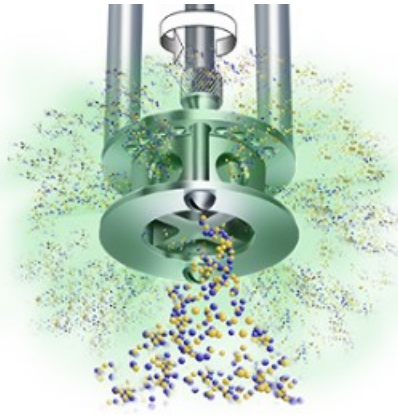
2.5.1 Silverson work head functioning

Now, we're going to describe the four-stage processing technique employed by Silverson technology, which make working-head functioning unique for its effectiveness (12):



-First stage: high speed rotation of the rotor blade exerts a powerful aspiration, pushing liquid or solid material in the container upwards from the bottom of the vessel toward the centre of the working head.

-Second stage: centrifugal force drives materials towards the periphery of the work head, then they're subjected to a milling action in the clearance between the ends of the rotor blades and the inner side of the stator.



-Third stage: intense hydraulic shear forces the material, out through the perforations in the stator to circulate into the main body of the mix

-Fourth stage: the material is expelled from the head and radially projected at high speed towards the sides of the mixing vessel.

Thus, the effect of the radial expulsion and suction into the head is to arrange a circulation pattern that minimizes aeration caused by the disturbance of the liquid's surface.

2.5.2 Protocol

The adopted protocol is no longer different to that of the low-shear mixing procedure and consists of several steps described in details:

- Place the tin can, filled with about 400-450 g of neat bitumen, into the oven at 150°C, until the bitumen becomes quite fluid. It could take a variable time from 60 to 120 minutes, depending on many environmental factors, like the base bitumen or the oven warm-up;
- Fasten the mixing unit with the two knurled nuts and the coupling pin, which must be kept fixed using the coupling sleeve. The coupling pin plays a role of preeminent importance to make it an integral system with the shaft and rotor;

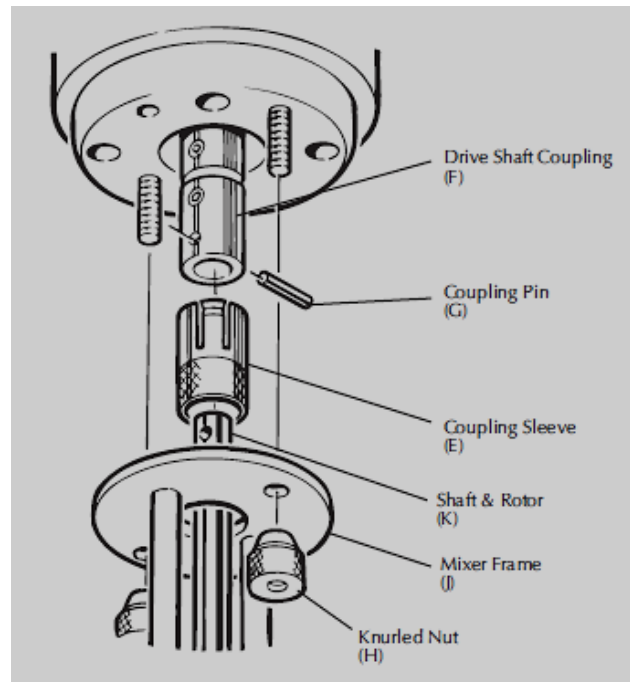


Figure 8 Standard Mixing Assembly

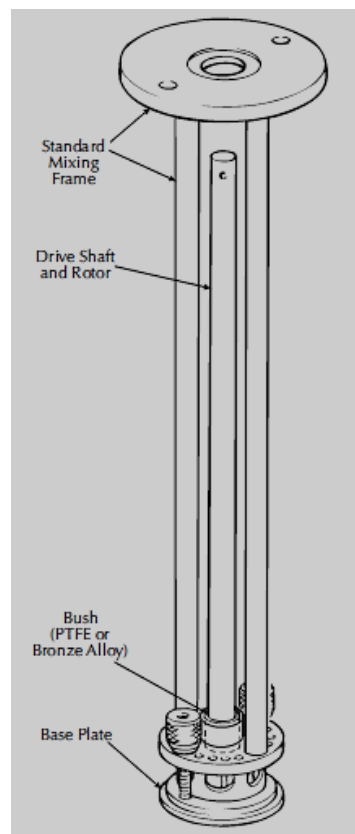


Figure 9 Standard Mixing Assembly - 2

- Choose the head type (the company provided us four different heads, selected on the basis of the expected function and the involved materials). In our peculiar case, we adopted a Vertical Slotted Disintegrating Head, usually suitable to fibrous or elastic materials such as rubbers and

polymers, and a Square Hole High Shear Screen, ideal for fine colloidal suspensions and nano-additives. They were alternatively employed in the protocols.



Figure 10 Vertical Slotted Disintegrating Head



Figure 11 Square Hole High Shear Screen

- Connect the chosen head to the mixing unit on the upper part and to the base plate on the lower side, by means of the knurled nuts;
- Place the can on the base assembly, which works as a platform for mixing containers, equipped with a removable non-slip mat with a groove surface, useful to prevent the can from slipping;

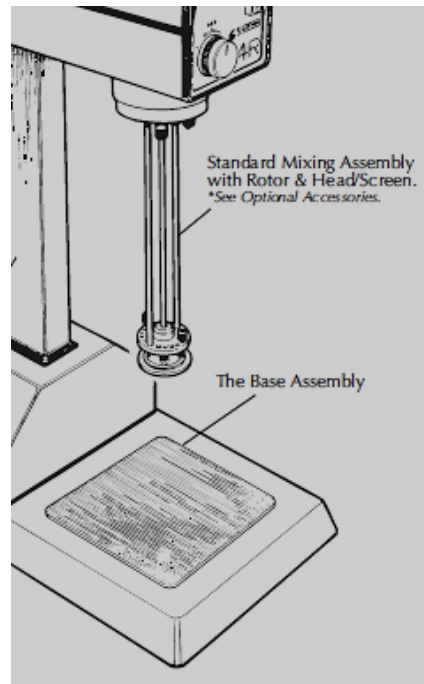


Figure 12 Base assembly

- Turn on the Silverson machine and lower the drive shaft, until it achieves around 20-30 mm from the can's bottom;
- The position of the stator within the vessel can affect the mixing performance of the machine. The recommended initial position is slightly off-centre, approximately 3-4 cm off the bottom of the vessel.

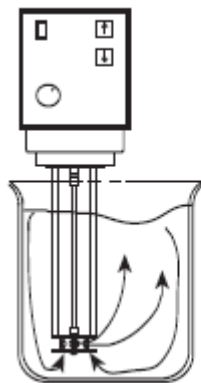


Figure 13 Correct rotor position

-A centrally positioned stator may cause aeration or splashing in the mixture. Moving the head out of the centre produces a smaller vortex enabling the mixer to operate at higher speeds without splashing or spillage.

- Connect to power supply and turn the power on by operating the switch located at the rear of the base assembly. The mixer frame must always be immersed in the fluid, which must cover the entire working-head and the bearing bushing before the machine is switched on. If this precaution is not taken overheating of the shaft will result.

- Increase the speed until 5000 rpm and check the amperage is kept under 5 Amp;
- In some cases, according to environmental conditions, a cooling system could be required, to avoid a sudden blend's temperature increasing due to the high speed. The more is the external temperature, the more the bituminous binder would overheat. Whenever it occurs, arrange a beaker under the sample, in order to fill it with cold water. Check the bitumen's temperature every 5 to 10 minutes;
- Keep the speed constant for 30 minutes
- Lift carefully the drive shaft, to avoid squirts;
- Remove the can and dry off eventual drops along the metal's surface;
- Clean thoroughly each machine's component.

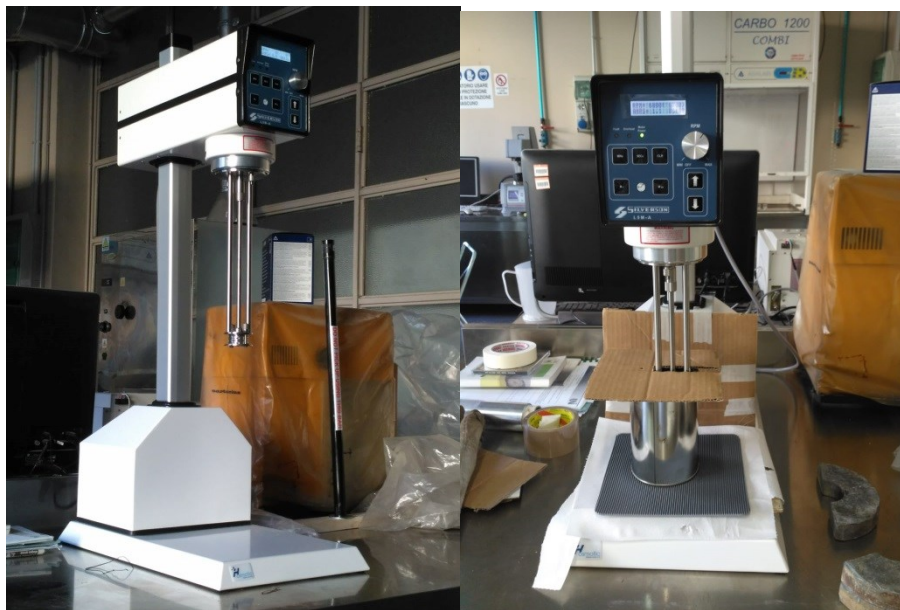


Figure 14 High-Shear Mixing procedure

Throughout high-shear mixing phase, some troubles came out, due to occasionally increase of specimen temperature, as a result of high speed achieved and depending on environmental conditions. We checked temperature conditions, cooling the container's surface by means of a cold fluid, to maintain as much as possible a constant temperature value. Sample overheating must be avoided to prevent early aging of the sample.

2.6 Sonication

Sonication represents the second phase of the blend's preparation protocol. While the low-shear and the high-shear mixing procedures are employed respectively in two protocols each, the sonication process constitutes a fix part for all of them (8).

The ultrasonic device placed in the laboratory is a UP200S[®] from the Heilscher GmbH company (13). It's well suited for all general ultrasonic applications in

small and medium scale. The applications are multiples and include operations as homogenization, disintegration, emulsification, cell disruption, degassing or sono-chemistry.

With the main purpose to maximize interactions between nano-particles and bitumen, encouraging outcomes have been obtained by means of ultrasound energy.



Technical Specifications

-Power: 200 W

-Frequency: 24 Hz

-Cylindrical titanium sonotrode
diameter: 7 mm

-Sample volumes: from 0.1 to 2000mL

Figure 15 ultrasonic device UP200S

Practically, ultrasounds are consequently generated, propagating within the material in the form of compression attenuated waves. As a consequence, separation of individual nanoparticles from agglomerates is promoted, leading to a more homogeneous dispersion degree (14).

Due to local energy provided by sonication, nanoparticles break free from the restraining forces of agglomerates.

The chosen sonication parameters, in order to achieve an adequate dispersion degree of nano-particles soaked into the bituminous matrix, were established on the basis of preliminary tests led in the past about the evaluation of sonication running time and wave amplitude influence on nano-reinforced blends (15). The adopted parameters were fixed: sonication running time of 60 minutes, as well selected amplitudes corresponding to 50% and 90% of the maximum value that can be attained by the equipment.

This choice was made in compliance with experimental works performed in the past, trying to maximise the overall efficiency of the system and to limit as much as possible any wearing phenomena, which may occur at the bottom of the

sonotrode in case of high viscosity of the blends. This case is quite realistic for CNTs blends, characterized by very high viscosity.

2.6.1 Protocol

The adopted protocol can be described as follows, (4), (5):

- First of all, place the tin can, filled with about 400-450 g of neat bitumen, already exposed to the first mixing phase, into the oven at 150°C, until the bitumen will become quite fluid. It could take a variable time from 60 to 120 minutes, depending on many environmental factors, like the base bitumen or the oven warmup;
- The two mixing phases may also be performed sequentially, in such case we can skip the previous step;
- Arrange a mechanical stirrer and put an heater on it, set at 150 °C;
- Place the can on the heater and keep the distance with the ultrasonic device;
- Lower the sonotrode system until around 40 mm to the bottom and thorough place the tip in a position as much central as possible;
- Activate the mechanical stirrer, set on speed 2. It will move at the same time the heater and the can too.
- Check the control knob of the amplitude level is set on the 20% value and choose the weave mode (0.5 means alternate, 1 means continue)
- Then, switch on the ultrasonic device and increase the amplitude to the established value (in our case it will alternatively be 50% or 90%)
- Keep it constant for 60 minutes;
- Switch off the device and the mechanical stirrer.

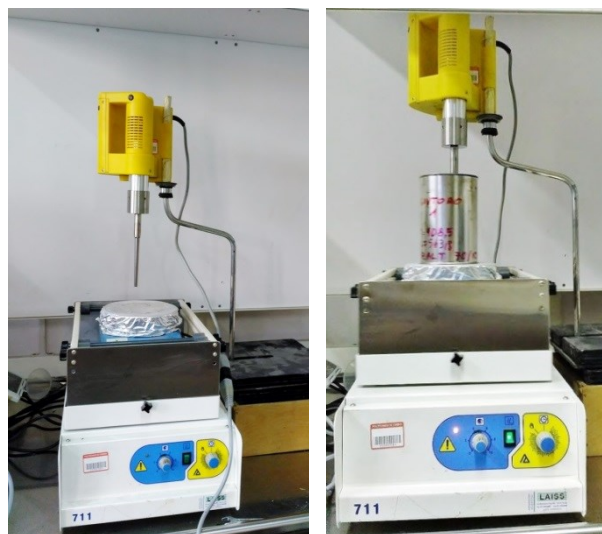


Figure 16 Sonication procedure

2.7 The four protocols (A/B/C/D)

In conclusion, four different mixing protocols were adopted, based on the use of the over mentioned equipment. Each protocol consisted of two steps (the shear mixing and the sonication phase), described in details as follows:

- PROTOCOL A:

Low-shear mixing phase	
<i>T_{bit}</i>	150°C
<i>Speed</i>	1550 rpm
<i>Running time</i>	90 min
Sonication phase	
<i>T_{bit}</i>	150°C
<i>Frequency</i>	24 Hz
<i>Running time</i>	60 min
<i>Wave amplitude</i>	90% (158μm)
<i>Wave mode</i>	Continue

Figure 17 Protocol A

- PROTOCOL B:

Low-shear mixing phase	
<i>T_{bit}</i>	150°C
<i>Speed</i>	1550 rpm
<i>Running time</i>	90 min
Sonication phase	
<i>T_{bit}</i>	150°C
<i>Frequency</i>	24 Hz
<i>Running time</i>	60 min
<i>Wave amplitude</i>	50% (88μm)
<i>Wave mode</i>	Continue

Figure 18 Protocol B

The noteworthy difference between the first two protocols regards the wave amplitude, chosen, as we previously said, on the basis of researches conducted in the past, trying to maximize the overall efficiency of the system.

- PROTOCOL C:

High-shear mixing phase (Silverson)	
<i>T_{bit}</i>	150°C
<i>Speed</i>	5000 rpm
<i>Running time</i>	30 min
<i>Head type</i>	Vertical Slotted Disintegrating
Sonication phase	
<i>T_{bit}</i>	150°C

<i>Frequency</i>	24 Hz
<i>Running time</i>	60 min
<i>Wave amplitude</i>	90% (158 μ m)
<i>Wave mode</i>	Continue

Figure 19 Protocol C

- PROTOCOL D:

High-shear mixing phase (Silverson)	
<i>T_{bit}</i>	150°C
<i>Speed</i>	5000 rpm
<i>Running time</i>	30 min
<i>Head type</i>	Square Hole High Shear Screen
Sonication phase	
<i>T_{bit}</i>	150°C
<i>Frequency</i>	24 Hz
<i>Running time</i>	60 min
<i>Wave amplitude</i>	90% (158 μ m)
<i>Wave mode</i>	Continue

Figure 20 Protocol D

Two different Silverson disintegrating heads were selected between the four provided by the company, in addition to the machine. We want to detect if such choice may lead to different nanoparticles dispersion degree or any other rheological changing evidence, in order to choose, whether possible, the best mixing protocol.

3.Acronyms

In order to make the composition as much readable as possible, we're going to introduce the acronyms utilized to specifically classify each blend.

Each acronym is made of three sections: the first letters are adduced to the material or the nano-additive type, then a number may be added according to the dosage percentage; finally, the last suffix specifies the followed mixing protocol. To better understand the classification system, each acronym will be widely described.

The abbreviation *NB* refers to the neat bitumen, lacking of any possible additive. The preeminent relevance covered by the neat asphalt binder has to do with its role of control sample.

The *NC* acronym is assigned to the nanoclay mixture, where the neat binder is combined with such nano-additive material. To help distinguish between the

twofold dosages, we'll add alternatively the percentage numbers, composing respectively *NC3* or *NC6*.

CNT indicates the Carbon nanotubes, *CNT.5* and *CNT1* are the peculiar percentages.

Once we've stated every acronym's meanings, we can illustrate the protocol identification system.

The four protocols previously exposed are summarized in the following way and added as a suffix at the end of each acronym identifying the material: on the basis of the variable parameter, number 90 is connected to Protocol A, number 50 to Protocol B, the V letter is associated to Protocol C and the Q letter to Protocol D.

Acronym	Material or nanoadditive type	Protocol
NB_90	Neat Bitumen	A
NB_50	Neat Bitumen	B
NBV	Neat Biumen	C
NBQ	Neat Biumen	D
NC3_90	Nanoclay 3% by weight	A
NC3_50	Nanoclay 3% by weight	B
NC3V	Nanoclay 3% by weight	C
NC3Q	Nanoclay 3% by weight	D
NC6_90	Nanoclay 6% by weight	A
NC6_50	Nanoclay 6% by weight	B
NC6V	Nanoclay 6% by weight	C
NC6Q	Nanoclay 6% by weight	D
CNT.5_90	Carbon nanotubes 0.5% by weight	A
CNT.5_50	Carbon nanotubes 0.5% by weight	B
CNT.5V	Carbon nanotubes 0.5% by weight	C
CNT.5Q	Carbon nanotubes 0.5% by weight	D
CNT1_90	Carbon nanotubes 1% by weight	A
CNT1_50	Carbon nanotubes 1% by weight	B
CNT1V	Carbon nanotubes 1% by weight	C
CNT1Q	Carbon nanotubes 1% by weight	D

Table 3 Summary of the names

The abovementioned acronyms will be used along the entire dissertation.

Chapter 2

Rheological analysis and results

Experimental tests

Within the process of measuring and determining bitumen's properties, primary emphasis seems to have the characterization of rheological behaviour.

Rheology is a complex and interdisciplinary science, which investigate the internal response of materials to stresses (16).

The world's meaning, as often happens, can help us to better get its topic. It has origin from Greek language, deriving from “ῥέω”, whose translation is “to flow” and “-λογία”, meaning “word, science”, and, thus, literally means “the study of the flow”.

The rheology science could appear, at a first sight, a modern knowledge, since it was mentioned for the first time in 1928 by Eugene C. Bingham, a pioneer in rheology's theory and practice, and well-known for the famous Bingham plastic fluid, named after it; nevertheless science's name is the only modern feature, while the theoretical base has an ancient history.

Rheology is, hence, the science of flow properties and the deformation of materials in terms of materials' elasticity and viscosity, whatever phase they are, i.e. liquid, melted or solid form. Since the stiffness of bitumen is time-dependent, which means that bitumen flows with time, it has been classified as rheological material.

Literature review

The determination of bitumen's rheological properties was conducted through several tests. Such properties are generally determined by means of a dynamic mechanical analysis, thanks to the dynamic shear rheometer (DSR) machine. Tests performed with DSR technology are usually led within the linear

viscoelastic response region, allowing to determine the viscous and elastic characterization over a wide range of temperatures and frequencies.

In the linear viscoelastic response region, the existing correlation between stresses and strains is just time-dependent, while the magnitude of the stress has no longer influence.

Before the explanation of the tests we performed to characterize the samples from a rheological point of view, some theoretical definition, explaining the physical meaning of the main variables, can guide the reader through the essay.

-The complex shear modulus G^* can be expressed as the ratio between the peak to peak shear stress τ and the peak to peak shear strain γ , both values are taken in absolute value. Since we operate within the viscoelastic domain, the complex modulus is independent from shear stress or strain. In other words, the complex shear modulus gives an estimation of the stiffness or the resistance to deformation under loading stress.

$$G^* = \frac{\tau_0}{\gamma_0}$$

The complex modulus is so-called because it's represented like a complex number:

$$G^* = G' + iG''$$

-The phase angle δ is expressed in radiant and has a twofold definition whether the test is led in controlled-stress or controlled-strain mode. According to the first case, it represents the angle between the applied stress and the resultant strain; while in the second case it's the angle between the sinusoidal applied strain and the resultant sinusoidal stress.

-Another variable of great importance is the storage shear modulus G' , which basically represents the complex shear modulus multiplied by the cosine of the phase angle, now expressed in degrees. From a physical point of view, it's a measure of the energy stored during a loading cycle.

$$G' = G^* \cos \delta$$

In conclusion, the complex shear modulus and the phase angle allows resistance estimation under shear deformation within the linear viscoelastic range (17).

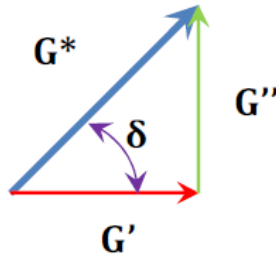
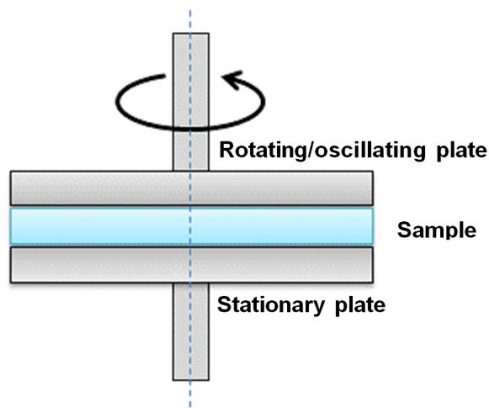


Figure 21 Complex shear modulus and phase angle - Vector representation

Performed tests

The employed equipment to perform rheological tests on binder compounds was a Physica MCR 301 and 302 DSR from Anton Paar Inc., which works as an air-bearing stress controlled machine, provided by a permanent magnet synchronous drive (18).

Such device allows complex shear modulus and phase angle measurement together with many other variables, in order to characterize rheological behaviour of the bitumen specimen, using a parallel plate geometry.



$$\tau = (2M)/(\pi R^3)$$

$$\gamma = \frac{\varphi \cdot R}{h}$$

Figure 22 DSR plate system

A parallel plate geometry was employed to test the samples, that is literally sandwiched between two parallel plates and then subjected to oscillatory shear stress, which substantially means that the strain varies in amplitude starting from zero in a sinusoidal manner.

Both a 8-mm and 25-mm plate systems, set with respectively a 1-mm and a 2-mm plates gap, were utilized.



Figure 23 DSR 8-mm and 25-mm plates

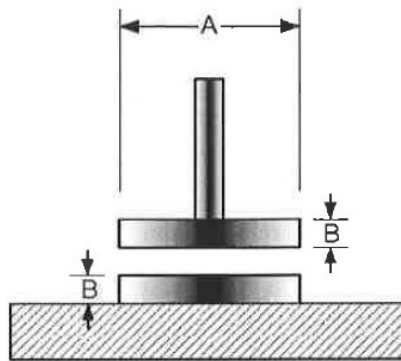


Figure 24 Plate dimensions

Dimension	8-mm Nominal	25-mm Nominal
A	$8 \pm 0.02 \text{ mm}$	$25 \pm 0.05 \text{ mm}$
B	$\geq 1.5 \text{ mm}$	$\geq 1.5 \text{ mm}$

Table 4 Plate dimensions

During the test, the upper plate is mobile and oscillates at pre-selected frequencies, working in a strain control mode (applying rotational deformation amplitudes) or in a stress control mode (applying torque amplitudes). The strain amplitude is selected within the linear viscoelastic region (19).

Oscillatory loading frequencies have a wide range, since they can vary from 1 to 100 rad/s by means of a sinusoidal wave. G^* and δ are automatically obtained connecting the device to a computer software supplied by the equipment provider.



Figure 25 DSR MCR 302 from Anton Paar

Technical specifications:

-Minimum torque:200mNm

-Torque resolution:0.1mNm

-Minimum angular frequency: 10^{-9} rad/s

-Max. temperature range: -160 to +1000

3.1 Frequency Sweep Test

A frequency sweep is a particularly useful tool, since it enables the sample viscoelastic properties to be determined as a function of timescale. Several mechanical parameters can be extrapolated, such as the Storage Modulus (G') and the Viscous Modulus (G''). The storage modulus (G') can be used as a measure of the elastic component of the sample, likewise the loss modulus measures the sample viscous component.

To surely conduct frequency sweep within the linear viscoelastic region, we selected strains values from previous experiments performed on nano-reinforced blends.

3.2 Sample preparation

We performed frequency sweep tests on the twenty blends, both with the 8-mm and 25-mm DSR plates.

Sample preparation procedure was quite similar in both cases; just slight differences were adopted during the pouring phase.

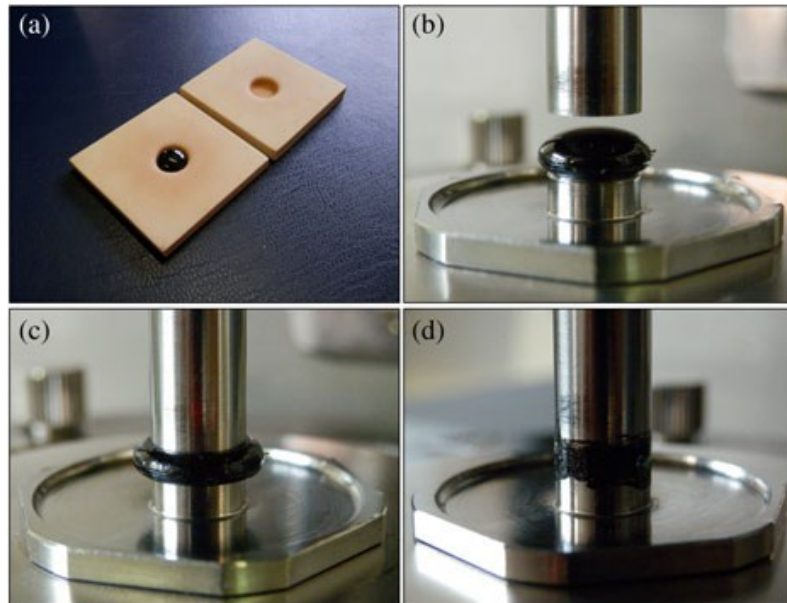


Figure 26 8-mm plate sample preparation phases (a-d)

To avoid as much as possible nano-additive sedimentation and aggregate formation on the bottom of the can, once the blend has cooled, we decided to re-

heat the specimen inside the oven, before testing it, and manually mix the blend forcefully. This method should ensure a better homogeneity, either on the surface and on the bottom, since the material amount needed in the test is very little.

Each DSR is equipped with an environmental chamber, which basically is a temperature controller, during heating or cooling phases, studied to keep a constant specimen environmental. Most of all, this component doesn't affect asphalt binder properties. Environmental chamber is also employed to control the specimen temperature, to avoid thermal gradients throughout the test.

3.3 RTFOT

According to AASHTO T240, we performed the Rolling Thin-Film Oven (RTFO) Test on the twenty samples to simulate short-term aging.

Practically, a fixed amount of bitumen is exposed to high temperatures to simulate manufacturing and placement aging. The test allows the measurement of heat and air effects on a moving film of asphalt binder. In addition, the aged bitumen can be employed to further rheological tests, such as the linear amplitude sweep test (LAS).

Basically, RTFO procedure consists in taking unaged bitumen samples into hollow glass bottles with a cylindrical shape and in placing them inside a rotating carriage sited inside the oven. The carriage rotates along the running time of the test, while 163°C temperature is sufficient to age the samples for 85 minutes. At the end, samples can be subjected to Pressure Aging Vessel (PAV) test to also simulate long-term aging, occurred during in-service life.

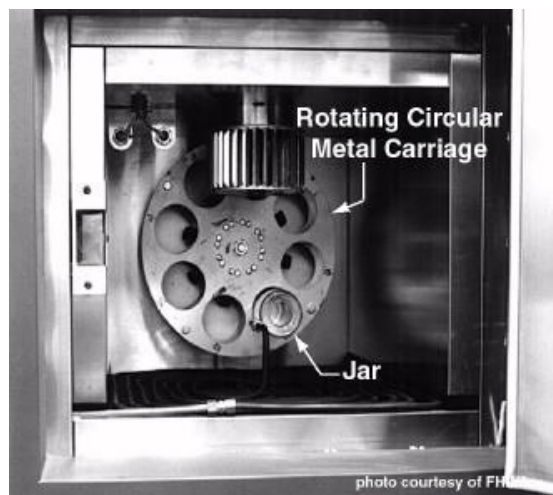


Figure 27 RTFOT device

The residue from the test is often used to determine bitumen's conditions after aging. The overall idea behind the procedure followed in the test is to take a realistic picture of asphalt binder's status after pavement construction.

The test also allows the measurement of water content and mass changes resulting from oxidation. The loss of smaller molecules, the “volatiles”, increases asphalt’s viscosity. In effect, during the manufacturing and placement processes asphalts lose volatiles. The high placement temperature ages it by driving off a substantial percentage of volatiles.

Performing rheological tests on aged samples allows the determination of the aging status and performance parameters, as fatigue and rut resistance.

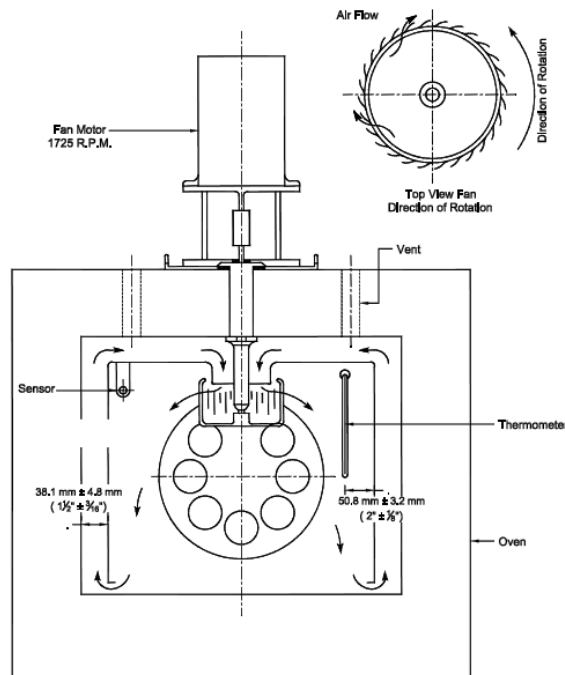


Figure 28 Air flow front view

Unaged bitumen samples are placed one by one in a cylindrical glass bottle, which is then placed in a carousel inside a specially designed oven.



Figure 29 RTFO glass bottles

The oven is pre-heated until it reaches a temperature of 163°C. Meanwhile, bitumen is poured in the bottles at quite high temperature, in order to let the asphalt binder easily flow, and then placed on a bottle rack to keep the specimen horizontal. Once the test started, the carousel was rotated at 15 RPM for 85

minutes, the running time of the test. The carousel rotation continuously exposes asphalt binder to heat and air flow and, due to rotation movement, it slowly mixes each sample. Once the test finishes, bottles are poured into the cans with the help of a scraper.



Figure 30 RTFO equipment

3.3.1 RTFO Test - Protocol

Test protocol illustrated by the T240 standard was thoroughly followed for all the specimens, and consisted of the following steps (20).

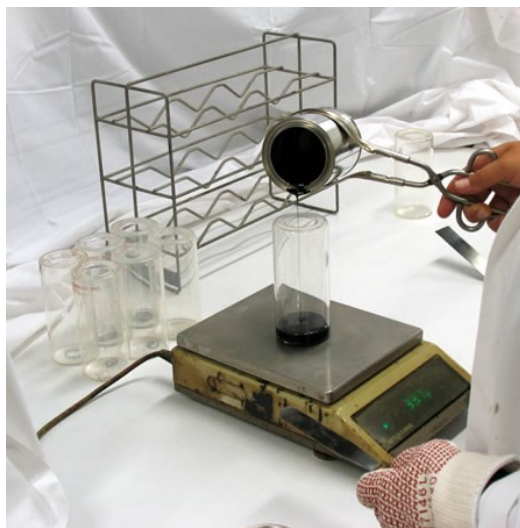


Figure 31 Pouring phase

- Heat the asphalt binder sample into the oven until it is fluid to pour;

- With the help of a scale, pour 35 g of material into each glass bottle and immediately turn the bottles on their side without rotating or twisting them;

- Place each jar on the bottle rack until they get cold for about 60 to 180 min, depending on the starting temperature;

- Put the bottles one by one in the RTFO

oven carousel (the maximum number of samples that can be tested at the same

time is 8), then close the door, and set carousel rotation at 15 RPM for 85 minutes. During this time, check whether the oven temperature and the airflow into the bottles at 4000 ml/min varies.

Once the time expired, remove the bottles from the carousel and transfer residue to a specific can. During the material removing phase, try to pour as much material as possible from each jar, also scraping the sides of the bottle by means

of a scraper. At least 90 percent of the asphalt binder should be removed from the bottle, especially whether weight loss measurement is expected.

The total running time of the test isn't fixed and depends on how much time it takes to reach the selected oven temperature and on the operator's experience.

3.4 Linear Amplitude Sweep (LAS) Test

In general, the Linear Amplitude Sweep test (LAS) is a powerful test which allows to evaluate asphalt binder resistance to fatigue damage (21). Basically, it consists in an oscillatory strain sweep test that provokes damages on the bitumen, following a loading scheme which linearly increases.

LAS test is a two-step procedure:

- as a first phase, frequency sweep test is performed, letting us to collect data about undamaged material properties and to evaluate bitumen rheological characteristics.
- the second step consists in applying a linear amplitude sweep test to characterize damage properties of the binder.

Practically, the sample to be tested is prepared according to the standard T 315 (DSR) using the 8-mm parallel plate geometry with a 2-mm gap setting. The sample is then tested using a series of oscillatory load cycles which increases linearly at a constant frequency to cause accelerated fatigue damage. The continuum damage approach allows fatigue resistance calculation thanks to rheological properties and amplitude sweep data.

Each test was performed in compliance with the TP 101-14 standard. Asphalt binder was previously aged following T 240 (RTFOT) procedure, according to the protocol described in the previous paragraph.

The first-step frequency sweep test is led within a frequency range of 0.2 to 30 Hz, at a strain of 0.1%. In order to perform the damage analysis, we can capture information regarding undamaged material properties, which are englobed in the parameter α . Thus, frequency sweep test allows α estimation, representative of the asphalt binder fatigue properties. The test is performed at room temperature (we set 25°C, since our bituminous binder is quite stiff) and applies oscillatory shear loading at constant amplitude over a range of loading frequencies.

The amplitude sweep test was performed at 10 Hz and the frequency kept constant. A linear load is applied from zero to 30% over 3100 cycles of loading. One replicate was averagely run for each binder, but in some cases, once the

results have been analysed, samples were tested again, whenever inconsistencies during the test occurred.

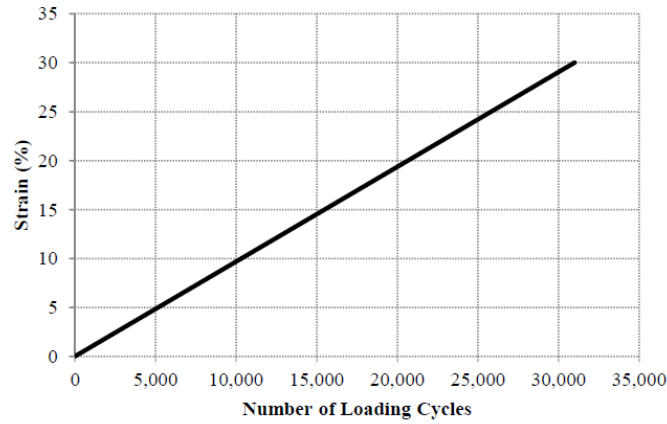


Figure 32 LAS - Loading scheme

LAS analysis was performed in compliance with TP 101-14 and TP 101-16 standards, to detect the discrepancy between the two approaches.

In LAS test, failure is defined as 35% reduction in the initial modulus, as expressed with the following equation:

$$N_f = A(\gamma_{MAX})^B$$

where A and B are two constants estimated by means of the viscoelastic continuum damage (VECD) analysis, dependent on the material characteristics.

Black diagrams

Data from frequency sweep tests were employed to draw Black diagrams, plotting the measured complex modulus versus the phase angle.

Data from several sources have identified Black diagrams as an effective resource to identify anomalies in rheological data, caused by mistakes occurred for an inappropriate use of the DSR plates and device (16).

In other words, Black diagrams represent a very powerful method to detect the eventual occurrence of any inconsistency in rheological data, caused, for instance, by irregularities during the testing phase (8).

As a second advantage, they don't require any manipulation of rheological data, since they don't need any shifting to draw one curve from data measured at

different test temperatures. The theoretical explanation of such benefit can be found in the fact that phase angle is plotted against complex modulus regardless of test temperature.

Moreover, the graphical representation of rheological parameters allows to display into a single diagram data collected in a wide time-temperature range, providing an overall portrayal of the mechanical response. On the other hand, this entails that errors occurred in temperature measurement won't display into a Black diagram (22).

After Black diagrams construction, smooth curves are expected, since asphalt binder is tested within the linear region.

In our case-study, they allowed to identify mistaken trials, in order to re-test the involved specimens.

An overall view of the constructed curves is presented in Figure 17. Successively, the following graphs allow to deeply focus on each material singularly.

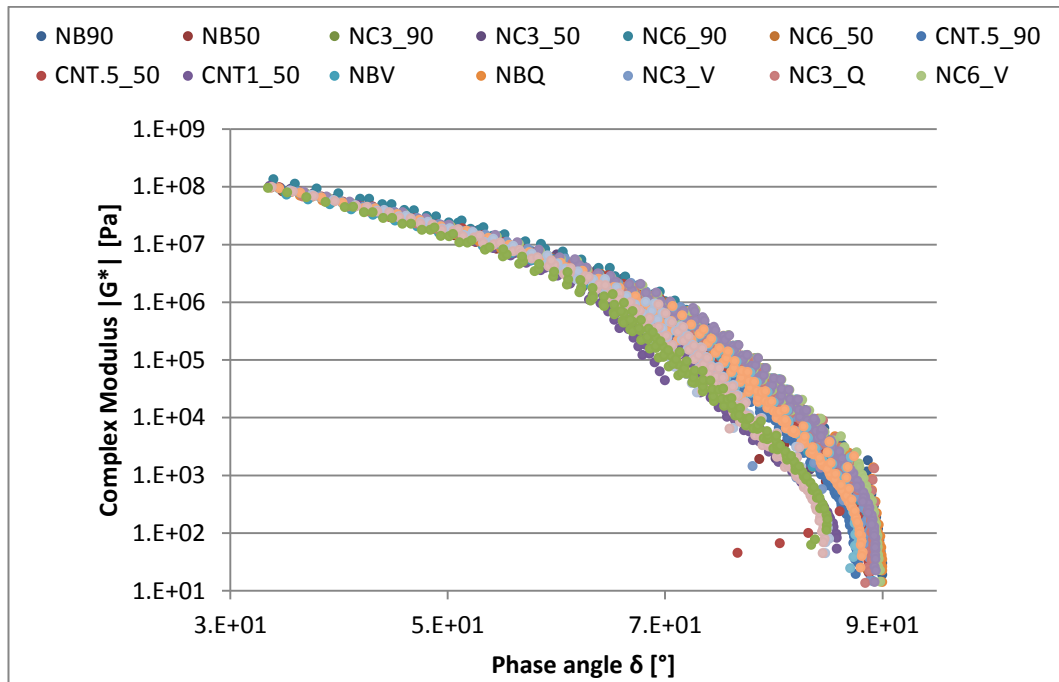


Figure 33 Black diagrams - All blends

Two comparative processes were established on the base of the chosen variable: at first, with the same material, protocols discrepancy will be assessed; then, in compliance with each protocol, we'll evaluate materials diversity.

3.1 Result's discussion: protocols comparison

In the first graph, we drew Black diagram's curves referred to the neat bitumen, our control sample, at different mixing protocols.

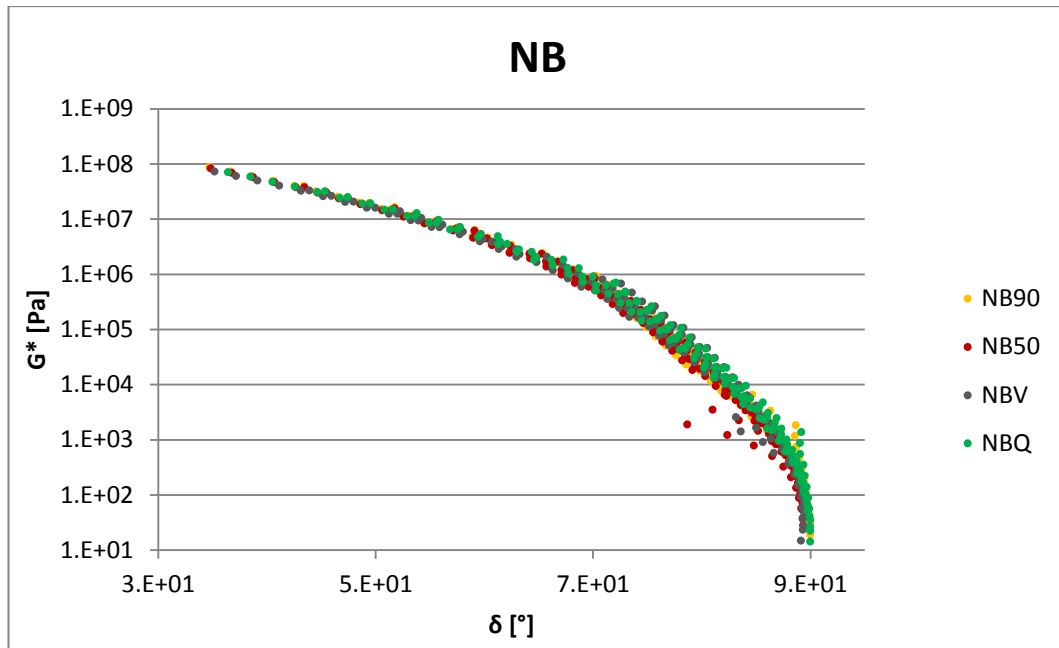


Figure 34 Black diagrams - Neat bitumen, Protocol comparison

As we would expect, the neat bitumen doesn't display any diversity, since no additives were added to the single base.

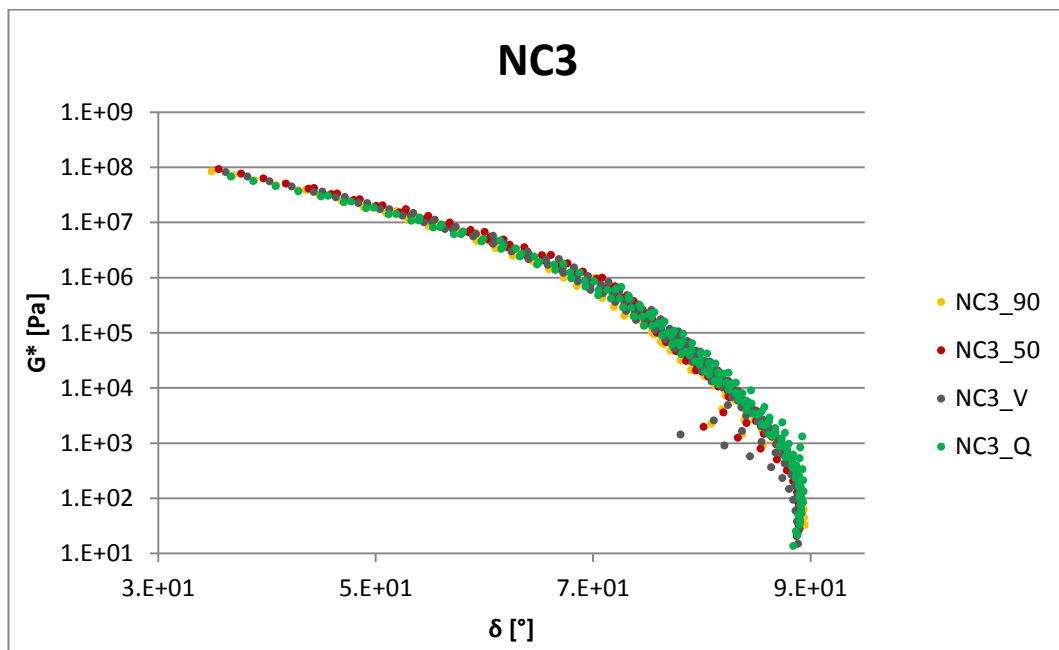


Figure 35 Black diagrams - Nanoclay 3% by weight , Protocol comparison

Closer inspection of the tables highlights the presence of outliers: such points don't reveal any surprise. All of them occur at the highest temperature (82°C) and the highest frequencies (over 10 to 100 hertz), as a proof that they can be neglected.

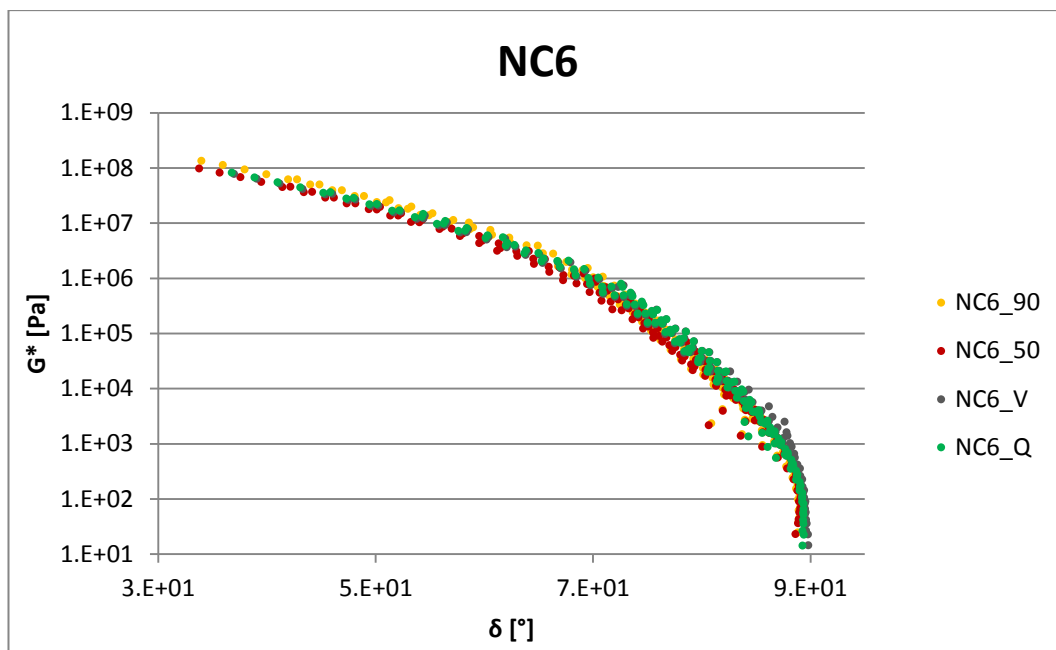


Figure 36 Black diagrams - Nanoclay 6% by weight , Protocol comparison

No evidence is detected about protocol's choice, due to very slight differences, which make hard the expression of undoubted preferences between them.

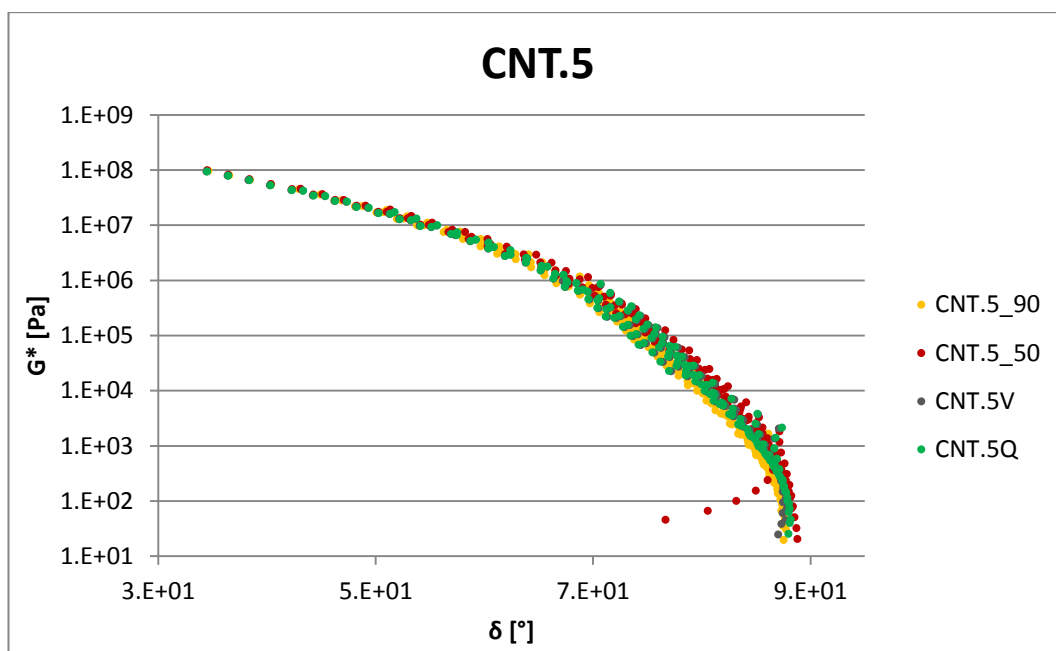


Figure 37 Black diagrams - Carbon nanotubes 0.5% by weight, Protocol comparison

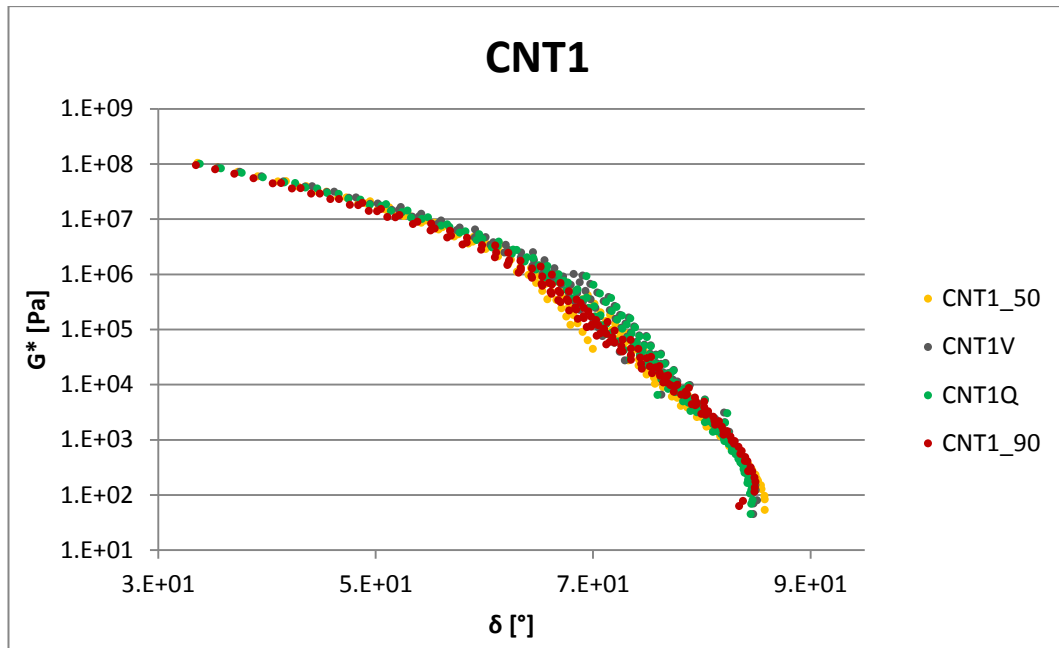


Figure 38 Black diagrams - Carbon nanotubes 1% by weight, Protocol comparison

Thanks to the easiness to identify anomalies in rheological data by means of black diagrams, we decided to test again the CNT1_90 specimen, whose trend was weird.

3.2 Result's discussion: materials comparison

In compliance to findings achieved by previous researches, it can be observed that curves show some sensitive to the additive type. CNT1 reveals the maximum discrepancy regardless of the adopted mixing protocol.

This is a remarkable result, since it implies lower phase angles and higher moduli; such evidence becomes more significant increasing the amount of reinforcement dosage.

From a practical point of view, it means an enhancement of stiffness and elasticity.

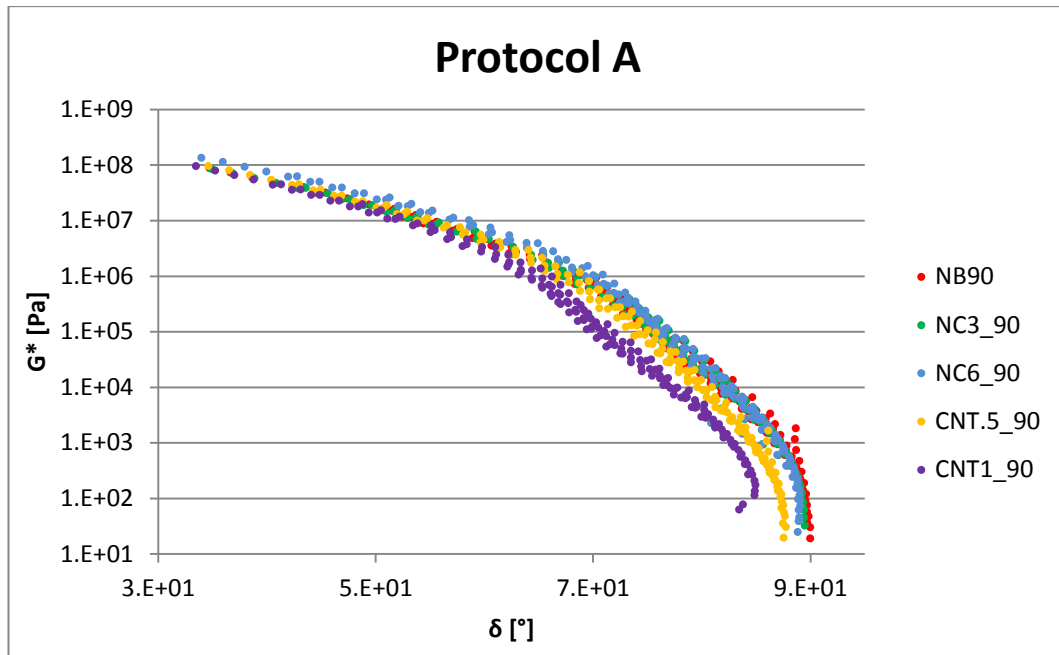


Figure 39 Black diagrams - Protocol A, material comparison

Previous experiments had also found none surprising evidence about NC curve's discrepancy.

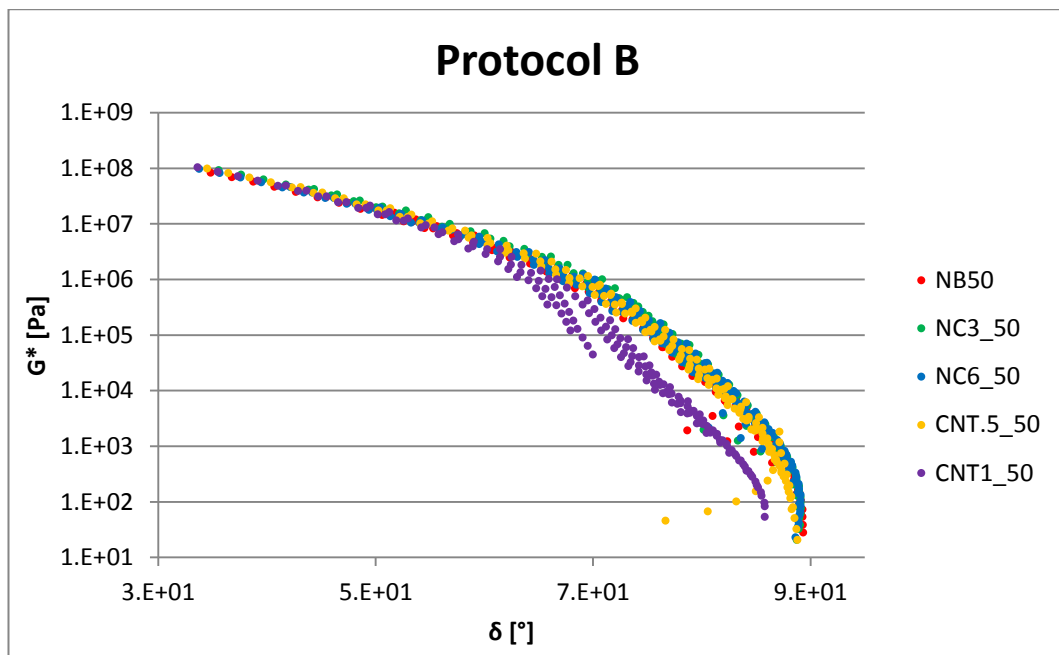


Figure 40 Black diagrams - Protocol B, material comparison

Collected data indicate as well that 0.5% CNT dosage causes a fairly low increase in elasticity, while the 1% addition produces some considerable improvement.

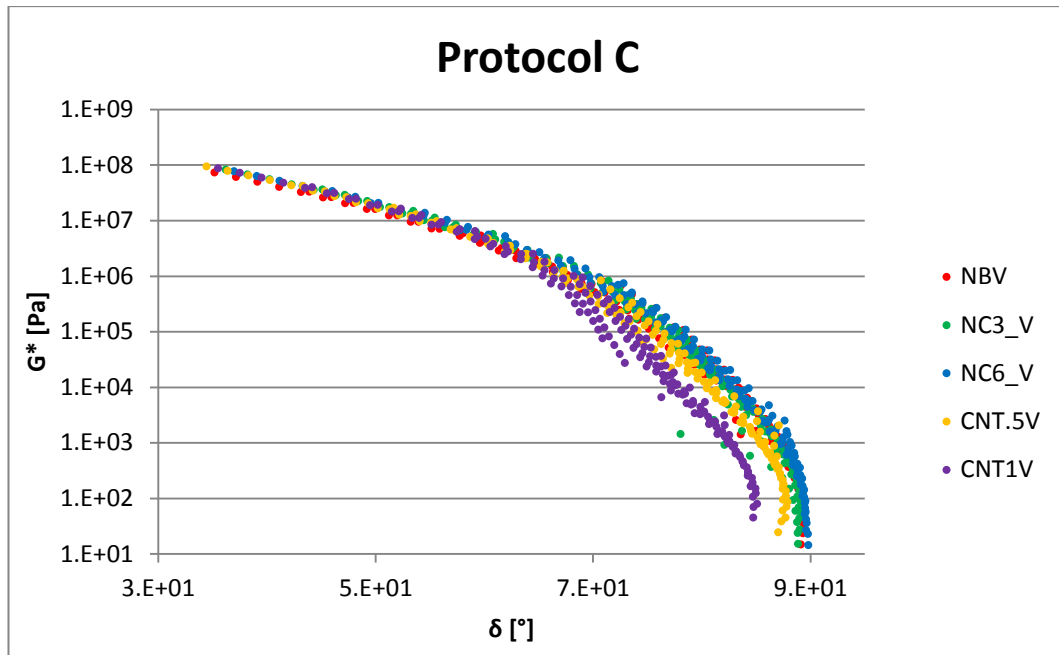


Figure 41 Black diagrams - Protocol C, material comparison

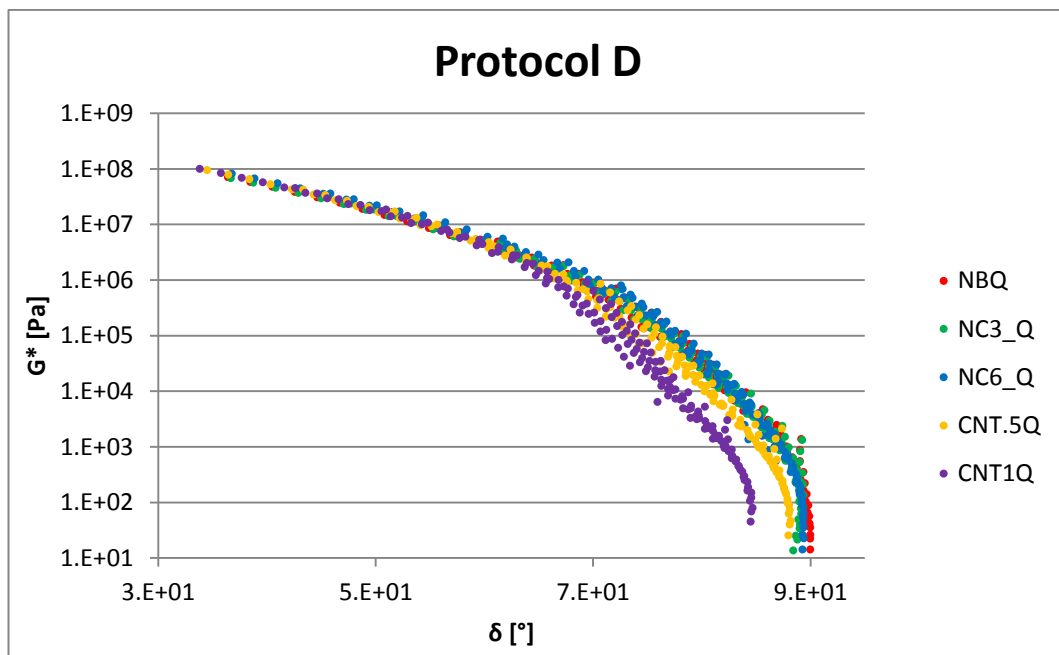


Figure 42 Black diagrams - Protocol D, material comparison

Black diagrams drawn for nanoclay-bitumen blends are very similar to those of the base bitumen, which indicates that, even if additives provoke changes in the mechanical response along specific time-temperature conditions, it doesn't affect rheological behaviour.

Thus, there's no evidence that nanoclays have a specific influence on curve's trends, since none of the detected differences were statistically significant.

Surprisingly, one of the most striking results is that CNT.5 doesn't show a distinctive deviation as we would expect, according to previous works, especially in Protocol B.

It is also remarkable that whenever stiffness and elasticity increases, this always implies the loss of thermo-rheological simplicity, as displayed by discontinuities in Black curves. Such discontinuous trend becomes significant for CNT-bitumen compounds, regardless of the protocol.

Master Curves

5.1 Literature review

A fundamental property employed in most of the mechanistic analyses of pavement response is the dynamic modulus as well as material input to design pavements.

Master curves may be constructed for asphalt binders, providing a relationship between the stiffness and the reduced frequency, over a wide range of temperatures and frequencies. Prediction of viscoelastic properties is allowed at any temperature (23).

Master curves' drawing process requires, first of all, complex modulus and phase angle measurement at multiple temperatures and frequencies, achieved by means of frequency sweep tests. Then, data are fitted thanks to a viscoelastic model.

Master curves play a preeminent role into the characterization of rheological properties of asphalt binders; as a demonstration, a considerable amount of literature has been published on such a concept and numerous researchers developed models whose validity is undoubted.

From a theoretical point of view, master curves are based on time-temperature superposition principle, used to determine temperature-dependent mechanical properties within the linear viscoelastic range and a unique reference temperature. This implies that master curves modelled at a reference temperature can be used as the prediction at various temperatures by applying computed shift factors (17).

The overall drawing schedule involves the following steps:

- determine frequency-dependent curves at several temperatures along a small frequency range
- compute shifting factors according to the chosen theoretical model

- use shifting factors to obtain modelled phase angle and complex modulus over the whole range of frequencies
- draw master curves

To clarify the role played by the over mentioned shift factors, they represent the amount of curve shifting required at each temperature to refer every point to a reference temperature.

In our case, shifting factors were determined by means of Williams-Landel-Ferry expression, which is typically used to describe the time/temperature behaviour of polymers in the glass-transition region.

The resulting master curve adjusted by means of shift factors provides a complete characterization of the stiffness-temperature response of a typical asphalt binder.

A typical master curve model that uses the complex shear modulus of asphalt binder to measure stiffness was developed by Christensen-Anderson. The complex shear modulus G^* and the phase angle δ are expressed by the following equations:

$$|G^*(\omega)| = G_g \left[1 + \left(\frac{\omega_c}{\omega} \right)^{\frac{\log 2}{R}} \right]^{-\left(\frac{R}{\log 2} \right)}$$

$$\delta(\omega) = \frac{90}{\left[1 + \left(\frac{\omega}{\omega_c} \right)^{\frac{\log 2}{R}} \right]}$$

where

$G^*(\omega)$ = Complex modulus at frequency ω

$\delta(\omega)$ = Phase angle at frequency ω

G_g = Glassy modulus

ω_c = Cross over frequency

ω = Reduced frequency

R = Rheological index

From a mathematical point of view, the linear viscoelastic CA method seems to be quite accurate and complete, and it allows to very quickly characterize bitumen viscoelastic behaviour.

Furthermore, each master curve variable assumes a specific physical meanings, letting us to estimate the rheological response along several conditions.

The crossover frequency, ω_c , is a measure of the overall hardness of the binder. As the crossover frequency decreases, the hardness increases. ω_c is function of the shift factor $\log a(T)$ and is equal to:

$$\omega_c = \omega^{\log a(T)}$$

The rheological index, R, is a shape factor indicating the rheological type. Graphically, it can be displayed as the difference between the $\log(G_g)$ and the $\log(G^*(\omega_c))$ at the crossover frequency. It's a sort of “speed indicator” of how much quickly the glassy modulus is reached.

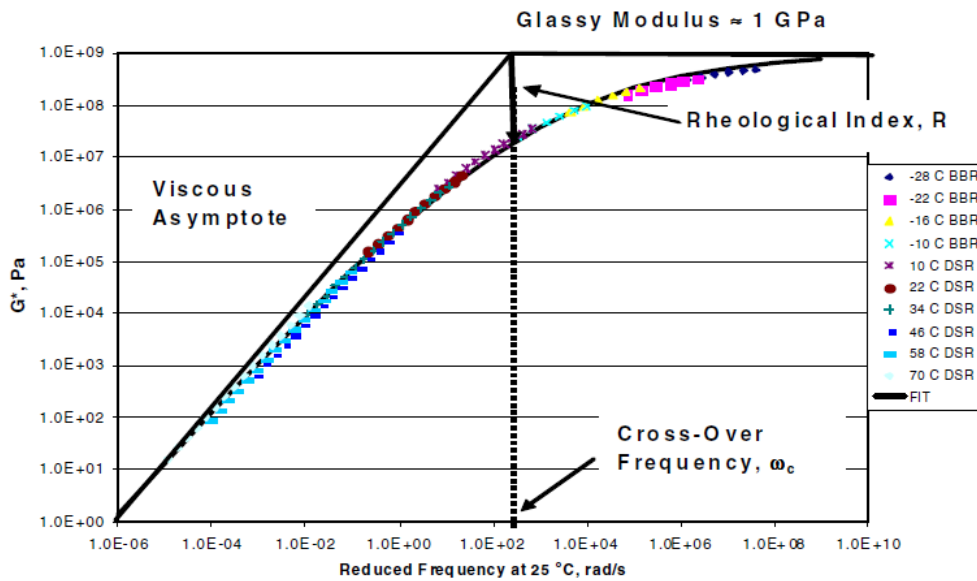


Figure 43 A typical mastercurve and physical properties

Whenever R value increases, master curves become flatter. In other words, it allows a more gradual transition from elastic behaviour to steady-state flow. In most cases, R value is sensible to oxidation state, and increases for oxidized asphalt.

Specifically, Master curves construction occurred at a reference temperature of 0°C, and time-temperature superposition was employed.

We plotted the logarithm of the complex shear modulus, measured at several temperatures, versus the logarithm of reduced frequency; then, curves were horizontally shifted. For those materials having a simple thermal-rheological behaviour, curves superposition requires only horizontal translations. In this case, horizontal shift factors $a(T)$ can be estimated; otherwise, vertical shift factors $b(T)$ may result also necessary. They're functions of the material's density (ρ) variability, which can't be neglected, occurred whenever temperature changes.

In our case study, temperature shift factors were made to fit the Williams-Landel-Ferry (WLF) function, in compliance with as follows:

$$\log a(T) = \frac{-C_1(T - T_R)}{C_2 + T - T_R}$$

where T_R is the reference temperature, C_1 and C_2 are constants empirically determined and T is the variable temperature.

In order to correctly draw the master curve, the unknown parameters revealed by Christensen-Anderson model, ω_c , R , T_d , C_1 and C_2 need to be estimated. T_d is the reference temperature, established on the basis of the specific case. Practically, it works with the Microsoft Excel Solver tool: the objective is to minimize the sum of the squared errors (SSE) of the logarithm of the predicted and measured G^* and δ by varying the four remaining variables.

The overall final view gives a visual picture of how viscoelastic properties change with temperature.

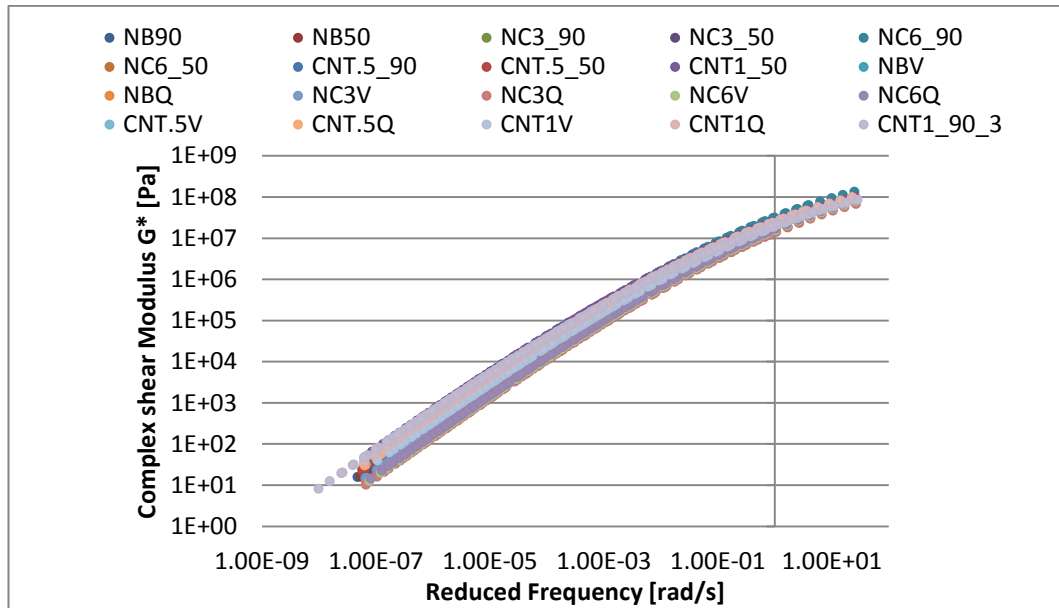


Figure 44 Master Curves- All Blends

5.2 Results discussion: protocols comparison

First of all, we based the first comparison on mixing protocol adopted during the blends preparation phase, highlighting the main differences and detecting any possible curve feature which could better explain protocol's influence on rheological properties.

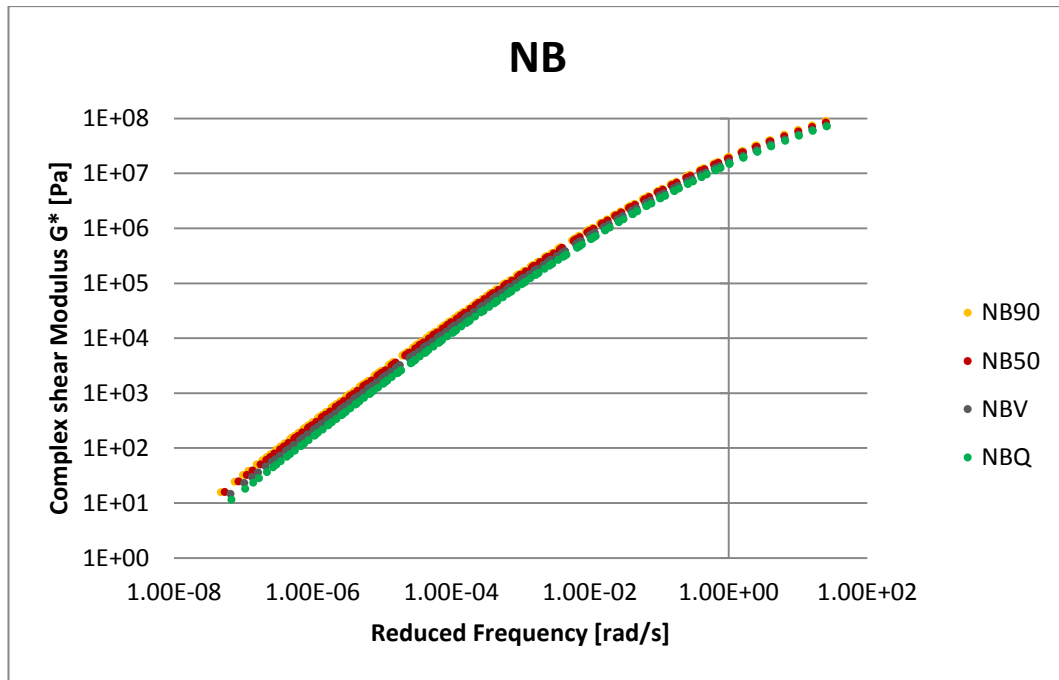


Figure 45 Master curve neat bitumen - Protocol comparison

According to results found with black diagrams, we can say in general that, since black space diagrams didn't reveal curves differences with such evidence, similar results are expected from master curves.

In fact, building curves by means of theoretical models and the time-temperature superposition principle, trends are getting smoother than those of black diagrams and discontinuities were rounded.

However, closer inspection of the table shows a slight shifting upward recorded for specimen prepared with low-shear mixing protocol. We can write down this shifting trend, since it could be confirmed by the following graphs referring to nano-additive blends.

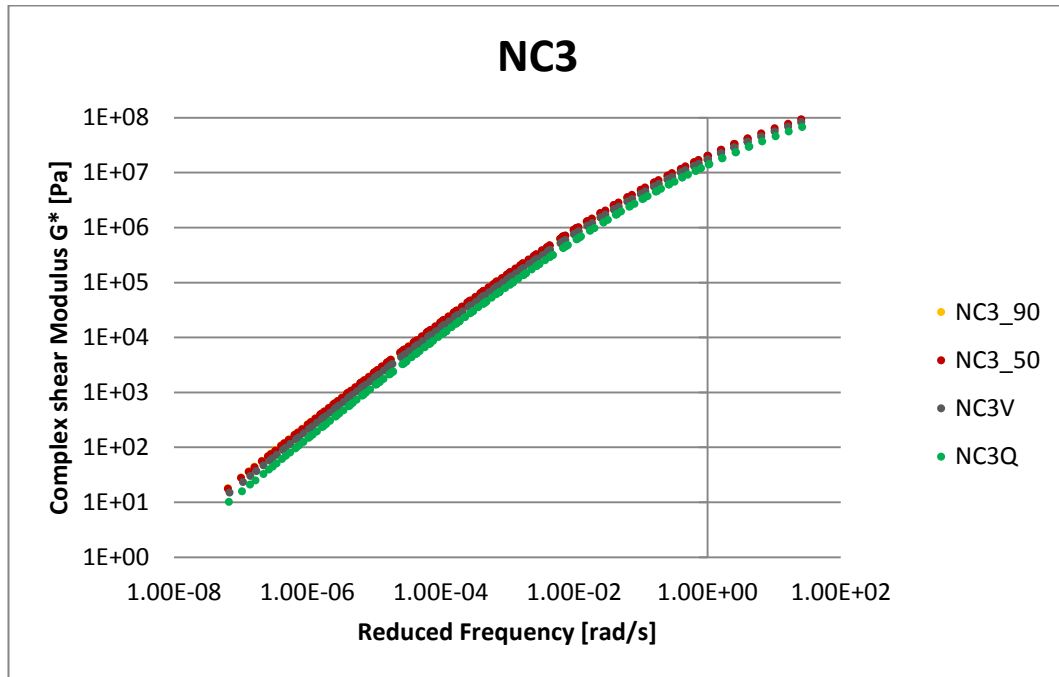


Figure 46 Master curve 3% nanoclay blends - Protocol comparison

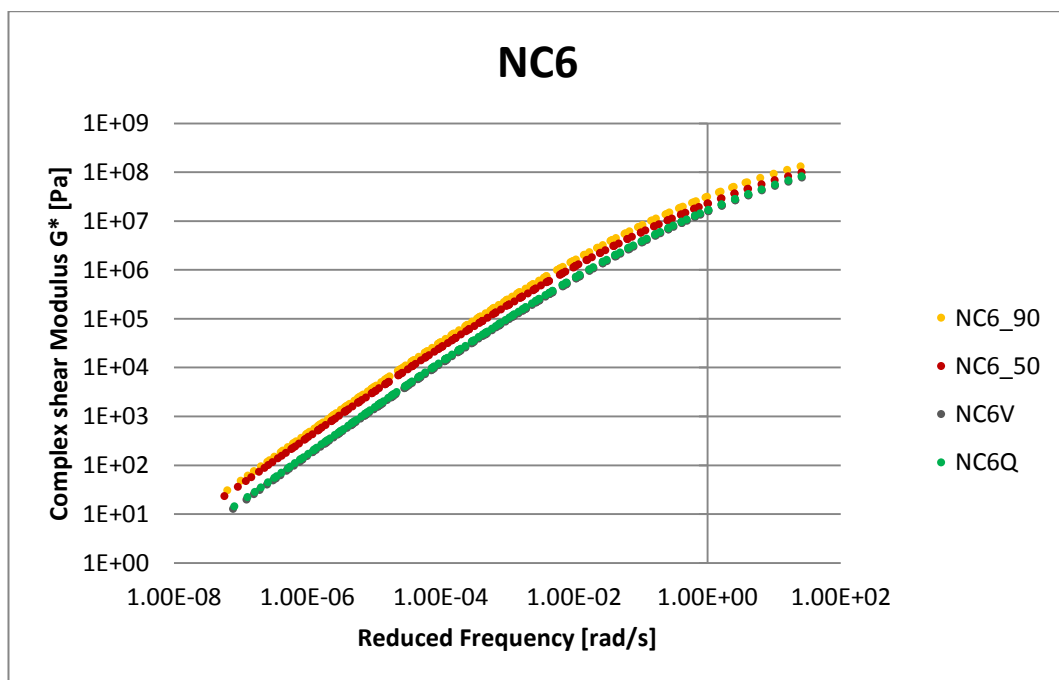


Figure 47 Master curve 6% nanoclay blends - Protocol comparison

Once more, the same tendency about protocols is displayed in both cases: blends prepared with Protocol A or Protocol B shows a more consistent shifting movement towards higher complex modulus values.

It's hard to give the right rational explanation, but research sometimes implies unexpected results, which require critical and deeper analysis.

Hence, we hypothesized that low-shear mixing, due to the long running time required to mix blends, would have caused an early aging of the specimen and thus an hardening of itself.

Discrepancy between protocols A/B or protocols C/D isn't noteworthy.

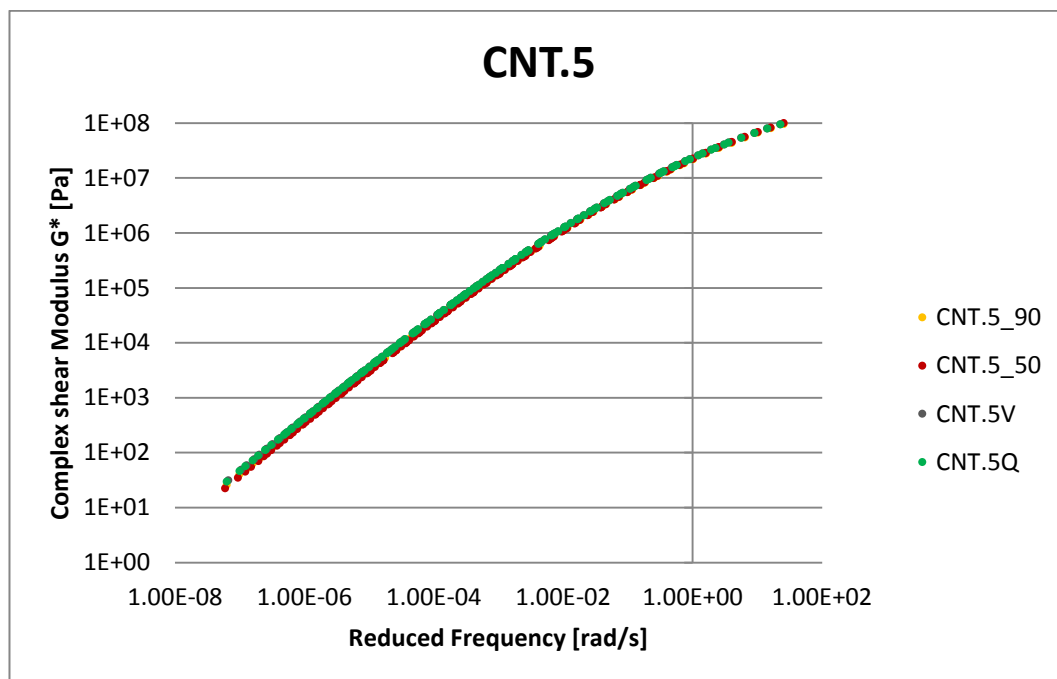


Figure 48 Master curve 0.5% carbon nanotube blends - Protocol comparison

On the contrary, none significant correlation was found between mixing protocols in case of *CNT.5* bituminous blends.

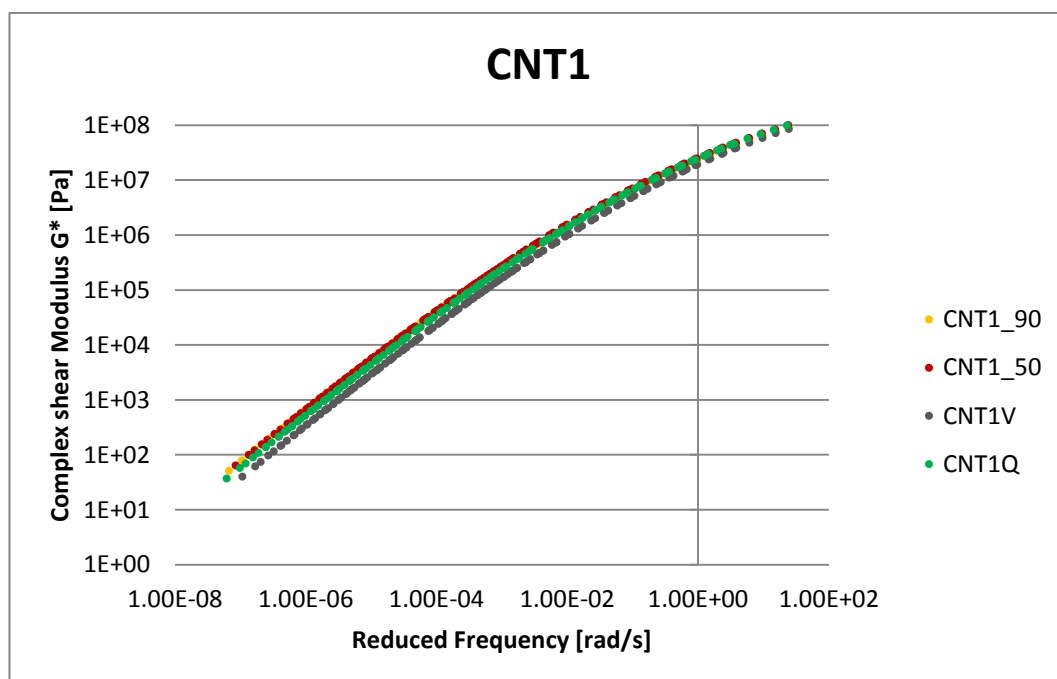


Figure 49 Master curve 1% carbon nanotube blends - Protocol comparison

Although slighter than *NB* and *NC* cases, *CNTI* blends again highlighted an hardening for those specimen prepared at low-shear mixing. The table presented at the bottom of the master curve topic paragraph, will help us to clarify if such a discrepancy is quantitative significant in terms of glassy modulus and crossover frequency.

5.3 Results discussion: materials comparison

Turning now to the next analysis, a comparison on the basis of materials differences was performed, as we want to detect the most significant changes occurred with nano-additive addition.

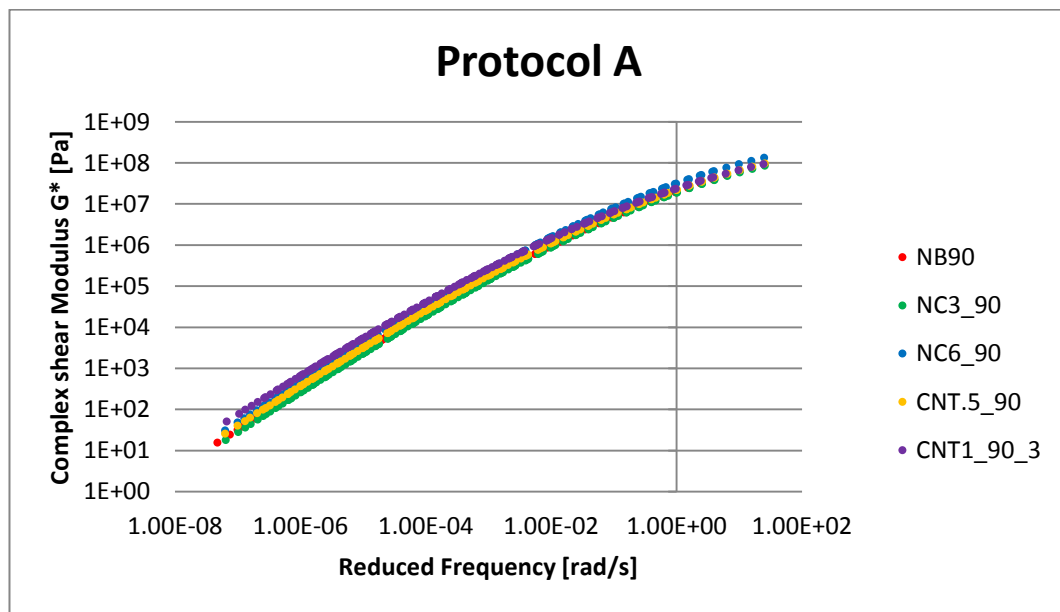


Figure 50 Master curve Protocol A, materials comparison

The central idea is that, as we would expect, *CNTs* addition leads to an increase in stiffness, which, in other words, means that higher complex modulus corresponds to the same reduced frequency. This result was expected and confirmed by experiments developed in previous literature.

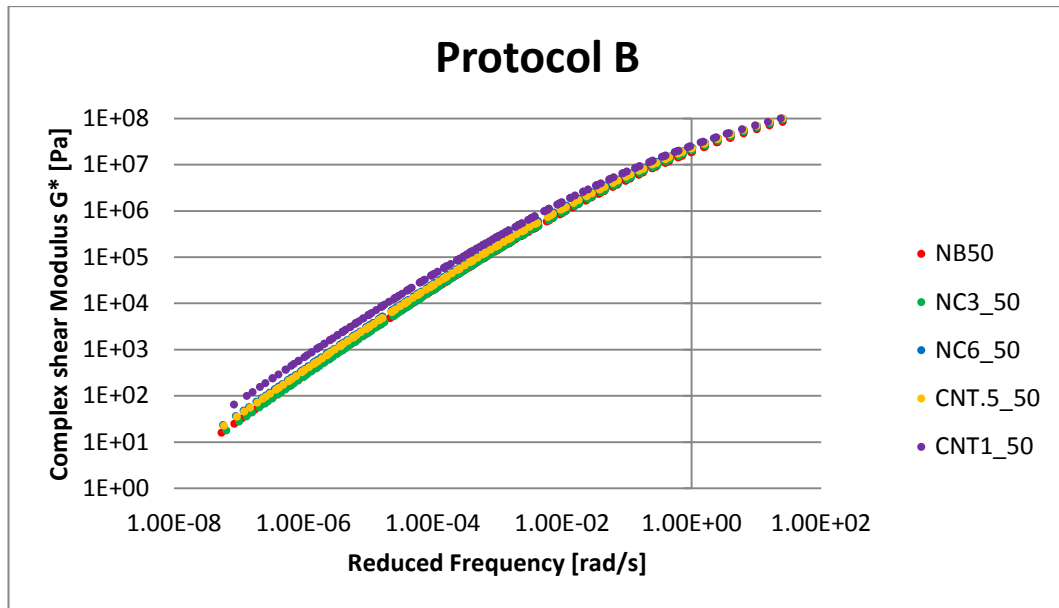


Figure 51 Master curve Protocol B, materials comparison

As nano-additive percentage increases, upward shifting occurs and performances improve. *NC* bituminous blends curves are almost overlapped to those of the control specimens.

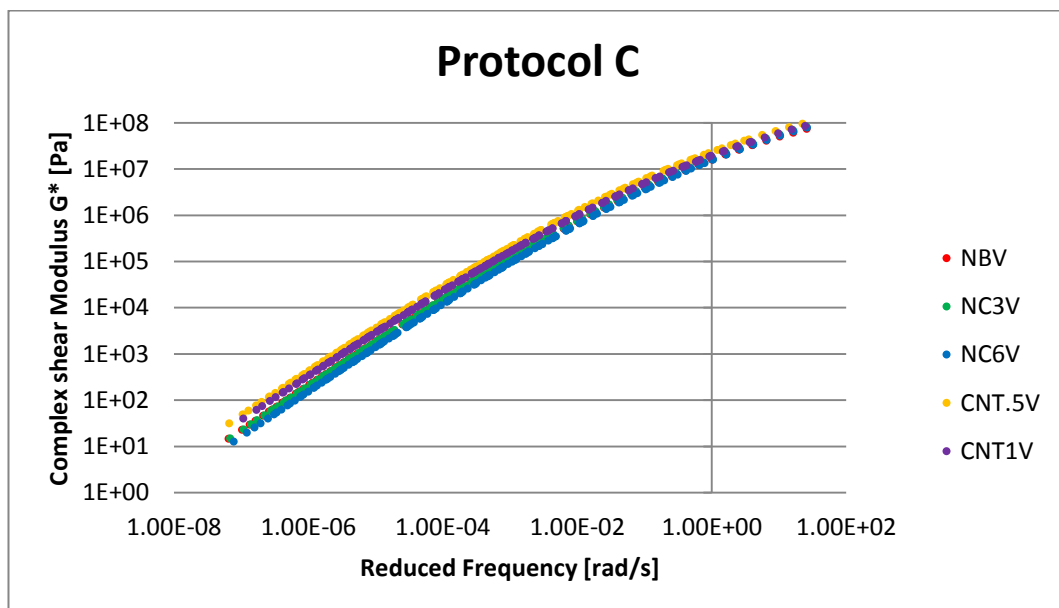


Figure 52 Master curve Protocol C, materials comparison

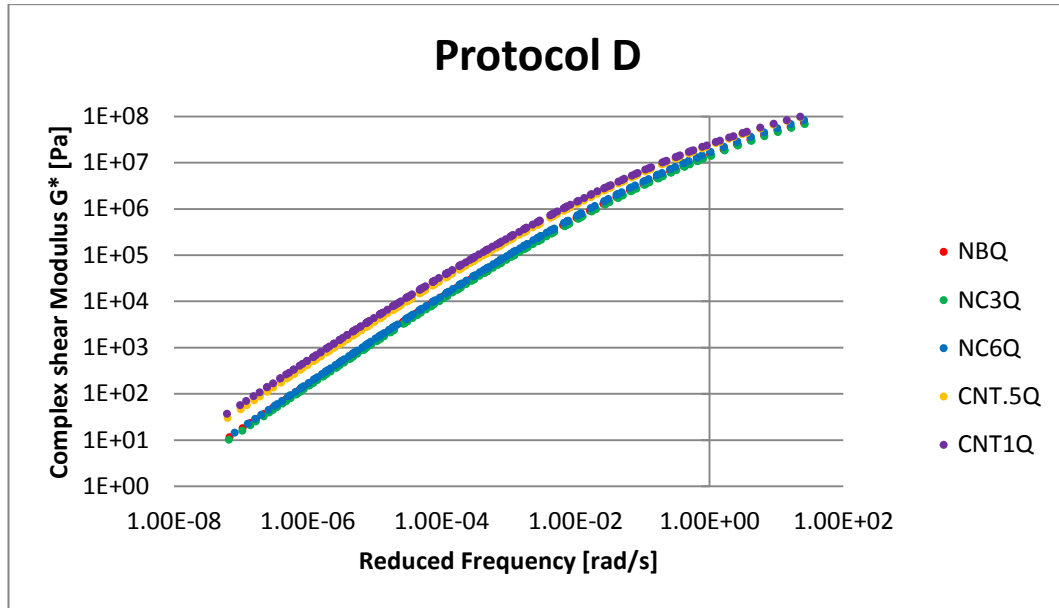


Figure 53 Master curve Protocol D, materials comparison

Protocols C and D display more clearly the *CNT* blends increase in complex modulus. We may assume that the use of Silverson equipment would be more appropriate for *CNT* particles dispersion within the bituminous matrix, since their tendency rises toward higher performances.

5.4 Comparison of variables from CA model

Henceforward, we can compare rheological parameters of the twenty blends contained in the following table, which extrapolates data deriving from the CA model and the WLF equation, applied to reach convergence and compute predicted variables.

Variables	$\log(Gg)$	$\log(\omega c)$	R	C1	C2
Materials	[Pa]	[rad/s]			
NB90	8.996	0.429	1.480	17.462	113.609
NB50	8.913	0.403	1.437	17.248	112.720
NC3_90	8.925	0.432	1.430	16.970	111.588
NC3_50	8.960	0.523	1.393	17.028	113.291
NC6_90	9.000	0.277	1.364	16.460	105.566
NC6_50	8.955	0.298	1.451	17.334	114.394
CNT.5_90	9.000	0.331	1.496	17.016	111.899
CNT.5_50	9.000	0.374	1.460	17.038	111.451
CNT1_90	9.000	0.006	1.689	26.768	192.227
CNT1_50	9.000	0.027	1.587	15.263	95.068
NBV	8.849	0.457	1.411	16.992	111.970
NBQ	8.864	0.600	1.383	17.095	113.566
NC3V	8.944	0.567	1.409	16.818	110.580
NC3Q	8.847	0.631	1.376	17.476	117.763
NC6V	8.917	0.670	1.369	16.810	111.897

NC6Q	8.929	0.648	1.364	16.611	110.106
CNT.5V	8.986	0.252	1.494	14.927	88.647
CNT.5Q	8.983	0.250	1.495	15.159	90.723
CNT1V	9.000	0.359	1.531	15.038	94.984
CNT1Q	9.000	0.156	1.533	15.236	91.391

Table 5 Master curve rheological modelled variables

We set a maximum limit to the logarithm of the glassy modulus equal to 9 GPa.

	SSE(G*)	SSE(δ)	Sum
NB90	0.008946	0.009642	0.018587
NB50	0.00632	0.009135	0.015454
NC3_90	0.005834	0.008988	0.014821
NC3_50	0.009169	0.00772	0.016889
NC6_90	0.008752	0.019367	0.028118
NC6_50	0.005446	0.010024	0.01547
CNT.5_90	0.011361	0.019595	0.030956
CNT.5_50	0.007077	0.009889	0.016966
CNT1_90	0.022444	0.043621	0.066065
CNT1_50	0.069097	0.106946	0.176043
NBV	0.005571	0.009452	0.015024
NBQ	0.005572	0.008787	0.014359
NC3V	0.004952	0.008764	0.013715
NC3Q	0.010385	0.0091	0.019484
NC6V	0.00513	0.008302	0.013433
NC6Q	0.005548	0.007914	0.013462
CNT.5V	0.020857	0.015846	0.036704
CNT.5Q	0.02359	0.019267	0.042857
CNT1V	0.055956	0.072009	0.127965
CNT1Q	0.038973	0.053884	0.092857

Table 6 Error Sum of Squares - Complex shear modulus and phase angle

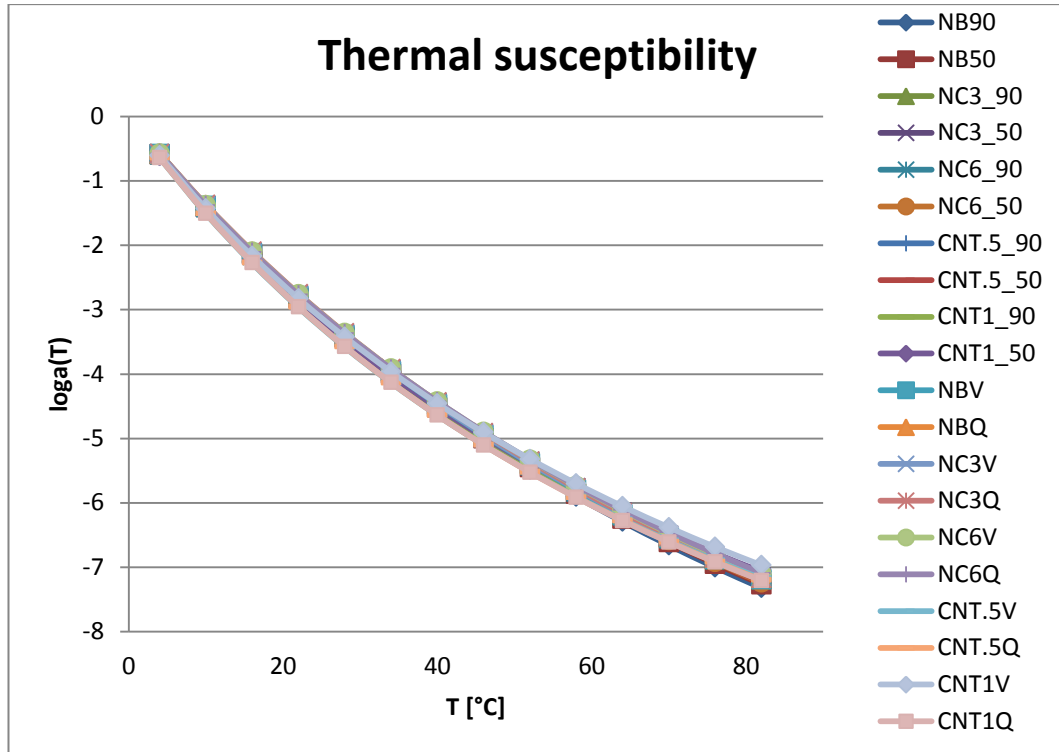


Figure 54 Shift factors plot in time

We plotted the logarithm of the estimated shift factors to focus on their development in time. The values are negative regardless of the temperature, since shift factors are numbers minor than one. However, as can be seen from the graph above, curves are almost overlapped. To thoroughly detect any discrepancy, since the picture could be less clear than we would, each curve was provided of intercept and slope's information.

Material	Intercept	Slope
NB90	-0.844508865	-0.08452
NB50	-0.843565375	-0.08382
NC3_90	-0.842037102	-0.0829
NC3_50	-0.826823213	-0.08254
NC6_90	-0.88334604	-0.08268
NC6_50	-0.830087036	-0.0836
CNT.5_90	-0.840937079	-0.083
CNT.5_50	-0.846845676	-0.08328
CNT1_90	-0.910753681	-0.08217
CNT1_50	-0.946893299	-0.08058
NBV	-0.838997159	-0.08286
NBQ	-0.827188593	-0.08276
NC3V	-0.845303449	-0.08254
NC3Q	-0.802643182	-0.08301
NC6V	-0.830790756	-0.082
NC6Q	-0.840020497	-0.0817

CNT.5V	-1.017738159	-0.08131
CNT.5Q	-1.001957588	-0.08174
CNT1V	-0.93404719	-0.07943
CNT1Q	-0.997167906	-0.08189

Table 7 shift factors - variables

6. Damage curves from LAS Test

In paragraph 3.4, we introduced LAS procedure standards, describing test phases, now we're going to focus on the analyses and results interpretation.

The LAS test was introduced by Bahia and his associates as a promising test to estimate asphalt fatigue performance. LAS test results are then analysed by means of the VECD (Viscoelastic Continuum Damage) model (24), which several researches demonstrated to be adequate to characterize asphalt binder fatigue performance.

A consistent number of problems came out in the past from the use of other theoretical models to predict fatigue performances of asphalt binders, i.e. the running time of the test and the effort in results explanation when modified bitumen was used (25).

6.1 TP 101-14 standard

As a first step in the analysis approach, determination of α fatigue parameter derived from frequency sweep test:

Storage modulus $G'(\omega)$ is already measured during frequency sweep test; a linear regression analysis is performed on a plot of $\log \omega$ versus $\log G'(\omega)$ using the expression:

$$\log G'(\omega) = m(\log \omega) + b$$

The m value is strictly connected to α parameter:

$$\alpha = \frac{1}{m}$$

Derived from amplitude sweep test phase, damage calculation can be performed:

$$D(t) \cong \sum_{i=1}^N [\pi \gamma_0^2 (C_{i-1} - C_i)^{\frac{\alpha}{1+\alpha}} (t_i - t_{i-1})^{\frac{1}{1+\alpha}}]$$

where

γ_0 is the applied strain for a given data point;

$C(t) = \frac{|G^*|(t)}{|G^*|_{initial}}$ is the norm of the complex shear modulus measured at the generical time t is divided by the initial undamaged complex shear modulus, represented by the second data point, since the first point could be affected by material changes. $D(t)$ is increased at each point adding the previous $D(t)$ value. This calculation is performed until the final data point corresponding to the 30% applied strain.

Then, C_1 and C_2 parameters can be estimated according to the following relationship, respectively as the anti-logarithm of the intercept and the slope:

$$\log(C_0 - C(t)) = \log(C_1) + C_2 \cdot \log(D(t))$$

where C_0 is taken equal to 1, the initial value of C . The standard suggest to neglect damage values lower than 10.

Damage failure value D_f is defined as the damage that corresponds to the reduction in initial complex modulus at the peak shear stress:

$$D_f = \left(\frac{C_0 - C_{at\ peak\ stress}}{C_1} \right)^{\frac{1}{C_2}}$$

The binder fatigue performance can be now estimated as:

$$N_f = A(\gamma_{MAX})^{-B}$$

where

γ_{MAX} is the maximum expected strain

$$A = \frac{f(D_f)^k}{k(\pi C_1 C_2)^\alpha}$$

$$B = 2\alpha$$

$$k = 1 + (1 - C_2)\alpha$$

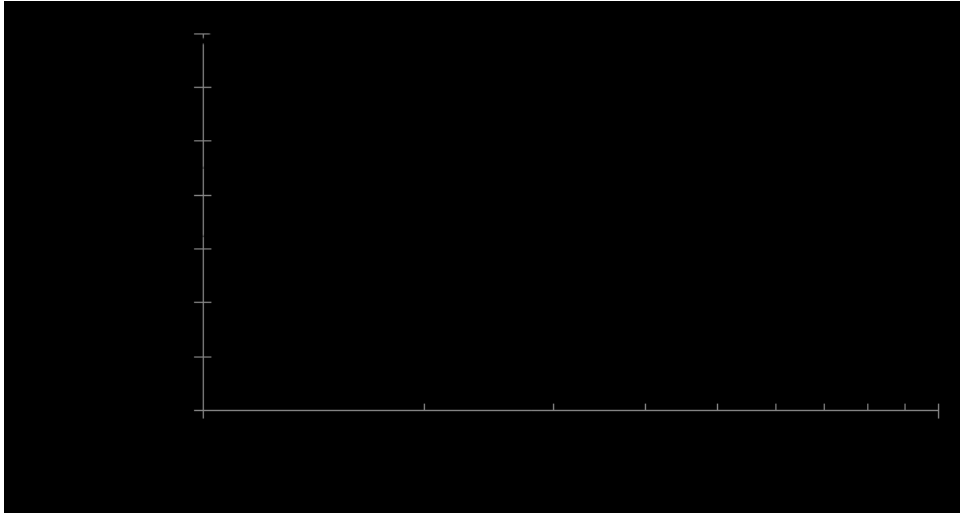


Figure 55 Plot of Fatigue Parameter N_f versus applied shear strain

Drawing the graph above, a log-log scale was employed and the fatigue parameter was normalized over 1 million ESALs.

6.2 TP 101-16 standard

The more recent standard follows also a VECD analysis, but some differences in damage estimation were detected, which led to sensitively different results.

First of all, amplitude sweep test is conducted in stepwise increasing loading scheme.

Undamaged material properties are expressed as:

$$\alpha = 1 + \frac{1}{m}$$

Indeed, damage accumulation:

$$D(t) \cong \sum_{i=1}^N [\pi I_D \gamma_0^2 (|G^*| \sin \delta_{i-1} - |G^*| \sin \delta_i)^{\frac{\alpha}{1+\alpha}} (t_i - t_{i-1})^{\frac{1}{1+\alpha}}]$$

where

I_D is the initial $|G^*|$ value corresponding to 1% applied strain and the other variables have been previously explained.

Another difference with the precedent standard consist in ignoring damages less than 100, to estimate C_1 and C_2 parameters.

The damage value at failure is slightly different:

$$D_f = \left(0.35 \frac{C_0}{C_1}\right)^{\frac{1}{C_2}}$$

The binder fatigue performance is defined as the damage that corresponds to a 35% reduction in $|G^*| \sin \delta (C_0)$ undamaged value:

$$N_f = A_{35}(\gamma_{MAX})^{-B}$$

6.3 TP 101-14 Results discussion and analysis

6.3.1 Protocol comparison

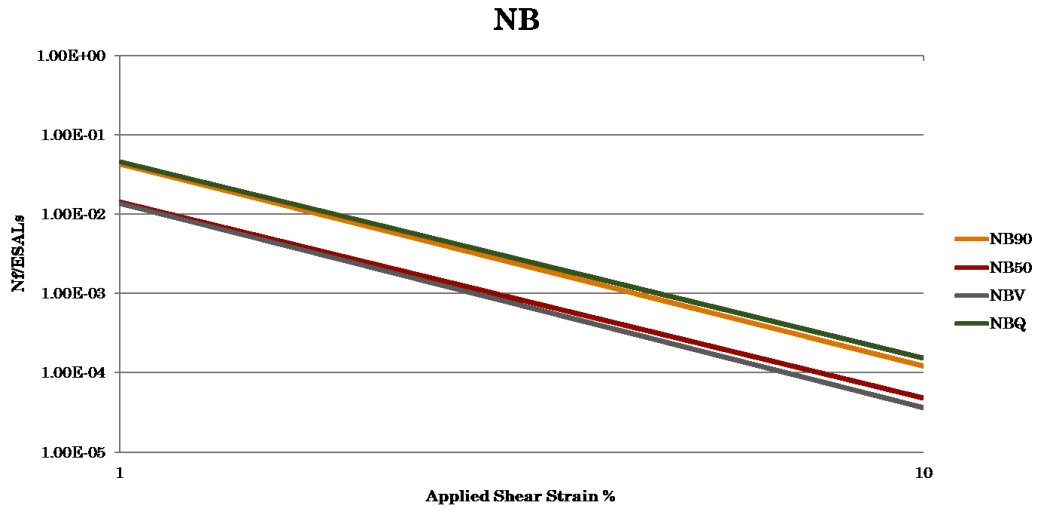


Figure 56 Fatigue parameter Nf - Neat bitumen, protocol comparison

The binder fatigue parameter presents a negative trend, since it decreases applying higher strains.

Unexpectedly, we found consistent differences in LAS curves for the control asphalt binder, as mixing protocol changed. This variability can't be confirmed, since just one repetition was performed. It could be due to the modelling phase, or to discrepancies occurred during the DSR test, or to other several reasons.

Protocol D works better than the others, while Protocol C is the worst one. However, univocal protocol tendency is not clearly recognizable.

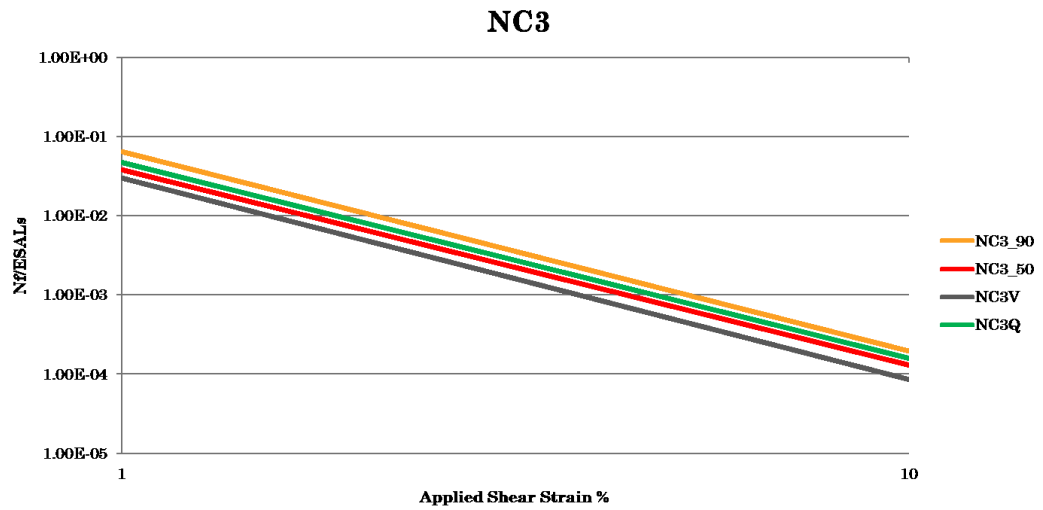


Figure 57 Fatigue parameter N_f - 3% nanoclay blends, protocol comparison

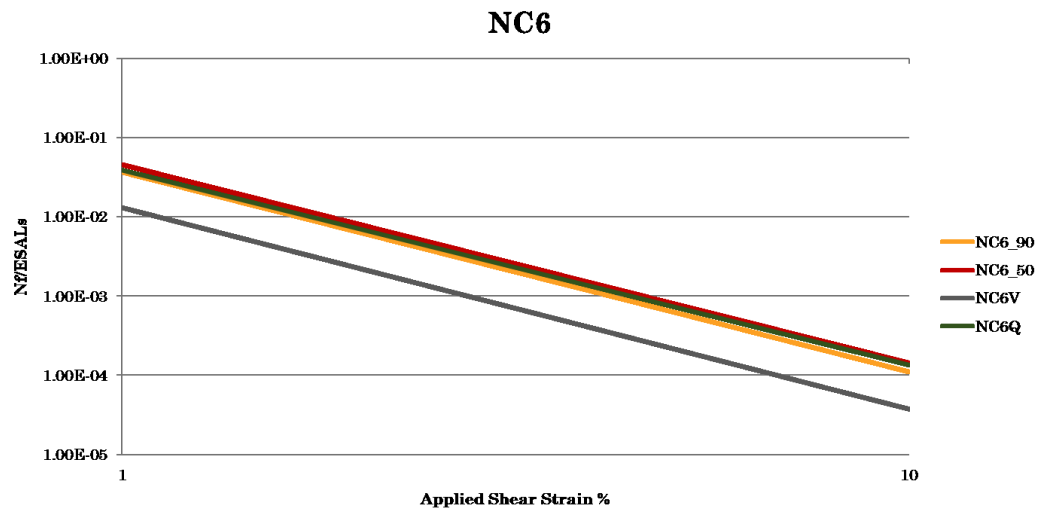


Figure 58 Fatigue parameter N_f - 6% nanoclay blends, protocol comparison

Again, Protocol C shows the lowest values in terms of fatigue performance. This tendency was displayed in all the graphs above.

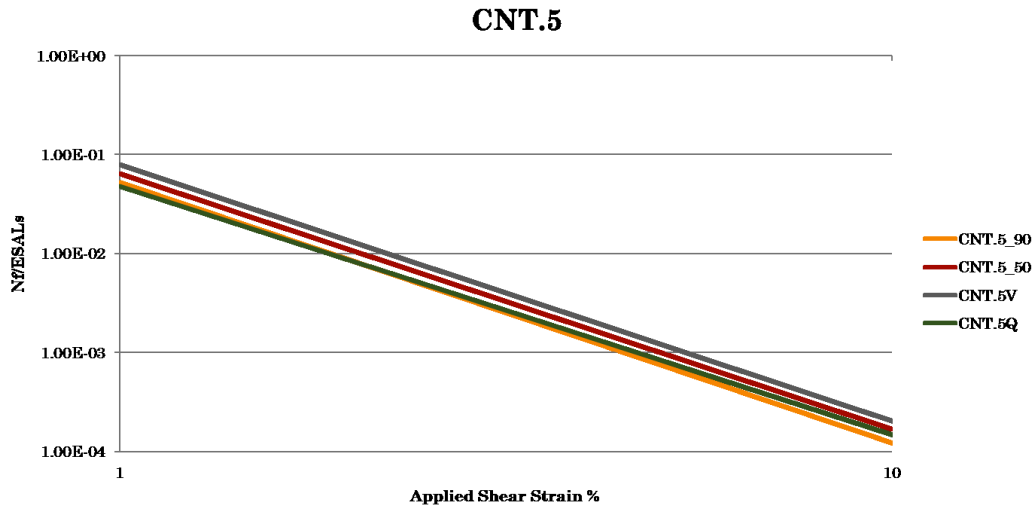


Figure 59 Fatigue parameter Nf - 0.5% carbon nanotube blends, protocol comparison

In case of *CNT* blends, curve's discrepancy becomes slighter and a turnaround was highlighted, since LAS curve constructed for Protocol C has the highest values.

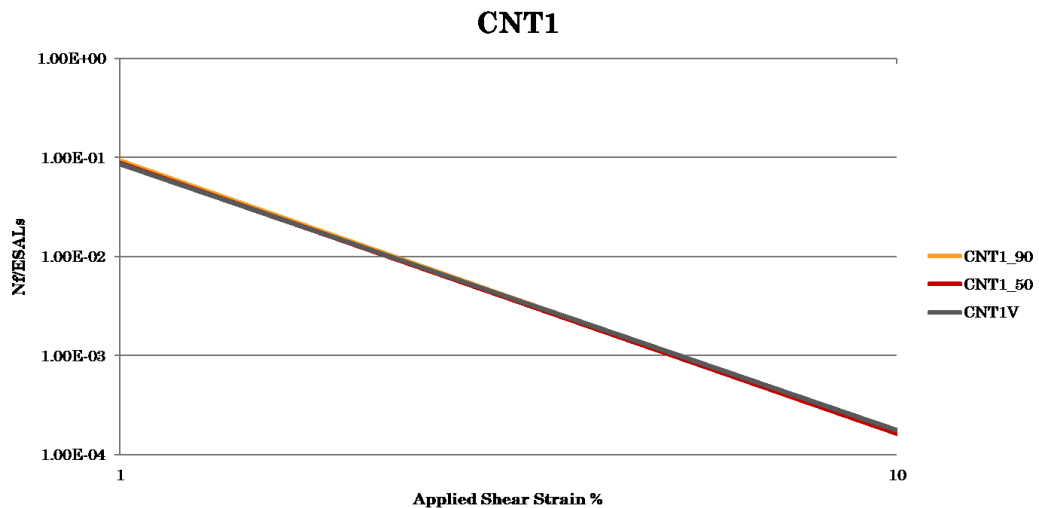


Figure 60 Fatigue parameter Nf - 1% carbon nanotube blends, protocol comparison

CNT1 curves are perfectly overlapped and none difference was displayed.

6.3.2 Fatigue parameters normalization

Due to unforeseen variability which stands out in case of the control samples, we decided to normalize the estimated value of A fatigue parameter on the control bitumen, at the respective protocols. Our aim was a trial to remove control bitumen's variability, in order to observe each specimen regardless of the non-modified asphalt binder protocol changes.

A and B represents, respectively, the intercept and the slope of damage curves. We can compare them for all the twenty blends, after performed normalization to the control bitumen:

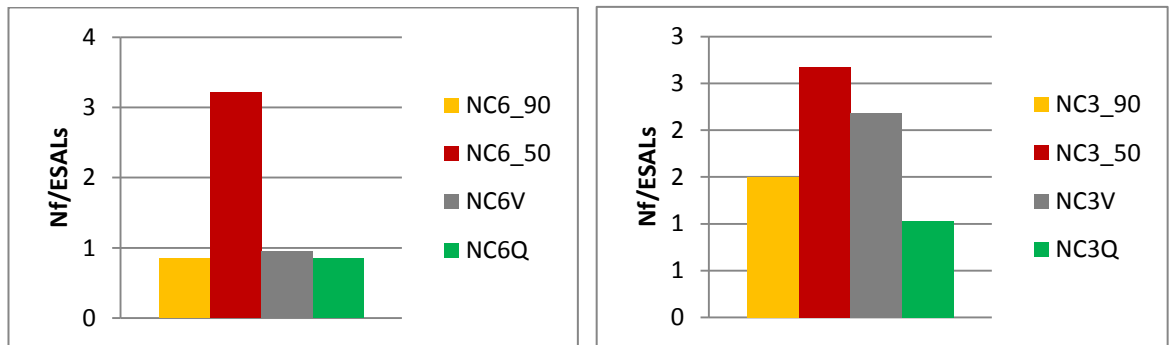


Figure 61 A parameter comparison - NC blends

For both *NC3* and *NC6* blends, Protocol B is the one that particularly stands out and shows better fatigue performance.

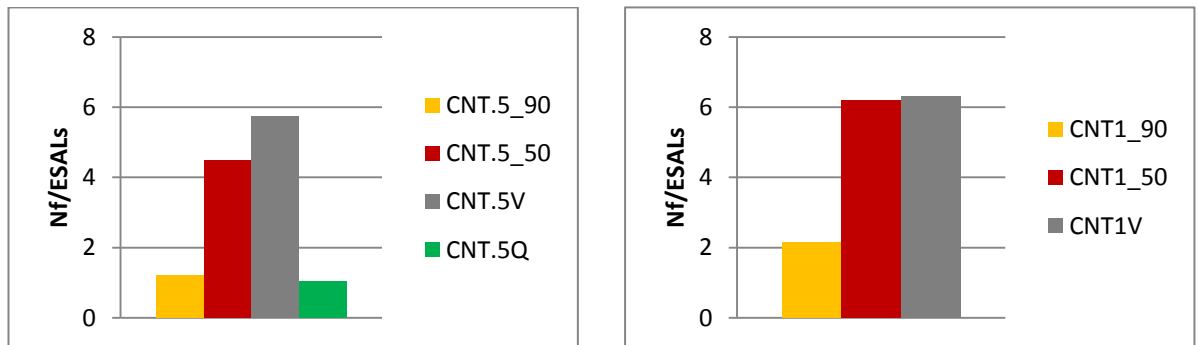


Figure 62 A parameter comparison - CNT blends

In case of CNT blends, differences become slighter, but a turnaround occurs, since Protocol C gives better fatigue performance in both cases.

However, since just one repetition was performed, there's no certainty that protocol's variability for the control sample was real, or caused by inconsistencies occurred during the test.

6.4 TP 101-16 Results discussion and analysis

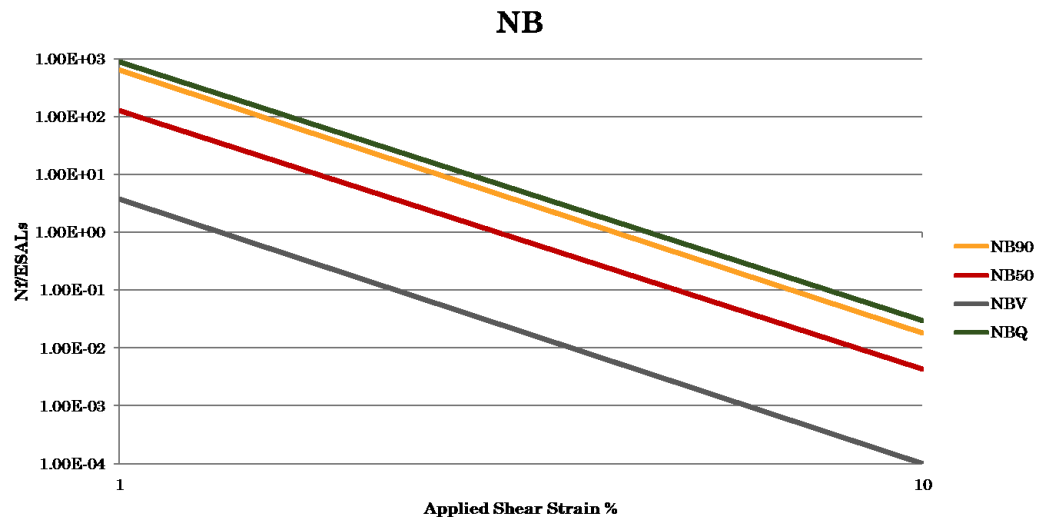


Figure 63 Fatigue parameter N_f - Neat bitumen, protocol comparison

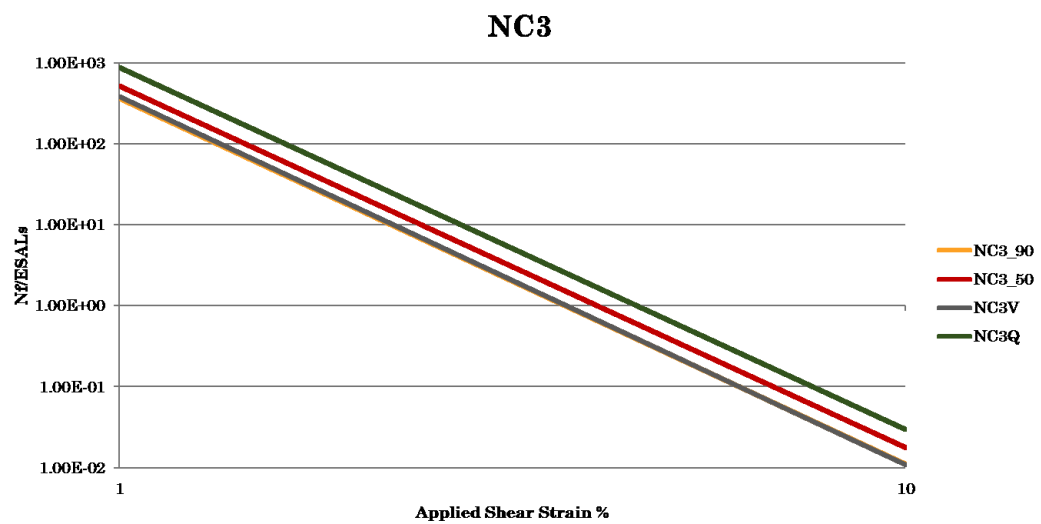


Figure 64 Fatigue parameter N_f - 3% nanoclay blends, protocol comparison

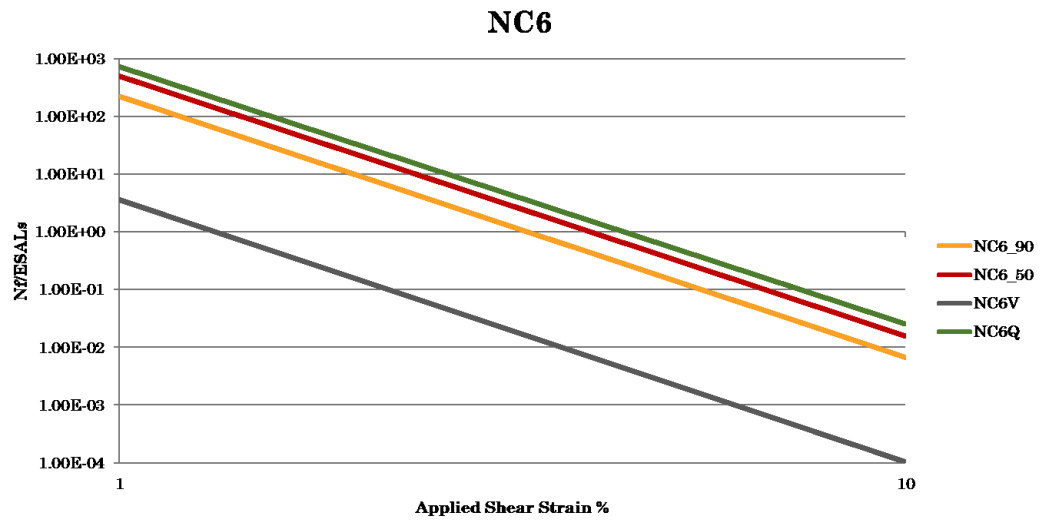


Figure 65 Fatigue parameter Nf - 6% nanoclay blends, protocol comparison

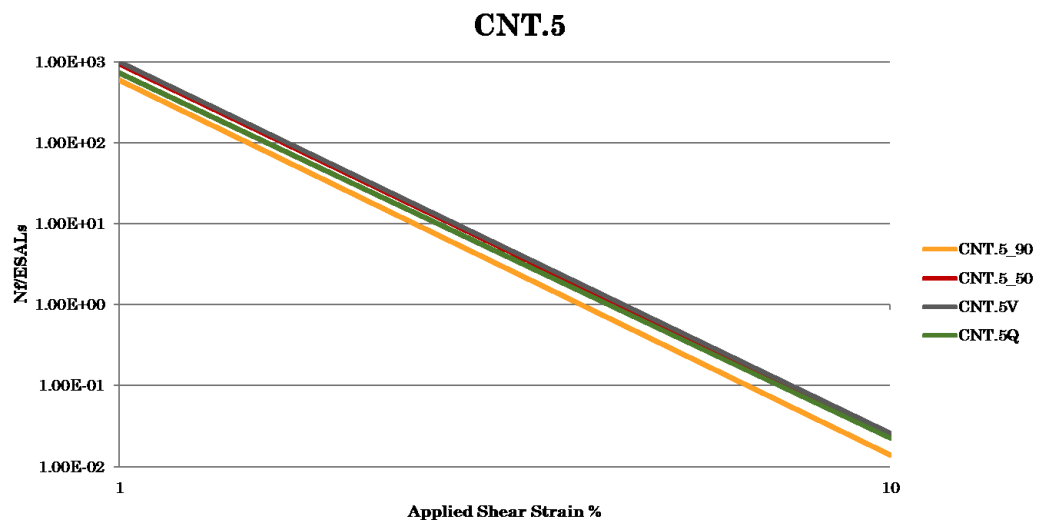


Figure 66 Fatigue parameter Nf - 0.5% carbon nanotube blends, protocol comparison

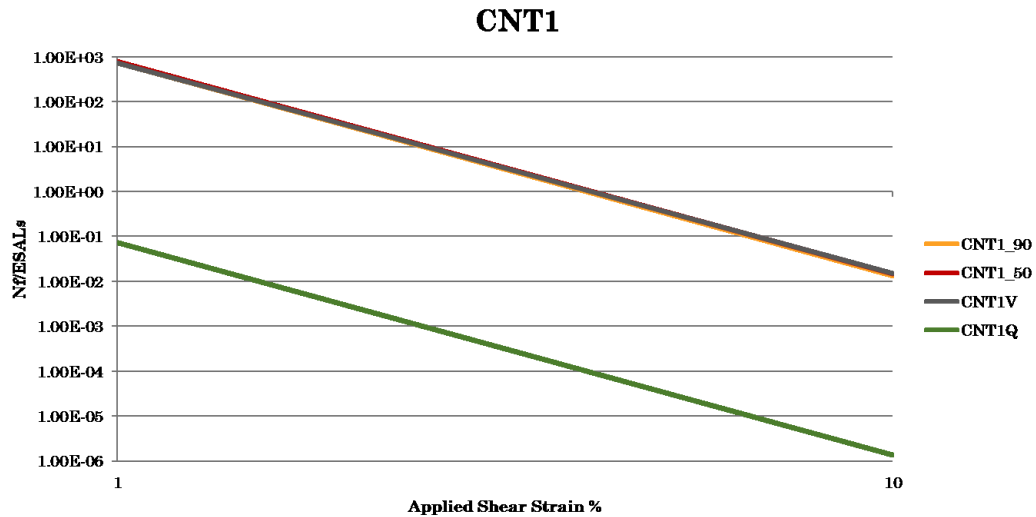


Figure 67 Fatigue parameter Nf - 1% carbon nanotube blends, protocol comparison

Analysis performed according to the most recent standard gave us results, which are substantially different, either from a qualitative and quantitative point of view. Protocol D results even worse, and normalization didn't work well in this case.

7. Apparent Molecular Weight Distribution (AMWD)

According to previous researches led in literature, new methods were found to connect rheological properties of asphalt binders to their molecular weights. Several times in the past it was found that the AMWD can be estimated from rheological and mechanical parameters, such as stiffness, or complex modulus, or phase angle, while the inverse process was harder. The validity of the direct approach consisting in MWs determination was demonstrated for polymers by Tuminello, 1986 (26) and McGrory, Tuminello, 1990 (27). Bitumens are like natural polymers with low molecular weight, nevertheless they present a more complex and variable structure, as bitumen molecules and MWs ranges are very wide (28).

Luckily, a new method, easy to implement, for determining the AMWD, starting from phase angle (δ) of the complex modulus measured within the linear viscoelastic region, was developed.

Bitumen's MWD is strongly dependent on its petroleum crude oil origin, on the refinement process adopted to produce it, on the ageing level and on the additive type added to improve its properties.

Such inverse determination process won't give specifically MWs in its strict sense, but rather the apparent MWs responsible for the observed mechanical behaviour.

Zanzotto et al., 1999 found that G^* is not that much sensitive to the higher MWs components, while δ seems to be more sensitive to the considered parameter. This assertion explains why the selected inverse method to determine MWD of asphalt binders focuses on the phase angle; thus, the approach is so-called δ -method. It is valid for every type of pure petroleum bitumens, or modified or artificially aged bitumens, whenever we operate within the linear viscoelastic domain.

First of all, before discussing results, we're going to briefly expose the consisting method and the theoretical approach, in order to help the reader to a more conscious and critical interpretation.

7.1 MWDs from the linear viscoelastic behaviour

MWDs can be expressed in terms of DMWD (differential MWD) or CMWD (cumulative MWD). From a mathematical point of view, DMWD corresponds to the semi-logarithmic plot of MW versus $f(MW)$, the respective probability density.

$$Fr(a \leq \log MW \leq b) = \int_a^b f(MW) d\log MW$$

where $Fr(a \leq \log MW \leq b)$ is the fraction of molecules which presents their molecular weight between a and b values.

On the other hand, CMWD is the semi-logarithmic plot of MW versus $cumf(MW)$.

$$cumf(MW^*) = \int_0^{\log MW^*} f(MW) d\log MW$$

where the asterisk indicates the apparent molecular weight. The hypothesized extension of MWs is from $\approx 100Da$ to $\approx 1000000Da$, in compliance with the typical values found for bitumens. Since the MWs range is consistently wide, a log-scale was used to better show the curve's trend.

As shown in the following picture, MW is focused in the rubbery zone of the LVE behaviour comprised between the terminal and the plateau zones.

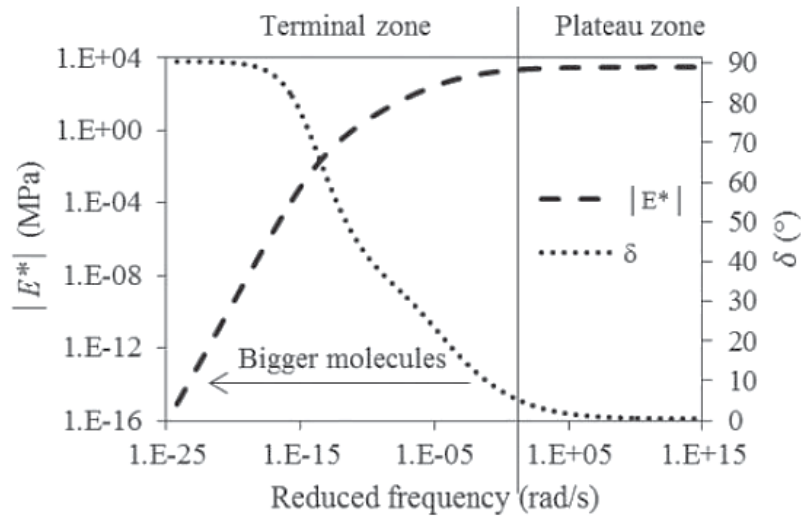


Figure 68 Modulus and phase-angle master curves

Each material molecule presents its own relaxation frequency, ω_i . Moving towards lower frequencies, molecules relax and their contribution can be neglected.

In order to derive a direct analogy between the measured rheological parameters and the MWD, as the oscillation frequency decreases, an increasing amount of molecules start relaxing and stop their modulus contribution, as we previously said, which explains why the modulus drastically decreases. On the other hand, the phase angle increases.

Such displayed trend allows to express the proportional relationship between the phase angle and the fraction of relaxed molecules at each given frequency. Thus, CMWD and δ connection has been justified and can be expressed as follows:

$$\log(MW) = 2.880 - 0.06768 \cdot \log(\omega)$$

Practically, we set up constant steps of MW, obtaining the corresponding ω value. The selected numerical differentiation was performed applying a numerical differential step of 1/3000 to the $\log(MW)$. The so-estimated ω value is plotted on the horizontal axis.

On the ordinate, we plot the phase angle master curve as a function of the MW.

$$cumf(MW) = A + B \cdot \delta(MW)$$

The two constants A and B are determined according to the conditions:

$$\begin{cases} MW \rightarrow 0; & \delta(MW) = 0, & cumf(MW) = 0 \\ MW \rightarrow \infty; & \delta(MW) = 90^\circ, & cumf(MW) = 1 \end{cases}$$

Substituting alternatively the two conditions in the previous expressions, we can easily find as result:

$$A = 0$$

$$B = \frac{1}{90}$$

The two parameters are defined universally for all materials.

Phase angle contained in the above expression was chosen from the one modelled during master curves, by means of Christensen-Anderson model and Williams-Landel-Ferry expression.

The last step model allows $f(MW)$ calculation:

$$f(MW) = \frac{dcumf(MW)}{dlog(MW)} \cong \frac{\Delta cumf(MW)}{\Delta log(MW)}$$

using the chosen step suggested by the method.

7.2 Results discussion

Since the bitumen crude oil is the same for all the blends, none difference is expected from the protocol comparison for each material. Indeed, the nanoparticle addition should affect MWD in any case.

In compliance with this hypothesis, we'll approach and discuss just graphs comparing the twenty blend materials.

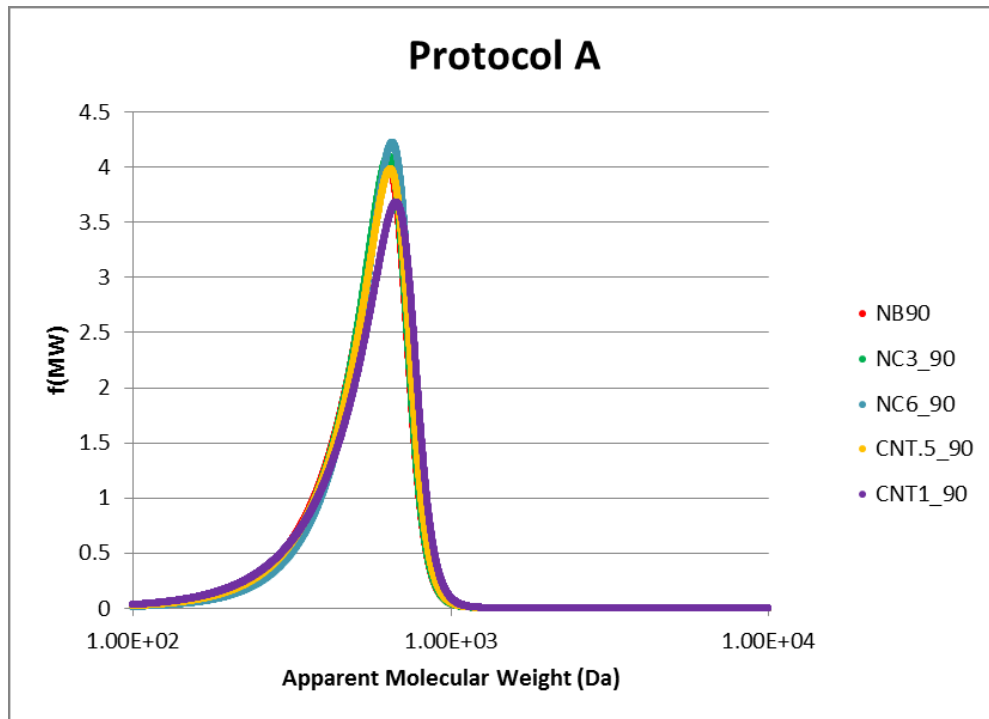


Figure 69 AMWD Material comparison - Protocol A

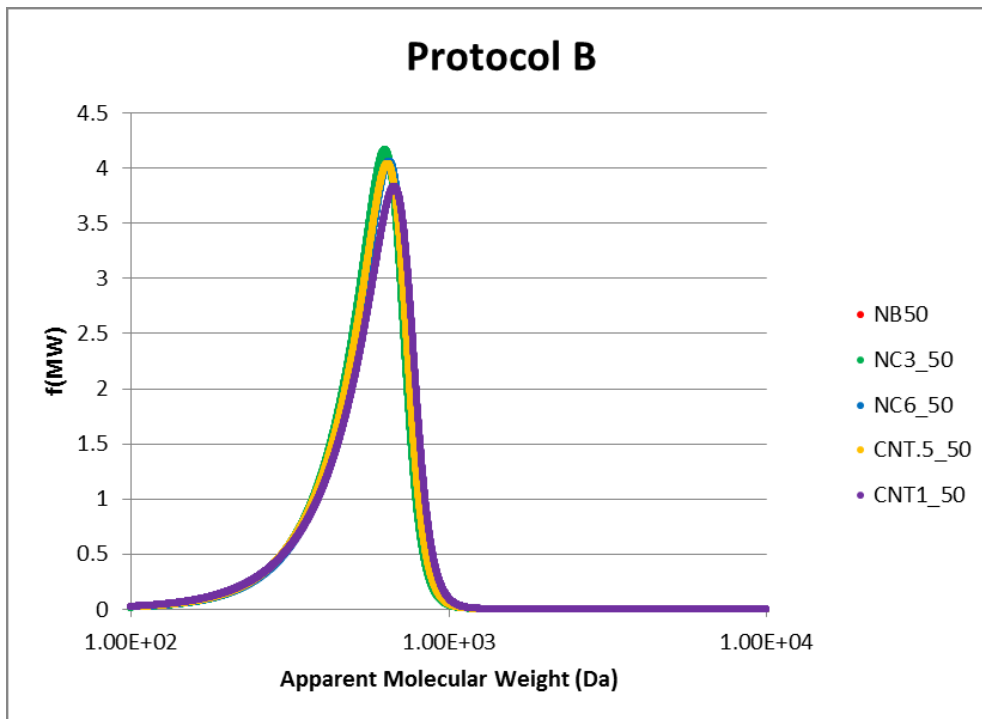


Figure 70 AMWD Material comparison - Protocol B

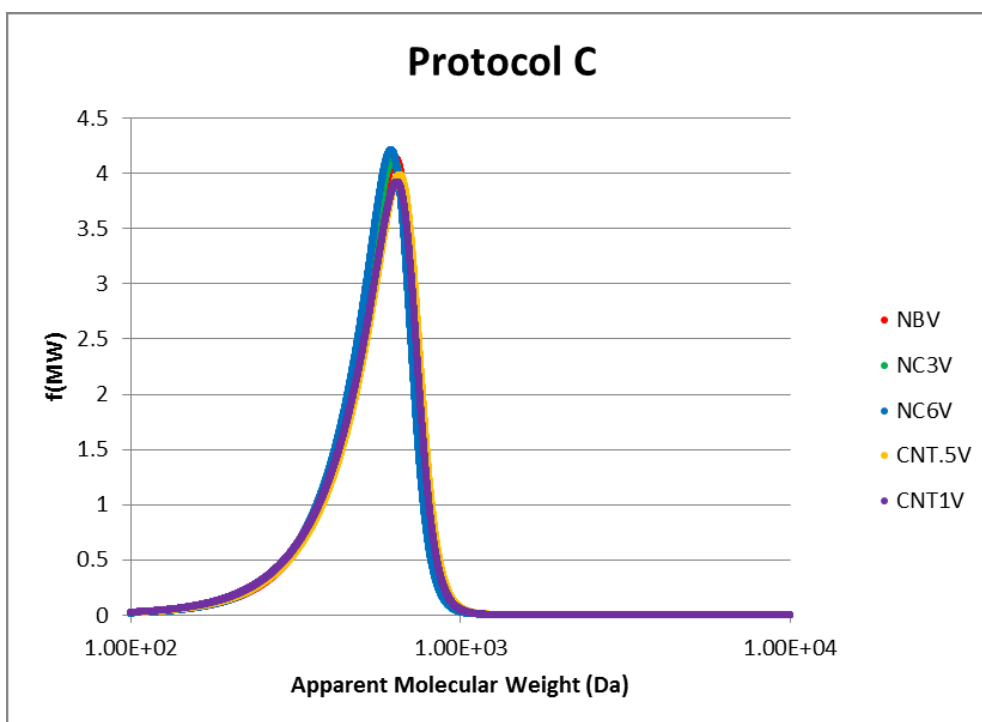


Figure 71 AMWD Material comparison - Protocol C

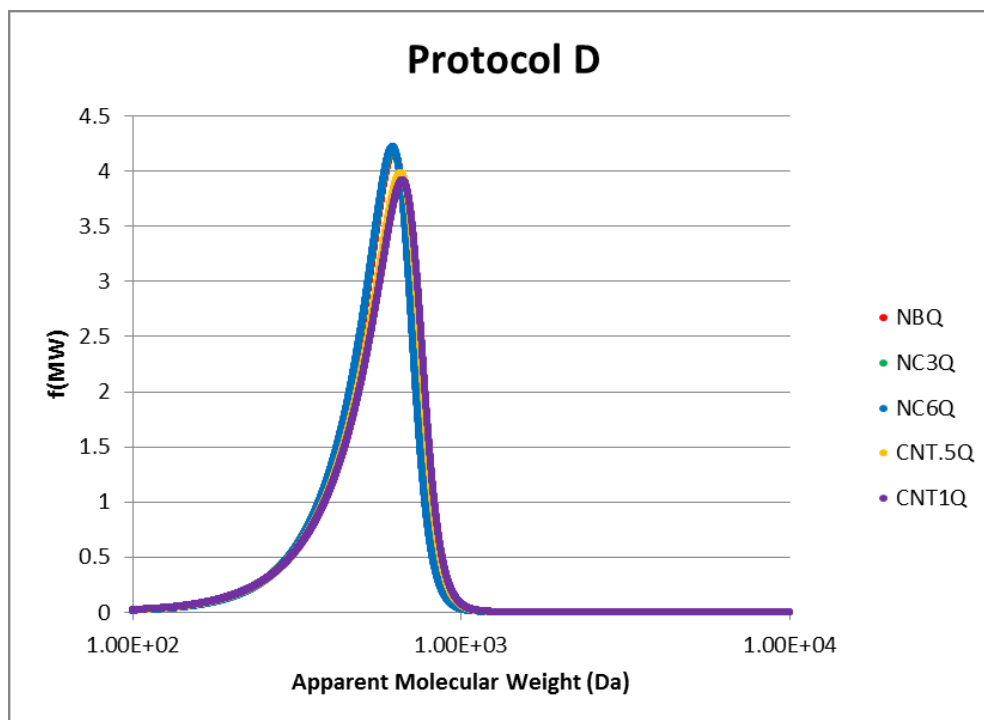


Figure 72 AMWD Material comparison - Protocol D

From the graphs above we can see that none of the curve difference was statistically significant. A slight decrease was constantly recorded in CNT blends; such a difference becomes more evident, as the nano-additive percentage increases.

Control binder curve and NC blends are almost overlapped.

Since graphical curve deviation wasn't that evident, we led a deeper analysis to compare the most significant variable, given by the mean distribution value.

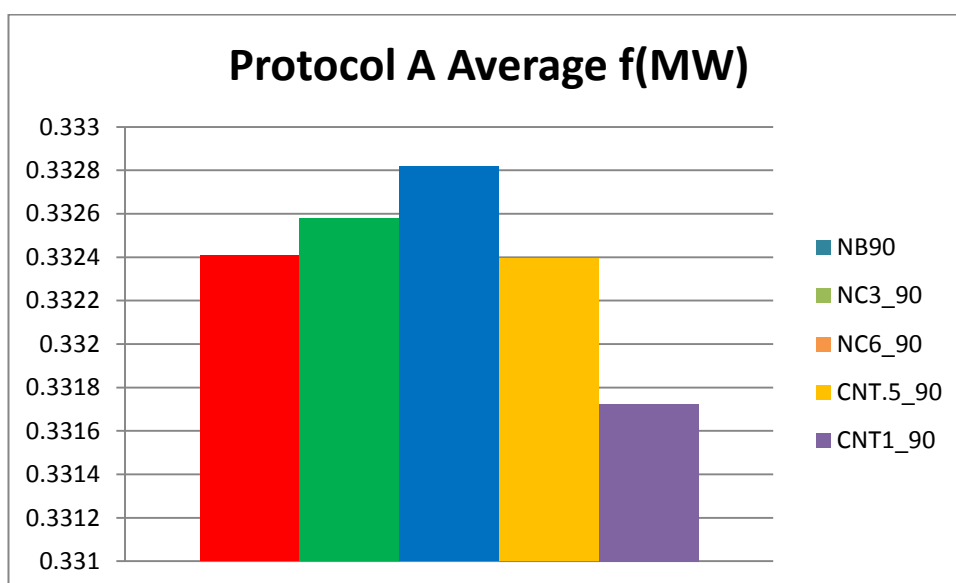


Figure 73 f(MW) average values, Materials comparison - Protocol A

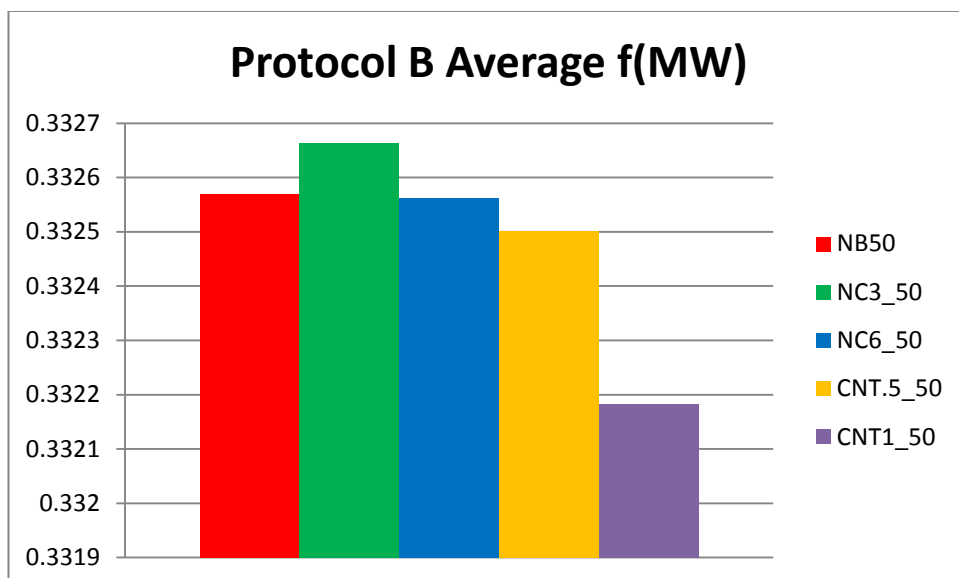


Figure 74 f(MW) average values, Materials comparison - Protocol B

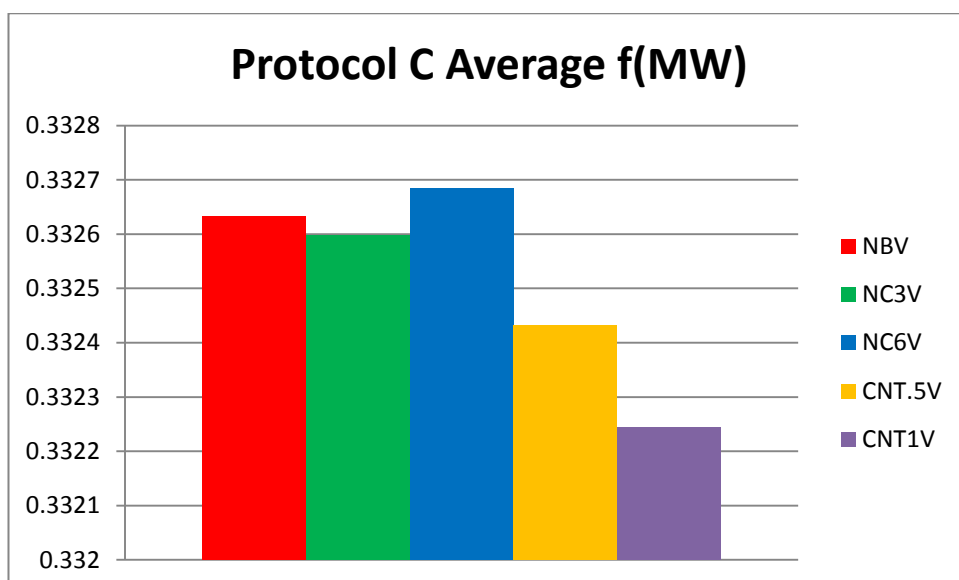


Figure 75 f(MW) average values, Materials comparison - Protocol C

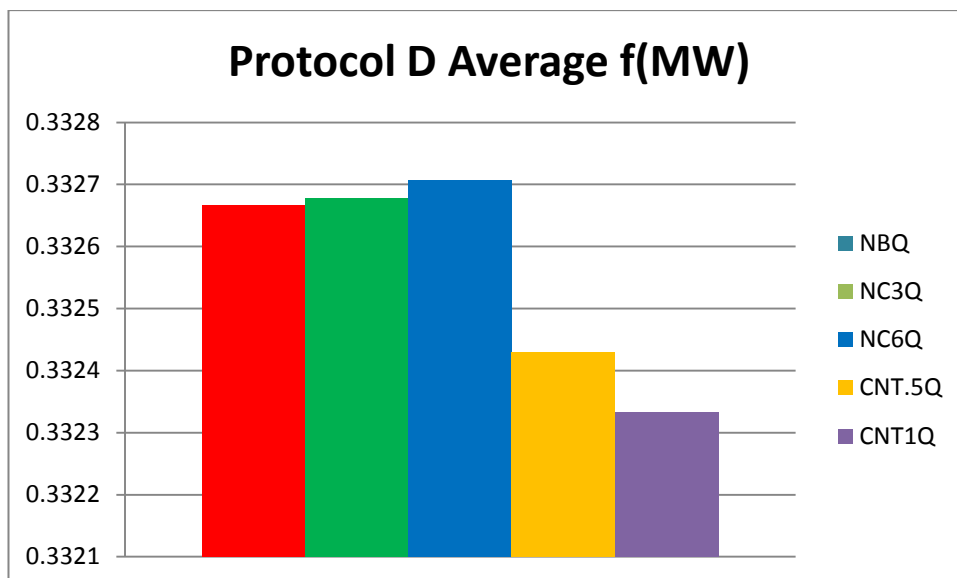


Figure 76 $f(MW)$ average values, Materials comparison - Protocol D

Comparing the results, *CNT0.5* and *CNT1* present in all cases lower $f(MW)$ values, and their peak is slightly moving rightward.

However, such a deviation, from a quantitative point of view, can't be assumed noteworthy as we would expect.

Probably, bitumen crude oil type employed during the refining process has a greater influence than the nano-additive type, which doesn't affect that much curve shifting and mean distribution values.

Chapter 3

ESEM Observation

1.Introduction

Microscopes are powerful tools employed to investigate materials morphology at micro and nano size level. Recently, Scanning Electron Microscopy (SEM) and Environmental Scanning Electron Microscopy (ESEM) have been used to explore bitumen's microstructure and their application fields widen day by day (29). SEM technology allows three dimensional images capture of specimen surface for a very wide material's range. Nevertheless, whenever a wet and non-conducting specimen is expected to analyse, ESEM technology gives better results.

SEM uses a focused beam of electrons to scan the surface and produces images as outputs. Electrons and sample atoms establish a continuous interaction, which produces signals containing information about superficial morphology and internal composition of the specimen. Practically, a finely focus electron beam irradiates sample's surface, which generates various signals, like backscattered or secondary electron or other photons provided of various energy, coming out from the surface, as a result of the electron interaction.

Investigating the source of electrons, they're produced at the top of the device column, then acceleration process occurs until they pass through a combination of lenses to produce a focused electron beam, that hits the surface of the specimen. On the other hand, the sample is placed on a stage into the chamber area and, unless the microscope is designed to operate at low vacuums, both the column and the chamber are provided of pumps.

The following picture easily displays how electron beam works, how much deep the penetration is, and in which way signals come out from the sample.

SEM, as we said before, produces images as output, scanning the specimen by means of a high energy electron beam. Substantially, when electrons and sample's surface begins to interact, secondary electrons (SE), backscattered electrons (BSE) and characteristic X-rays are produced and collected by detectors, which employ them to structure images that are then displayed on the computer screen (30).

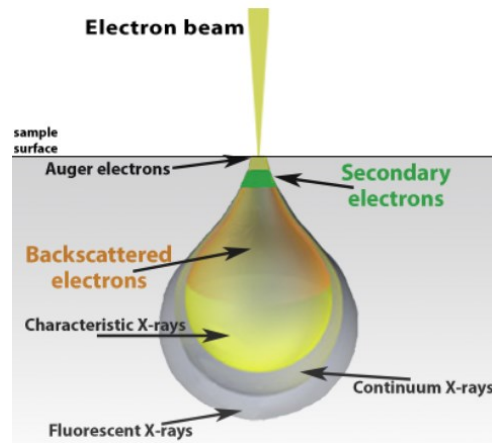


Figure 77 SEM interaction model

SEM is also equipped with detectors specialized to identify each signal, considering that they're singularly located into specific parts of the specimen and have explicit functions, such as topography identification or composition characterization. Whenever the applied electron beam hits the surface, it penetrates up to few microns depth; penetration thickness depends on the accelerating voltage and on the sample's density. The denser the material, the lower is the penetration depth. To be more specific, two detectors are dedicated to topographical imaging, using both SEs and BSEs: Everhart-Thornley detector (ETD) and through the lens (TLD).

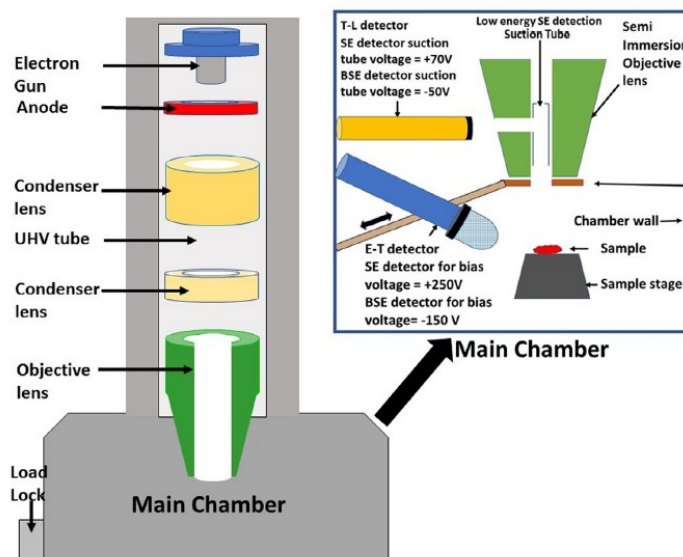


Figure 78 SEM System representation

Images produced by SEs give us information about sample's topography, whereas images generated by BSEs provide information about the composition of the sample.

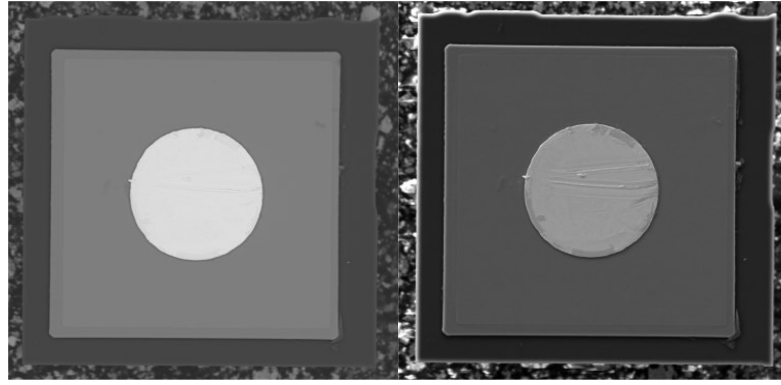


Figure 79 Respectively, SE and BSE image

SE images are strongly connected to the signal quality, which is influenced by: sample composition and electrical properties, geometrical angle between the hitting electron beam and the surface normal vector.

Whatever is the material, and even if the electron beam isn't affect by any modification, shadow zones occur, depending on surface orientation toward the electron gun. As darkness increases, it corresponds to an adverse orientation.

To summarize what we explained about SEM operation mode, it provides insight of fracture nature, allowing also the detection of healing phenomena in asphalt binder; such application helps to implement new materials for civil engineering employment. Tough, one of the most negative aspect, is that this technology requires a sample coating system, which could distort its original features.

2. SEM drawbacks

Nevertheless, SEM technology showed several drawbacks, that limit its use in asphalt binders field (29).

First of all, bitumen is subjected to volatility in the vacuum chamber; furthermore, it's extremely susceptible to electron beam damage and surface charging can sometimes occur. The last phenomenon takes place when the specimen surface amasses excessive electrons number, causing image distortion, since charged zones deflect the incident electron in a wrong and irregular way during scanning process, which leads to instability of electron signal. It mainly happens when non-conducting samples are tested. In such cases, a thin conductive metal layer is requested to cover the non-conductive surface, preventing charging process activation.

It also requires to test clean and dry samples; whether they were dirty, wet or oily, it would be impossible to lead the observation in a conventional SEM chamber. At

least a conducting film covering the sample's surface is needed. Although such specifications have fulfilled, not always SEM images would have displayed perfect resolution for several reasons. In fact, due to high temperature and high vacuum conditions, coating layer get smaller since it has volatile properties. On the other hand, a thin coat is required, 5 to 20 nanometres, otherwise it would distort the original topographic features.

Another problem is associated to thermal damage possibility for sensitive specimens. When they're heated, cracking and pitting phenomena may occur, especially for organic specimens, and molecule scattering may interest wet materials or soft specimens. Volatile particles cause damages to SEM chamber pumps; in case of soft materials significant surface damage occurs during the imaging in high vacuum mode.

In conclusion, high vacuum may also cause sample evaporation. In such cases, a control technique of environmental conditions would require the physical separation between the electron generation chamber and the electron imaging chamber.

3. ESEM technique

To analyse wet, soft or non-conducting samples with scanning electrons, a technique called environmental SEM or ESEM was originally designed by G. Danilatos. The choice to adopt the word "environmental" derives from the fact that sample imaging is possible thanks to sample environmental variation in terms of pressure, temperature and gas composition. ESEM provides the same advantages and performances discussed about SEM microscope, meanwhile it removes high vacuum constrain (29). Indeed, even wet, oily and non-conductive samples can be examined without modifying the surface, and without requiring any state alteration. None sample preparation is performed; consequently, none damage occurs.

Thus, the only way to analyse asphalt binder's microstructure without any concerns and possible specimen's damage, by means of scanning electrons, is to employ ESEM technology (31).

The Environmental Scanning Electron Microscope (ESEM) is the most valid alternative to SEM observation, because of its possibility to observe viscous oil bearing specimens at high vacuum. Volatile specimens are less exposed to

damage risks with ESEM, thanks to the higher capacity of chamber pumps to handle volatile particles.

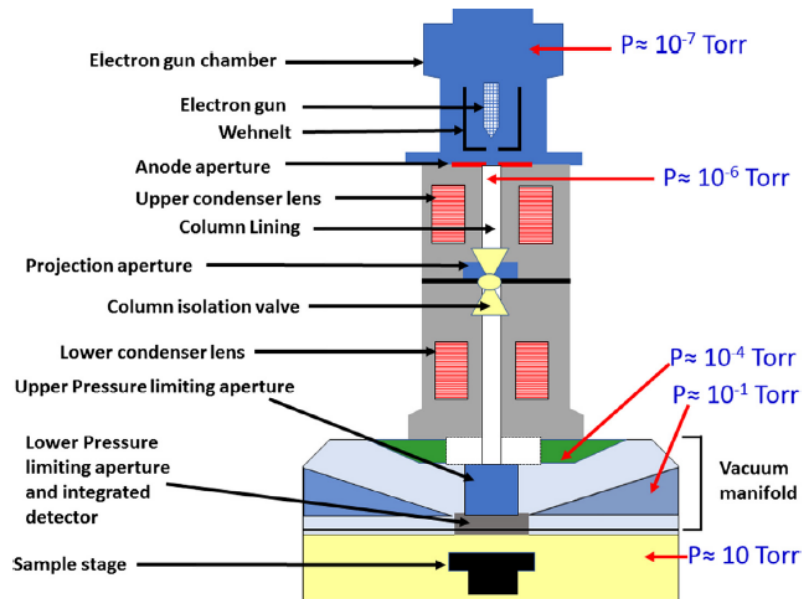


Figure 80 ESEM System representation

From the picture above, several pressure zones can be identified. A complex system of pumps and pressure apertures keep the chamber at low and controlled pressure. Since it deletes the problem of sample preparation, ESEM technology is particularly adequate to investigate samples during dynamic process.

Recently, researchers have shown an increasing interest in morphological investigation of asphalt binders (32). The topic is quite absorbing and many steps need to be covered to bridge the gap in terms of scientific knowledge. The issue presents wide applications and requires combination between chemical and engineering proficiency.

Collected pictures shows, according to previous literature researches, that aging implies, as the main consequence, effects on asphalt fibril's structure: hence, fibrils become denser and coarser. Such evidence can be connected to the performance grade of asphalt binder.

It allows to directly get observations of phase separation between fibrils and bitumen.

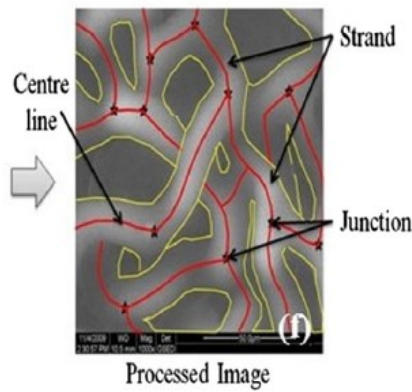


Figure 81 Example of SE images derived from ESEM observation

4. ESEM procedure

Many studies were led in the past to observe bitumen microstructure using the SEM microscope, few researches were conducted with ESEM, thus we followed the procedure established by the Centre For Pavement And Transportation Technology (CPATT), sited at the University of Waterloo, which is easily reproducible (33).

The ESEM model utilized is a FEI Quanta 250 FEG Model, which includes six variable-pressure and can accommodate multiple sample (we chose a maximum of three specimens for each observation session).



Technical specifications:

- Magnification: 14 to 1000000 x
- Electron beam resolution: high, low and extended vacuum mode
- Accelerating voltage: 200 V to 30 kV
- Geometry: 45° objective lens with through-the-lens differential pumping and heated objective apertures
- Maximum horizontal width: 5 mm at analytical working distance (10 mm); 8.8 mm at 25 mm WD

Samples can be studied in three different pressure conditions (34):

- high vacuum condition ($<6 \cdot 10^{-4}$ Pa): it's suitable for conductive specimens, as SEM microscope.
- low vacuum condition ($10 \div 130$ Pa): it allows observation of wet and non-conductive samples, without surface alteration performed with conductive coating layers. It's the case of polymers, ceramics, fibres, textiles and asphalt binders.
- environmental ESEM condition ($10 \div 2600$ Pa): to observe wet samples, even if they contain high amount of water. None specific sample preparation is required and the device works in 100% humidity conditions inside the chamber. Since the pressure level is very high, materials containing volatile particles can be analysed.

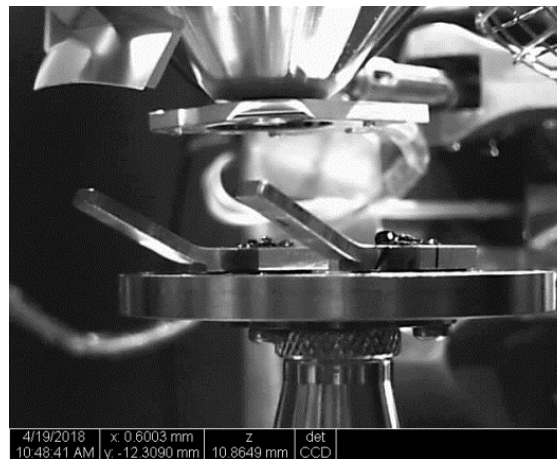


Figure 82 Sample stage

Sample preparation protocol was determined after many attempts, the same about magnification and ESEM settings employed along microstructure observation. Establishing analysis parameters selected to compare specimens and detect any difference was hard, since observation's output was just made of pictures and videos. Hence, quantitative comparison variables were extrapolated according to literature, such as fibrils' relative sizes, their abundance and microstructure evolution in time. The overall idea is to lead morphological observation in order to predict asphalt binder rheological properties and performance parameters.

As a first sight, bitumen appears initially featureless, since focalization takes time; then, a network of fibrils shapes. Time employed to stabilize the fibrils was recorded and analysed as a comparison parameter. Experimental studies led by CPATT team-work (33) stated that such network isn't merely a product of electron beam, because fibrils tends to be aligned along stress direction, and this

behaviour is typical of bitumen material. Basically, the structure is induced by electron beam, but connected to material's properties.

Previous studies also conducted observations on aged specimen, highlighting a clear trend: strands after aging becomes smaller, their average diameter decreases, and fibrils appear more numerous and dense (31); furthermore, they lengthen and assume a more parallel arrangement. There's a specific reason which explains the described tendency: after aging, molecular weight increases, which implicates a denser structure, and packing increase.

Sample preparation procedure was previously developed in details, since many variables play an important role, as temperature heating, sample size, mould features, sample storage and ESEM images acquisition.

4.1 Protocol and mould description

Regarding the shape and the size of the mould designed to contain the bitumen sample, we know that a very limited quantity of material can be introduced within the ESEM chamber, since microscopes usually analyses small specimens. Thus, the same dimensions employed in DST test were established: 8-mm diameter and 2-mm height. Another variable was the constituting material of the sample holder: in fact, some foams can experience troubles when subjected to vacuum conditions. Hence, DSR foam made of polymeric materials weren't use and a stainless steel holder was selected. Such material, in fact, resulted compatible with two of the main issues, which are heating the sample and bearing vacuum conditions (both low and high pressure).

The mould dimensions are those expressed in the following figure: beyond the 8-mm DSR plate standard dimensions, an external square perimeter was arranged, and a 15-mm long grip was added to help the operator during moving manoeuvres.

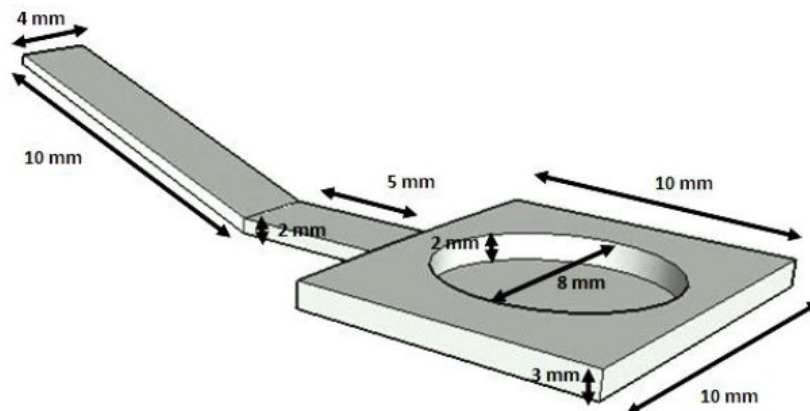


Figure 83 Stainless steel mould

The bitumen, placed in covered containers, was heated inside the oven at a temperature of 110°C until it could flow. A quantity which corresponds to about 0.1 g was transferred from the can to the sample mould by means of a spatula.

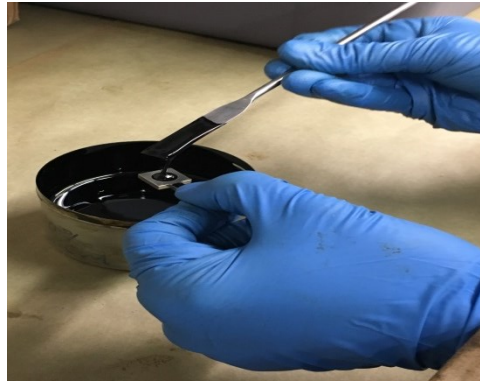


Figure 84 Mould pouring phase

Then, the holder was directly placed on a heater at 150°C to flatten the bitumen for approximatively 30-60 s, and after that it was stored in a cooler at 8°C for many hours.



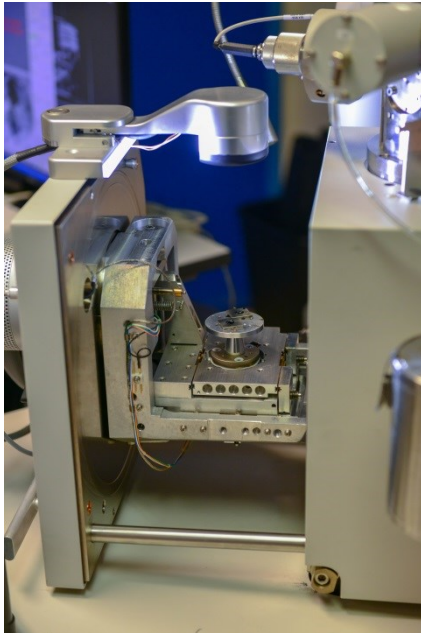
Figure 85 Sample flattened on a heater

It's possible to leave the sample for one whole night before microscope observation. All of the steps just described were led under a fume hood to avoid dust contamination, which could worsen examination phase.

4.2 ESEM observation

We directly performed ESEM observation, in order to analyse the microstructure of the twenty blends and capture the main morphological differences, detect whatever stand out a variability between the protocols adopted in blending preparation, moreover in terms of nano-additive dispersion degree, and investigate how the microstructure could affect rheological and physical properties.

We used the FEI Quanta 250 FEG model, with the following settings:



- Acceleration Voltage: 20 kV
- Chamber pressure: 0.8 mbar
- Low vacuum mode
- Magnification: 1000, 5000 and 10000 x
- Acquisition: SE images
- Spot size 3.5

Figure 86 ESEM observation

SE imaging mode is ideal to observe in a clearly way bitumen microstructure. The electron gun was held at about 15 mm from the sample's surface. The choice of an acceleration voltage of 20kV was performed in compliance with previous experiments, which demonstrated that, with lower voltages, images are less clear.

4.3 Results discussion

In order to introduce the reader to a more conscious and critical results interpretation, we can first introduce the qualitative and quantitative variables on which the analysis is based. It was quite hard to extrapolate considerations valid for our research study, since the only outputs provided by the machine are pictures and videos.

Being inspired by existing publications, we adopted the following interpretation criteria, (31), (32), (33):

-Timing necessary to focus the fibres clearly and to stabilize the videos (we recorded them just for *NB* and *NC* samples). In fact, while the bitumen sample initially appears featureless, a network of fibrils or strands is observed after few minutes of electron beam exposure. At first, we tried to record movies for *CNT* samples, but in conclusion it was useless, since fibrils are too small to show strands.

-Fibril's diameter: it's a variable, which evaluates the average fibrils' diameter. According to previous researches, it's expected to reduce its size in case of aged samples.

-Fibril's density: it's a qualitative analysis about the amount of fibrils in a limited area (like the picture): the denser they are the more stiff is the bitumen. This general assertion was found in the past, and must be verified for our samples. The densest samples are the CNT ones, which effectively are the stiffest.

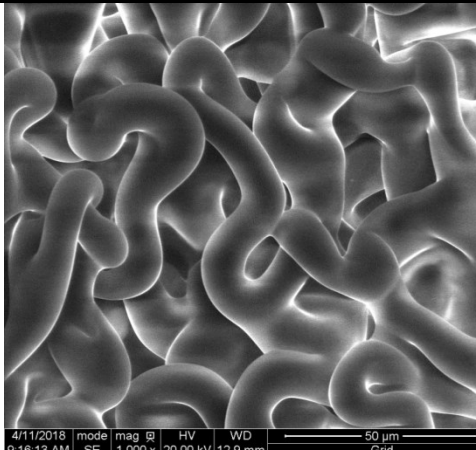
-Fibril's alignment: it's a brief description of how fibrils are arranged and of fibril's compaction level.

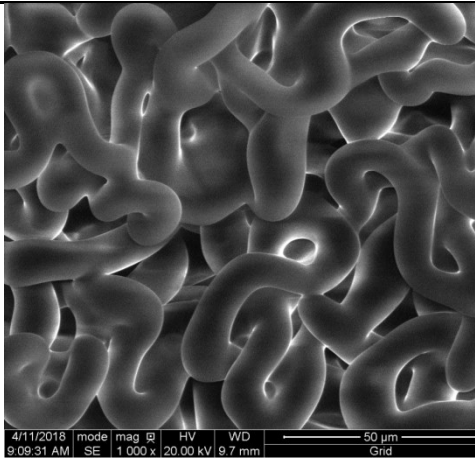
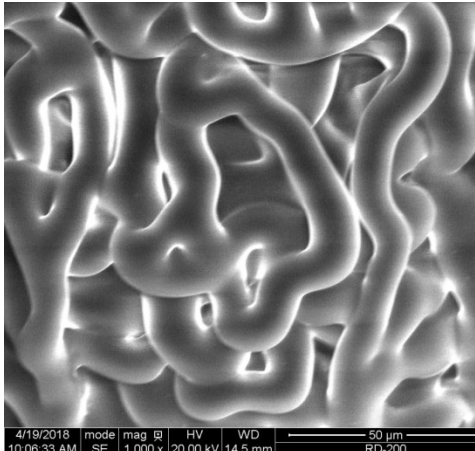
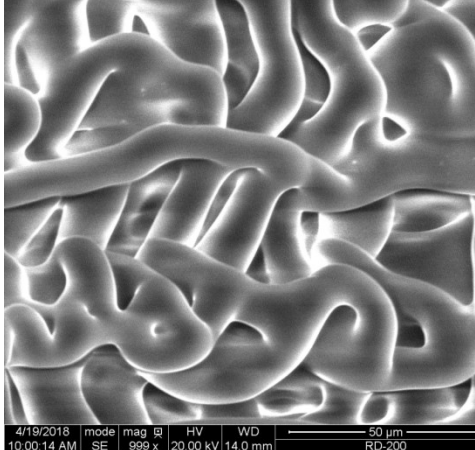
These parameters were compared just for *NB* and *NC* samples, since *CNT* images were completely different, thus it was impossible to compare them by means of the same variables.

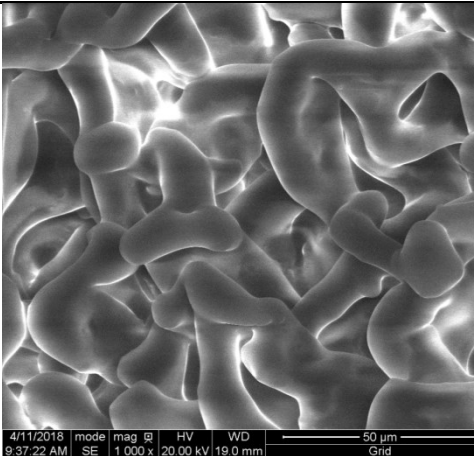
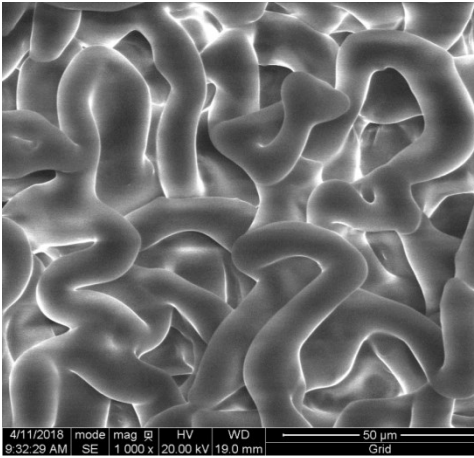
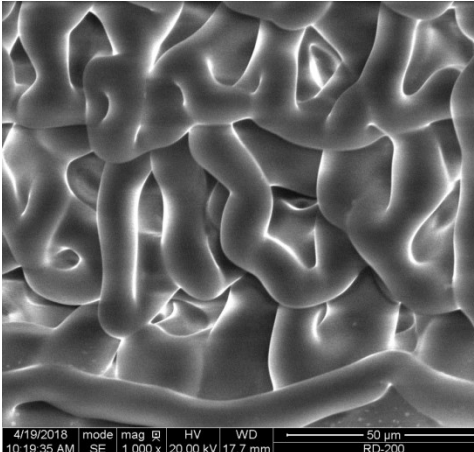
Once we collected all the images, they were compared to detect whether there's any evidence in the microstructure's profile, with the main aim to study if the mixing procedure gave any proof of discrepancy in nanoparticles dispersion degree, due to the adopted mixing protocol.

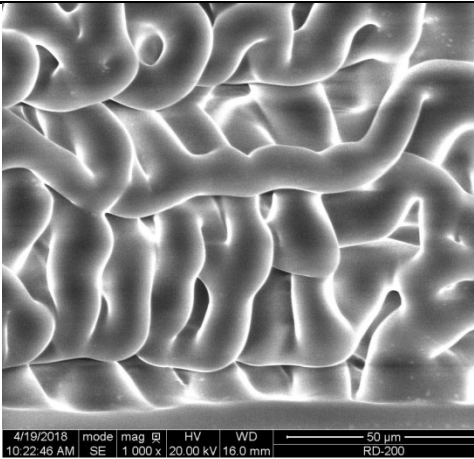
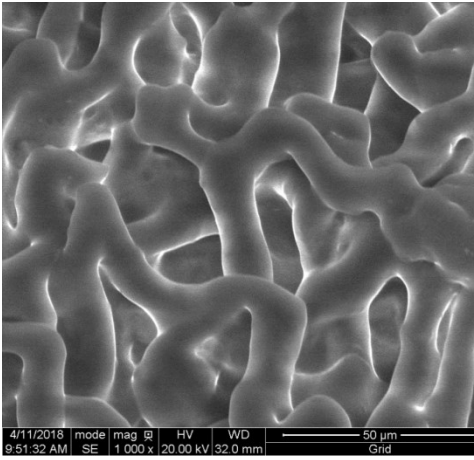
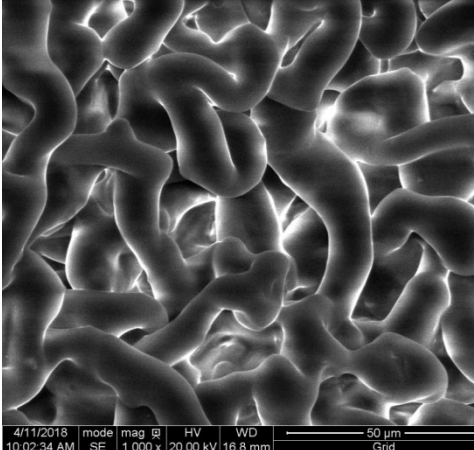
ESEM observation was performed one more time after RTFOT on aged bitumen, allowing us to get short-term aging influence on bitumen's microstructure.

4.3.1 NB and NC results

Sample	ESEM image	Fibril alignment	Timing	Diameter
NB90		Loose and tangled fibrils	26	10-13

NB50		Loose and tangled fibrils	32	10-12
NBV		Sparse and aligned fibrils	27	10-12
NBQ		Sparse and extended fibrils	28	10-12

NC3_90		Nodes and lumps	24	13-17
NC3_50		Nodes and lumps	33	12-15
NC3V		Aligned and parallel fibrils	29	11-13

NC3Q		Dense and structured fibrils	24	11-13
NC6_90		Lumps and tangles of fibrils	33	10-15
NC6_50		Lumps and tangles of fibrils	35	11-16

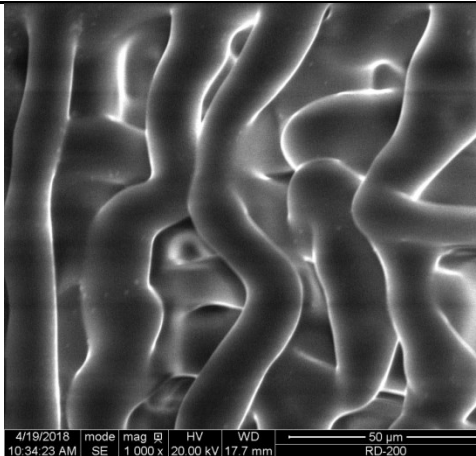
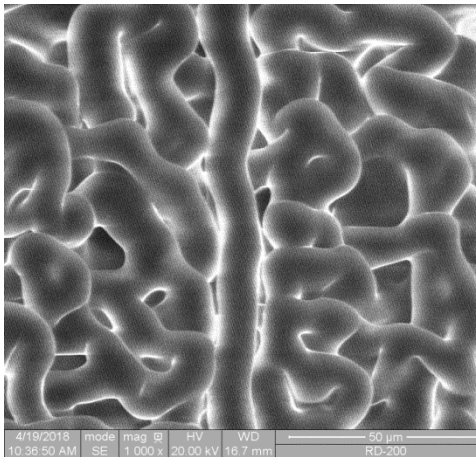
NC6V		Aligned and extended fibrils	20	13-18
NC6Q		Parallel and extended fibrils	26	10-13

Table 8 ESEM evaluation – NB, NC samples

As can be seen from the collected images shown above, there are several evidences:

- samples prepared following low-shear mixing protocols present evident nodes and lumps. Such lumps' dimension is averagely compatible with NC size, which means that they could be nano-additive particles aggregated, that didn't appropriately disperse into the bituminous matrix
- samples prepared following high-shear mixing protocols display much denser, aligned and parallel fibrils. A similar behaviour was seen in literature in case of aged samples, which means that, due to very high speed achieved under Silverson machine, and high temperatures, specimen have been exposed to early aging.

According to the variables mentioned in the previous paragraph, it's possible to highlight that:

- Timing requested to clearly visualize fibrils in the recorded videos is averagely higher in case of samples mixed in compliance with

Silverson procedure. Such evidence was already experienced in previous studies.

- None clear trend was found regarding average fibril's diameter, since it depends on each case.

4.3.2 CNT results

At first, we found noteworthy difficulties in observing *CNTs* blend samples, since the microstructure appeared completely altered. Fibrils seemed disappeared and it was impossible to focus any strand.

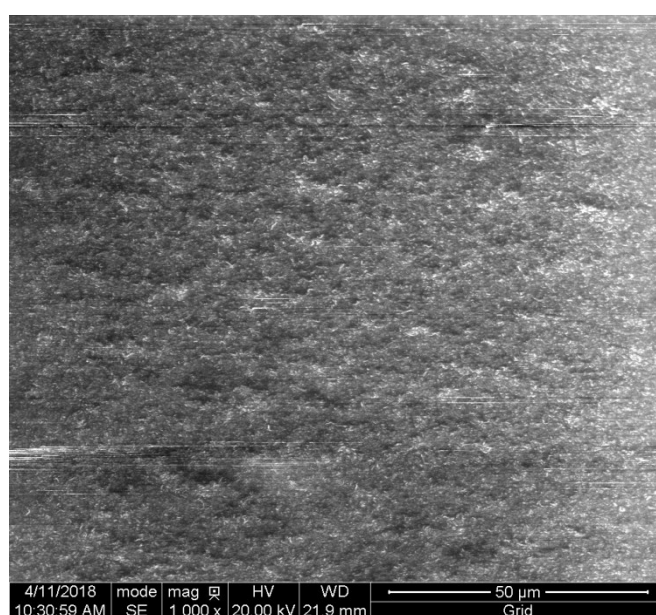
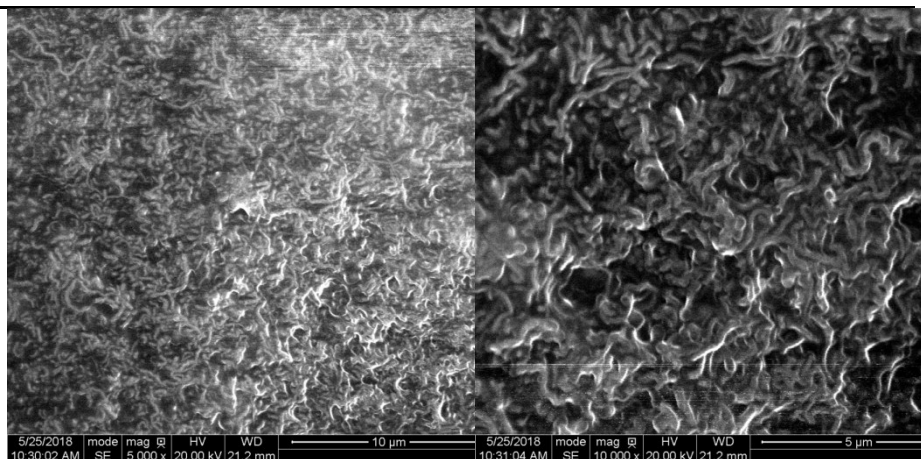


Table 9 ESEM observation CNTs 1000 x magnification

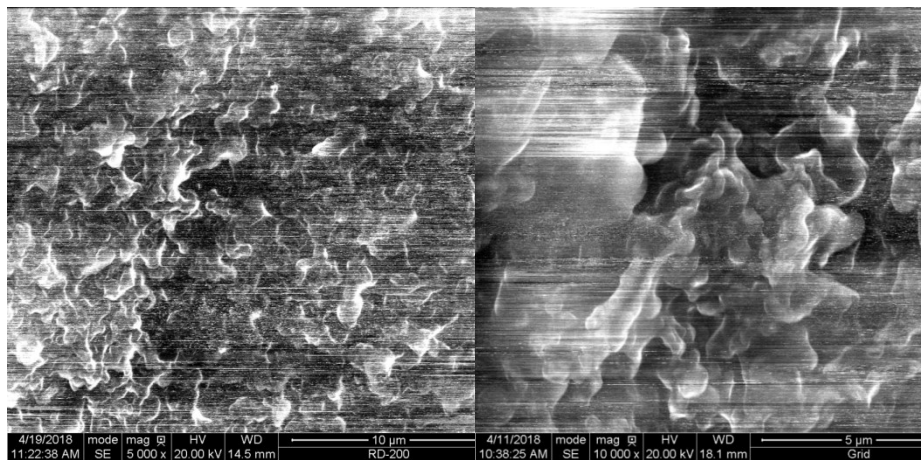
Thus, we had to increase the magnification of 5 and 10 times. Such an increase in enlargement features provoked higher troubles in imaging samples, since fibrils moved very quickly, thus we didn't record any videos for *CNT* samples.

Sample	Magnification: 5000 x	Magnification: 10000 x
--------	-----------------------	------------------------

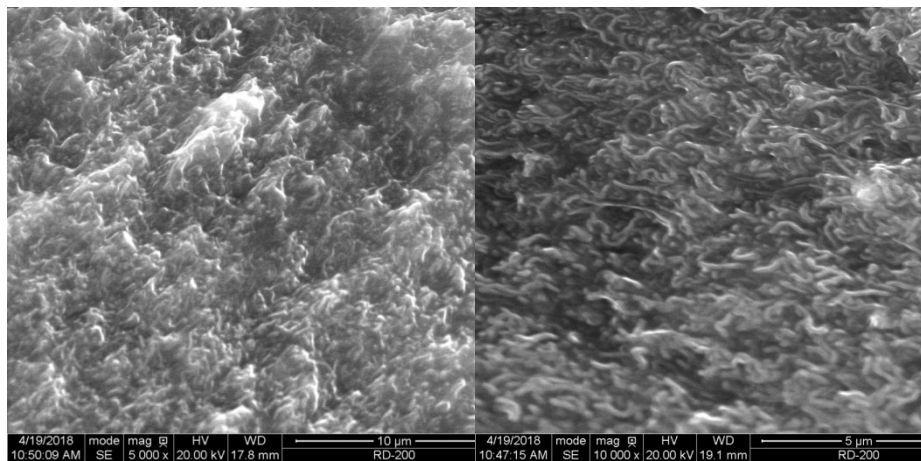
CNT.5_90



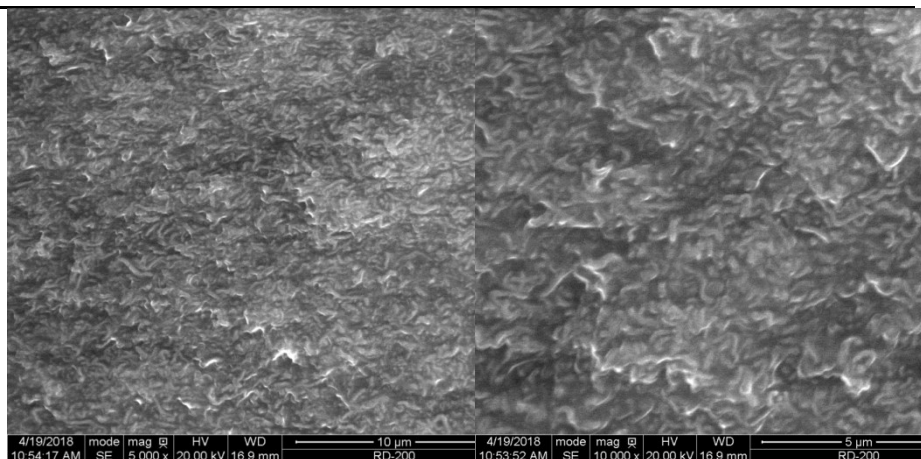
CNT.5_50



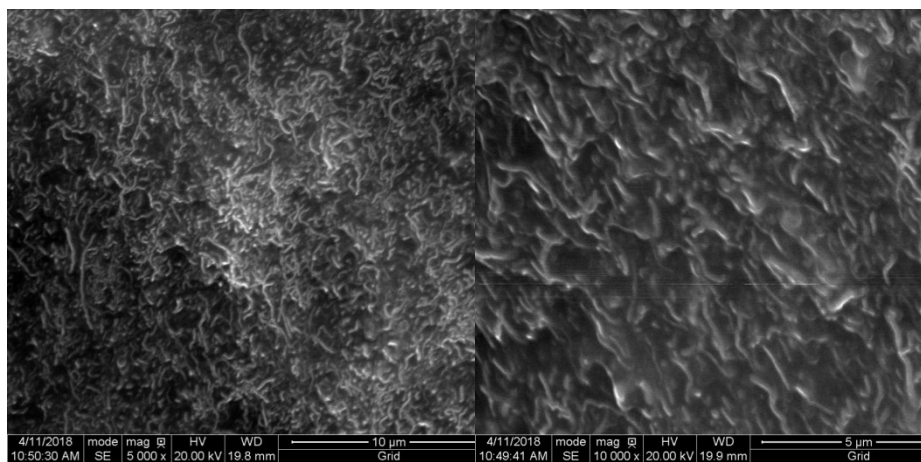
CNT.5V



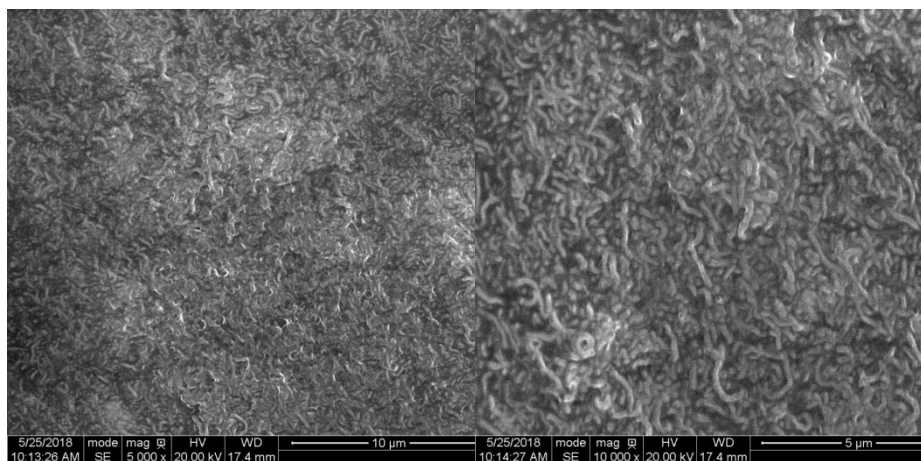
CNT.5Q



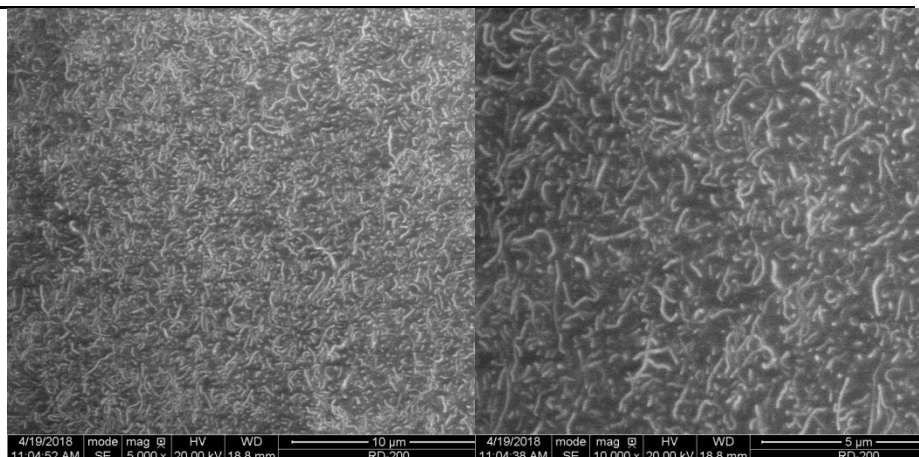
CNT1_90



CNT1_50



CNT1V



CNT1Q

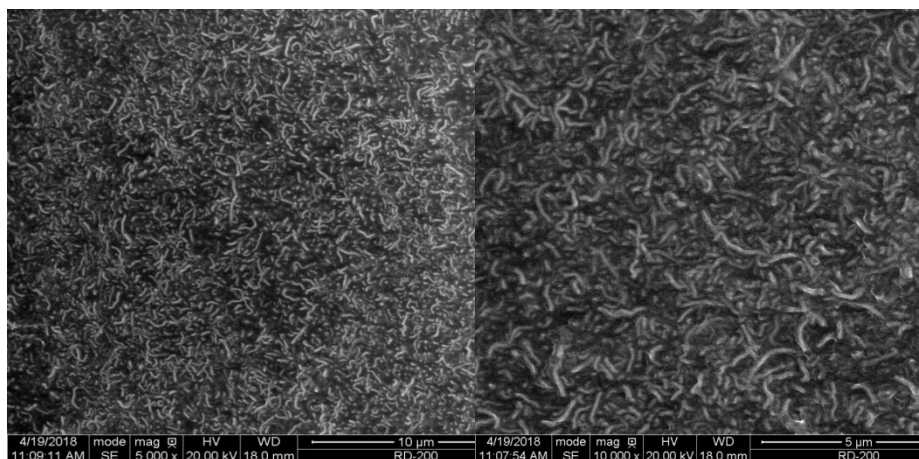


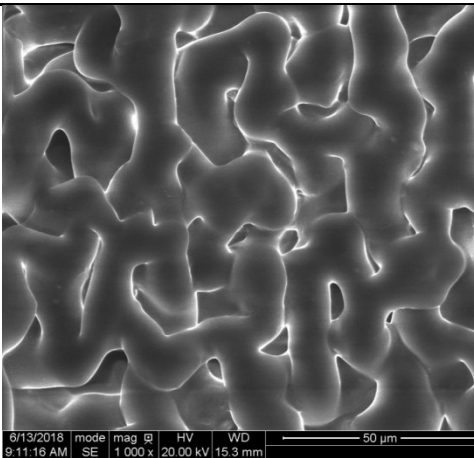
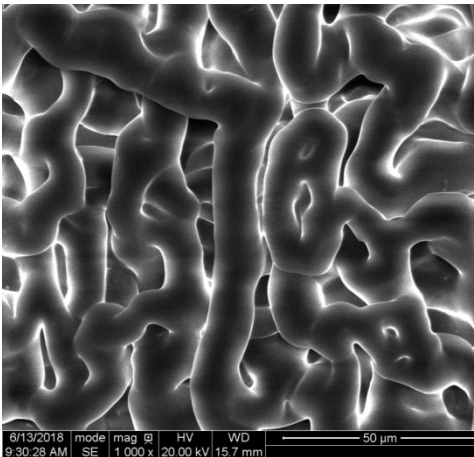
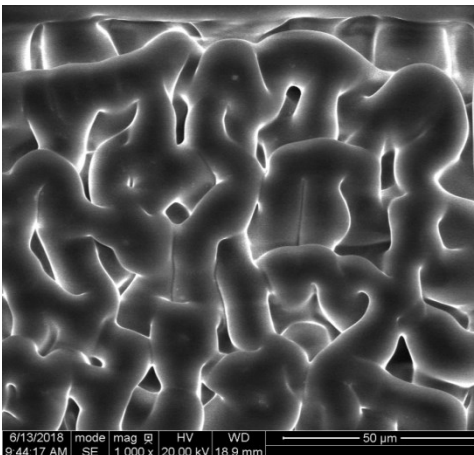
Table 10 ESEM evaluation: CNT samples

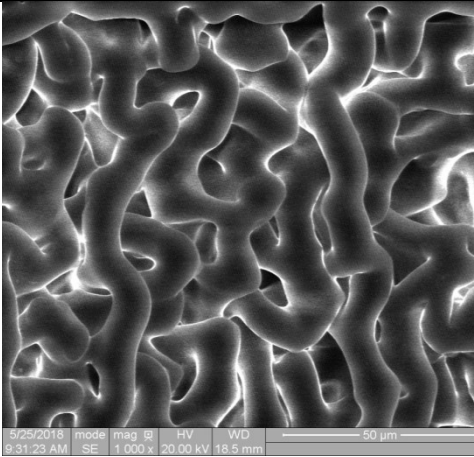
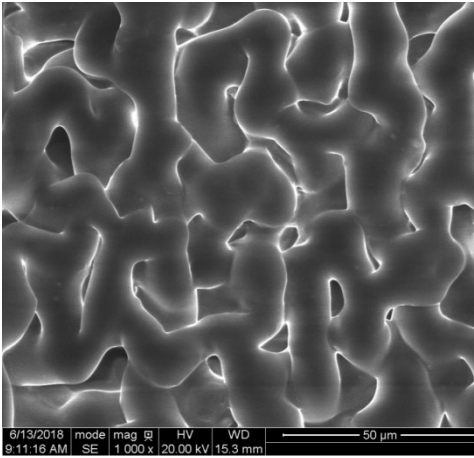
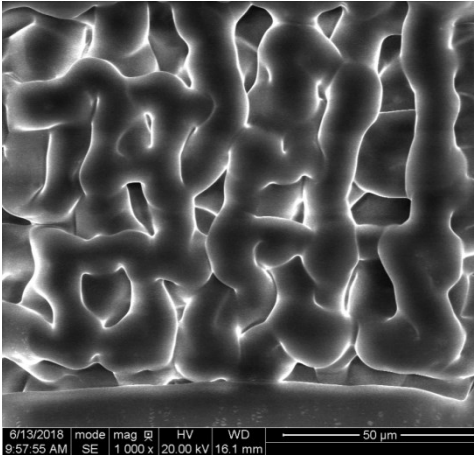
Due to the very minute fibril's size, it was impossible to record any videos in case of *CNT* blends, since they moved very fast.

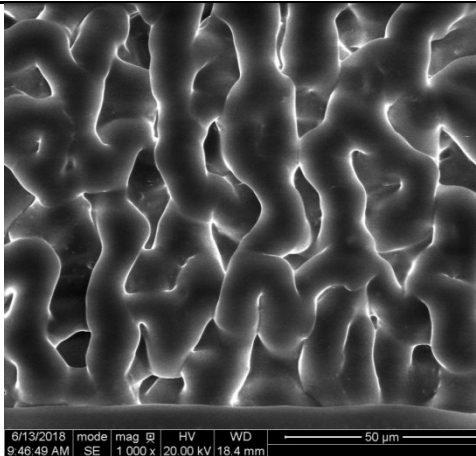
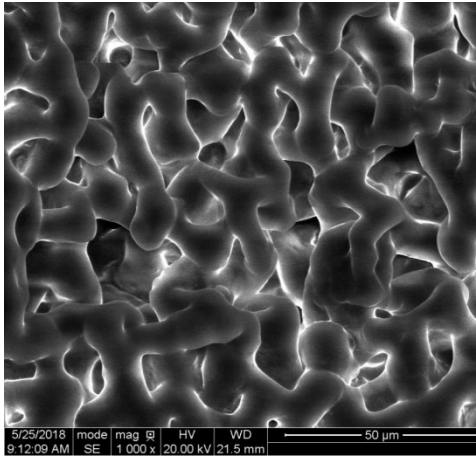
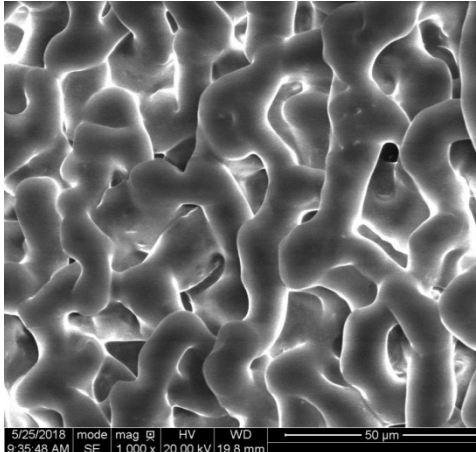
From the images above, results immediately evident that outputs are overturned, as fibril's structure seems disappeared. Comparing fibril's size to that of *CNTs*, the nano-scale demonstrates the analogy with the NC7000 size.

At first, the output left us astonished, surprised by a such huge difference. However, we think that it may be attributed to an incorrect use of the ESEM microscope. In fact, after a careful study, we found that low vacuum mode is selected in case of wet or non-conductive samples. Whereas, NC7000 is characterizes, as we said in the first chapter, by high electrical conductivity. Hence, electrical properties maybe altered ESEM observations, showing *CNTs* nanoparticles in the foreground.

4.3.3 Aged samples: NB and NC results

Aged Sample	ESEM image	Fibril alignment	Timing	Diameter
NB50	 <p>6/13/2018 mode mag @ HV WD 9:11:16 AM SE 1 000 x 20.00 kV 15.3 mm 50 µm</p>	Dense fibrils	39	11-17
NBV	 <p>6/13/2018 mode mag @ HV WD 9:30:28 AM SE 1 000 x 20.00 kV 15.7 mm 50 µm</p>	Dense and aligned fibrils	39	10-15
NBQ	 <p>6/13/2018 mode mag @ HV WD 9:44:17 AM SE 1 000 x 20.00 kV 18.9 mm 50 µm</p>	Dense fibrils	40	9-14

NC3_90		Dense and compact fibrils	43	9-13
NC3_50		Dense and featureless	31	11-16
NC3V		Dense and structured fibrils	38	10-13

NC3Q		Dense and structure d fibrils	35	10-13
NC6_90		Dense and confused d fibrils	39	8-11
NC6_50		Dense and confused d fibrils	34	11-13

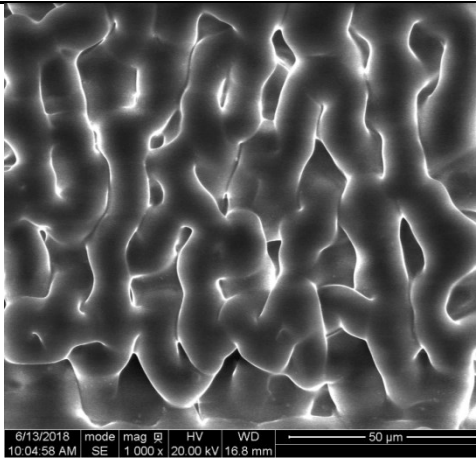
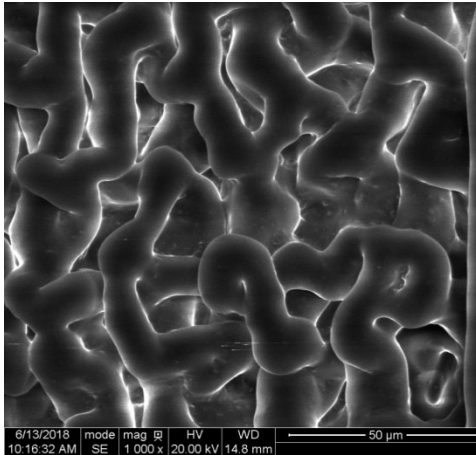
NC6V		Dense and featureless fibrils	39	12-15
NC6Q		Dense and chaotic fibrils	41	11-14

Table 11 ESEM evaluation – NB, NC aged samples

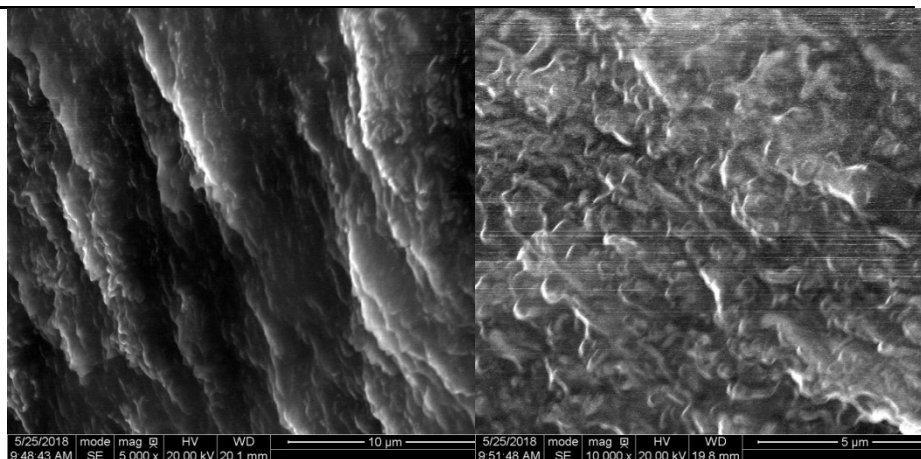
According to existing experimental studies, in case of aged samples, fibril's structure appears featureless, and fibrils tend to be clearly focused. As we performed just a short-term aging, differences in the pictures weren't so evident.

Apparently, timing necessary to visualize well-defined fibrils was averagely increased, which is consistent with literature's findings. In the past, also a decrease in fibril's diameter was found, despite this tendency wasn't confirmed in our sample, probably because of the low aging level.

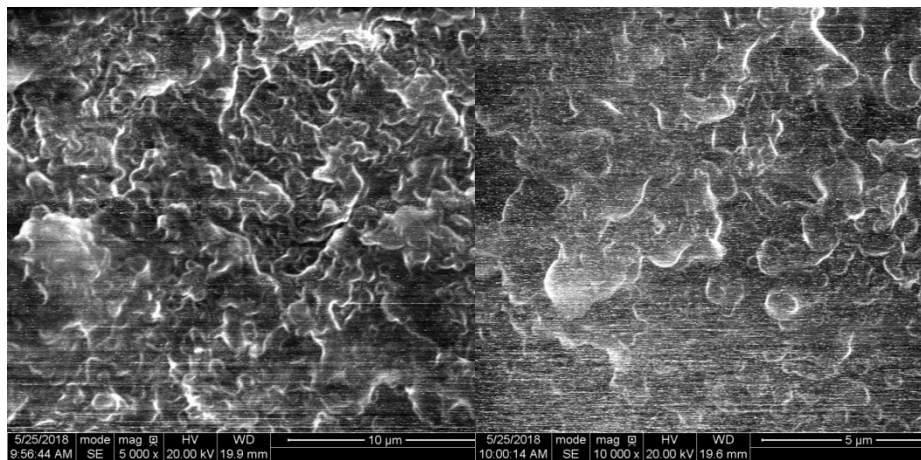
4.3.4 Aged samples: CNT results

Aged Sample	Magnification: 5000 x	Magnification: 10000 x
-------------	-----------------------	------------------------

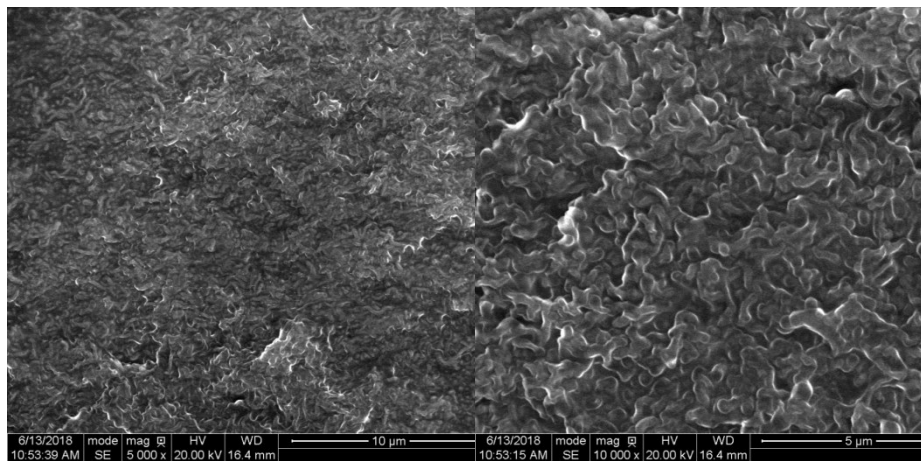
CNT.5_90



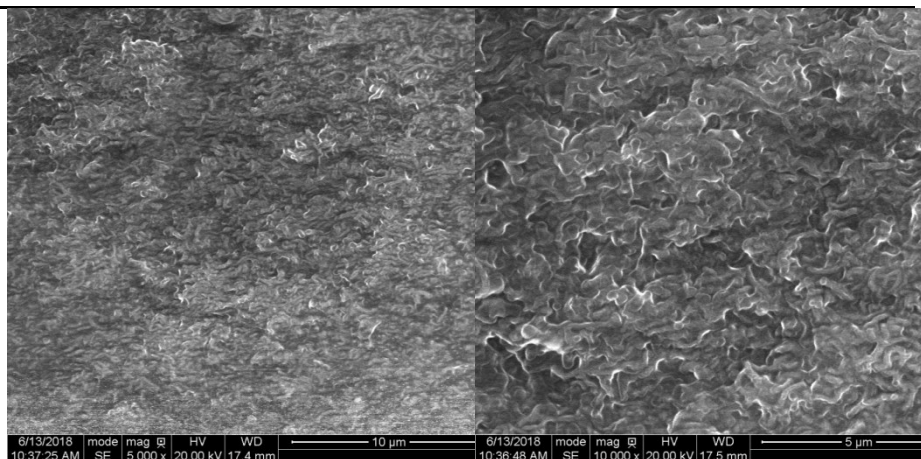
CNT.5_50



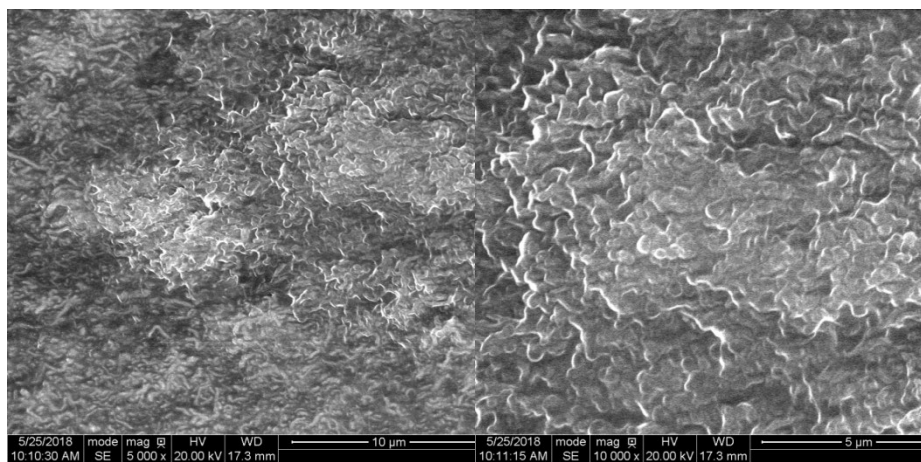
CNT.5V



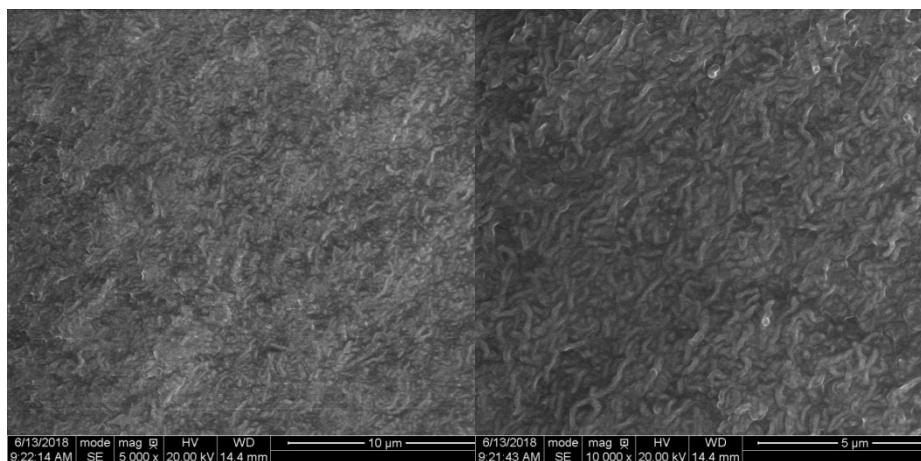
CNT.5Q



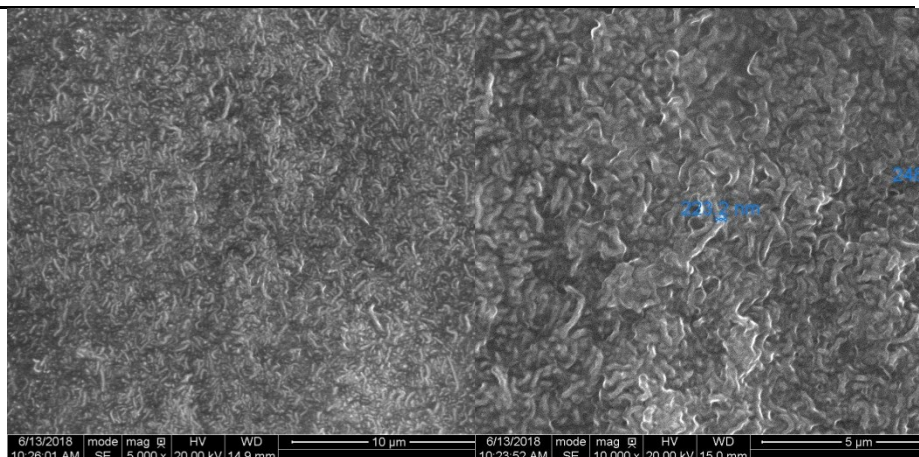
CNT1_90



CNT1_50



CNT1V



CNT1Q

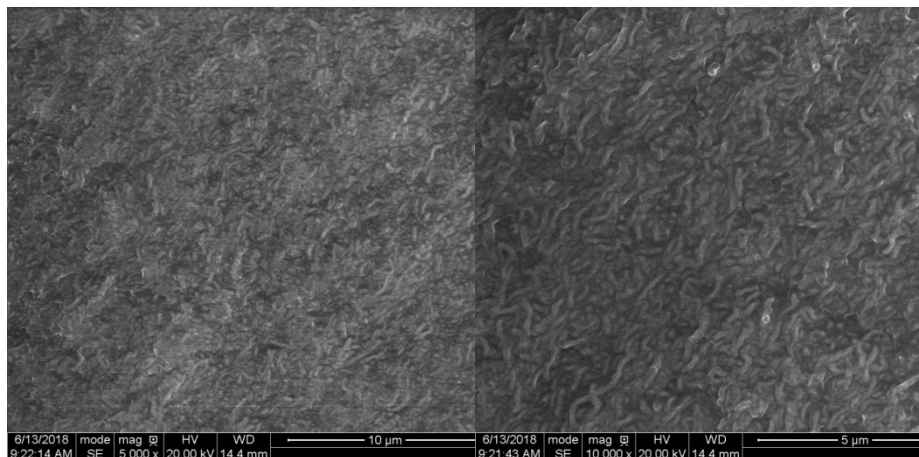


Table 12 ESEM evaluation – CNT aged samples

Images from sample CNT.5_50 were damaged, as small white stripes altered the picture and couldn't be hidden. We tried to prepare the sample again, for a second observation session, but output pictures presented the same stripes. We followed up examples of similar cases, unsuccessfully. Then, we hypothesized that an excessive humidity amount within the sample could have caused *CNT* oxidation reaction: during oxidation process, the carbon-carbon bonded network of the graphitic layers is broken allowing the introduction of oxygen units and may cause the carbon nanotube break up into fragments. The picture is vague and confusing: it's impossible to recognize fibrils, and bubbles take form on sample's surface during observation.

Pictures captured after aging process didn't show any discrepancy with non-aged samples. But, we can highlight that images collected for specimens prepared in compliance with Protocol C or D shows fibrils more clearly and precisely.

Conclusions and perspectives

At the end of our involving research study, extreme importance is covered by a “looking back” phase, consisting in giving an overall view and critical interpretation of findings, to evaluate the effectiveness of the employed methods and to lay the foundation for future investigations.

We moved forward on a variety of fronts, since analyses were performed on numerous academic fields of study. Hence, it's convenient to jump to final conclusions making a bulleted list, which let us methodically articulate our outcomes.

Our main purpose was to evaluate the mixing protocol influence on rheological properties and nanoparticles fine dispersion level. It was performed by means of rheological tests and microstructure investigations.

- Regardless of the adopted mixing protocol, what basically stands out from black diagrams and master curves is that, as a consequence of carbon nanotubes addition, phase angles reduces and complex shear modulus slightly increases. In other words, it physically means an improvement in stiffness and elasticity, especially at high temperatures. Such a tendency occurs in every case, and was confirmed by existing researches. The more the nano-additive dosage grows, the more rheological properties enhances.

Whereas, base bitumen modified with nanoclays displays curves which are almost overlapped to those of the control samples. Throughout the rheological characterization, it becomes distinctive that bituminous blends prepared according to mixing protocol A or B had early hardening, since their complex modulus is moderately higher.

- After drawing damage factor at the end of fatigue analysis, blends prepared according to mixing protocol A or B presented, once more, averagely higher performances within the non-linear domain. The just mentioned attitude was typical of the neat bitumen (*NB*) and of nanoclay blends (*NC*), nevertheless carbon nanotube blends (*CNT*) showed a turnaround, since high-shear mixing gave better fatigue behaviour. It's noteworthy that just one repetition was carried out for LAS test. We recommend, for future experiments, to repeat it once more, to confirm the outcomes.
- ESEM observation gave us relevant findings: first of all, it was stimulating working on emerging aspects of asphalt binder nature, and this research has thrown up many questions in need of further investigation. Additional studies need to be carried out in order to validate our outcomes: Silverson mixing protocol seems to achieve better nano-additive dispersion into the bituminous

matrix, preventing agglomeration development. Furthermore, fibril's alignment inside those blends prepared according to high-shear mixing protocol resulted denser and structured, as well as aligned and parallels. This behaviour typically characterizes aged samples, thus high-shear mixing protocol, due to high speed mixing and high temperature process, could provoke an early aging in terms of microstructure. The just expressed outcomes may give an explanation of worse fatigue performance occurred in Protocol C and D samples.

Clearly, none foregone conclusion comes out, since unequivocal judgement in research field would be hurried and rashly articulate.

Further research is needed to generalise the expressed outcomes of the current study and to directly verify them:

- Firstly, we suggest to extend investigations to several single base bitumen, since it sensitively affects nano-additive influence on rheological behaviour.
- Regarding the ESEM observation, the challenge now is to perform the analysis for *CNT* blends at high pressure settings, or by means of SEM technology, to investigate whether bitumen's fibrils stand out.
- Moreover, nanoparticles dispersion into the base bitumen requires the development of a reliable mixing technique, which should also prevent the occurrence of segregation phenomena. Thus, it could be useful to arrange a protocol to prevent specimen overheating during high-shear mixing protocol, in order to detect if a correlation exists between such phenomenon and early aging observed with ESEM technology; even if, on the other hand, higher temperatures allow, especially for *CNT* blends, easier nanoparticles dispersion, since viscosity decreases with temperature.

In conclusion, future experiments are needed, to perform a deeper investigation of relationship between rheological analyses and bitumen morphological characterization, to validate results by considering a wider array of base materials and mixing protocols.

Bibliography and sitography

1. **Ezio Santagata, Orazio Baglieri, Lucia Tsantilis, Giuseppe Chiappinelli, Davide Dalmazzo.** Bituminous-based nanocomposites with improved high-temperature. *Composites Part B* 99. 2016, pp. 9-16.
2. **Pinnavaia TJ, Beall GW.** Polymer-Clay. Nanocomposites. *Wiley Series in Polymer Science*. Chichester: Wiley, 2000.
3. **Paul DR, Robeson LM.** Polymer nanotechnology: nanocomposites. *Polymer*. 2008, 49(15):3187-204.
4. **V., Anania.** Stabilità allo stoccaggio di leganti bituminosi modificati con nanoargille. Politecnico di Torino : Master thesis defense, 2014.
5. **A., Bolla.** Stabilità allo stoccaggio di leganti bituminosi modificati con nanotubi. Politecnico di Torino : Master thesis defense, 2014.
6. **Ezio Santagata, Orazio Baglieri, Lucia Tsantilis, Davide Dalmazzo.** Rheological Characterization of Bituminous Binders Modified with Carbon Nanotubes. *Procedia - Social and Behavioral Sciences*. 2012, Vol. 53, 546-555.
7. Nanocyl. <http://www.nanocyl.com/>. [Online]
8. **Ezio Santagata, Orazio Baglieri, Lucia Tsantilis, Giuseppe Chiappinelli, Ilaria Brignone Aimonetto.** Effect of sonication on high temperature properties of bituminous binders reinforced with nano-additives. *Construction and Building Materials*. 2014, 75 (2015) 395–403.
9. *Effects of nano-sized additives on the high-temperature properties of bituminous binders: a comparative study.* **Santagata E, Baglieri O, Tsantilis L, Chiappinelli G.** Stockholm : International RILEM symposium on multi-scale modeling and characterization of infrastructure materials, 2013. 297–309.
10. **Santagata E, Baglieri O, Tsantilis L, Dalmazzo D.** Rheological characterization bituminous binders modified with carbon nanotubes. . *Procedia – social and behavioral science*. 2012, Vol. 53, 546–555.
11. Heidolph Italia. <http://www.heidolph-italia.it/> . [Online]
12. Silverson. <http://www.silverson.com/us/products/laboratory-mixers/> . [Online]
13. **Technology, Hielscher – Ultrasound.**
http://www.hielscher.com/200s_p.htm?gclid=EAIaIQobChMI8MHxmrbZ3gIVwee aChIXLAdwEAAYASAAEgIpefD_BwE. [Online]

14. **Lam C-K, Lau K-T, Cheung H-Y, Ling H-Y.** Effect of ultrasound sonication in nanoclay clusters of nanoclay/epoxy composites. *Mater.* 2005, 59:1369–72.
15. **Montazeri A, Chitsazzadeh M.** Effect of sonication parameters on the mechanical properties of multi-walled carbon nanotube/epoxy composites. *Mater.* 2014, 56:500–8.
16. **Airey, Gordon D.** Use of Black Diagrams to Identify Inconsistencies in rheological data. *Road Materials and Pavement Design.* 2002, Vol. 3:4, 403-424.
17. **F., Petretto.** *Le reologia dei leganti bituminosi stradali: studio delle proprietà meccaniche a seguito di processi di “aging” in laboratorio.* Bologna : PhD Defense, 2012.
18. Anton Paar. <https://www.anton-paar.com/in-en/products/details/rheometer-mcr-102-302-502/>. [Online]
19. **Ezio Santagata, Orazio Baglieri, Lucia Tsantilis & Giuseppe Chiappinelli.** Fatigue properties of bituminous binders reinforced with carbon nanotubes. *International Journal of Pavement Engineering.* 2015, Vol. 16:1, 80-90.
20. Pavement interactive. <https://www.pavementinteractive.org/reference-desk/testing/binder-tests/rolling-thin-film-oven/>. [Online]
21. **Mohammadreza Sabouri, Danial Mirzaiyan, Ali Moniri.** Effectiveness of Linear Amplitude Sweep (LAS) asphalt binder test in predicting asphalt mixtures fatigue performance. *Construction and Building Materials.* 2018, Vol. 17, 281–290.
22. **Podolsky, Joseph H., et al., et al.** Effects of aging on rejuvenated vacuum tower bottom rheology through use of black diagrams, and master curves. *Peer Reviewed.* 2016, Vol. 185, 34-44.
23. **Booshehrian, Abbas, Mogawer, Walaa S. e Bonaquist, Ramon.** How to Construct an Asphalt Binder Master Curve and Assess the Degree of Blending between RAP and Virgin Binders. *Journal of Materials in Civil Engineering.* 2013, Vol. 25, 1813-1821.
24. **Mirhosseini, Ali Foroutan, et al., et al.** Evaluating fatigue behavior of asphalt binders and mixes containing Date Seed Ash. *Journal of Civil Engineering and Management.* 2017, Vol. 23.
25. **Sabouri, Mohammadreza, Mirzaiyan, Danial e Moniri, Ali.** Effectiveness of Linear Amplitude Sweep (LAS) asphalt binder test in predicting asphalt mixtures fatigue performance. *Construction and Building Materials.* 2018, Vol. 171, 281-290.

26. **Tuminello, W. H.** Molecular weight and molecular weight distribution from dynamic measurements. *Polymer Engineering & Science*. 1986, Vol. 26, 1339–1347.
27. **McGrory, W. J., & Tuminello, W. H.** Determining the molecular weight distribution from the stress relaxation properties of a melt. *Journal of Rheology*. 1990, Vol. 34(6) , 867–890.
28. **Andrea Themeli, Emmanuel Chailleux, Fabienne Farcas, Cyrille Chazallon & Bernard Migault.** Molecular weight distribution of asphaltic paving binders from phase-angle measurements. *Road Materials and Pavement Design*. 2015, 228-244.
29. **Mazumder, Mithil, et al., et al.** SEM and ESEM techniques used for analysis of asphalt binder and mixture: A state of the art review. *Construction and Building Materials*. 2018, Vol. 186, 313-329.
30. **Wang, Peng, et al., et al.** Micromorphology of Asphalt Modified by Polymer and Carbon Nanotubes through Molecular Dynamics Simulation and Experiments: Role of Strengthened Interfacial Interactions. *Energy & Fuels*. 2018.
31. **Mikhailenko, Peter, Kadhim, Hawraa e Baaj, Hassan.** Observation of bitumen microstructure oxidation and blending with ESEM. *Road Materials and Pavement Design*. 2017, Vol. 18, 216-225.
32. **Mikhailenko, P., et al., et al.** Observation of asphalt binder microstructure with ESEM. *Journal of Microscopy*. 2017, Vol. 267, 347-355.
33. *Observation of Asphalt Binder Microstructure with ESEM.* **Mikhailenko, Peter, et al., et al.** Toronto : Conference of the 12 Transportation Association, 2016.
34. National Research Council of Italy.
<http://www.istec.cnr.it/index.php/eng/resources/expertises/95-microstructure-and-texture/527-environmental-scanning-electron-microscope-esem>. [Online]